REPUBLIC OF TURKEY
YILDIZ TECHNICAL UNIVERSITY
GRADUATE SCHOOL OF NATURAL AND APPLIED SCIENCES

INVESTIGATION OF BURIED STRUCTURES UNDER EARTHQUAKE LOADING

SEFA UZUN

MSc. THESIS
DEPARTMENT OF CIVIL ENGINEERING
PROGRAM OF STRUCTURAL ENGINEERING

ADVISER
PROF. DR. YUSUF AYVAZ

İSTANBUL, 2019

REPUBLIC OF TURKEY

YILDIZ TECHNICAL UNIVERSITY

GRADUATE SCHOOL OF NATURAL AND APPLIED SCIENCES

INVESTIGATION OF BURIED STRUCTURES UNDER EARTHQUAKE LOADING

A thesis submitted by Sefa UZUN in partial fulfillment of the requirements for the degree of **MASTER OF SCIENCE** is approved by the committee on 04.01.2019 in Department of Civil Engineering, Structural Engineering Program.

Thesis Adviser

Prof. Dr. Yusuf AYVAZ

Yıldız Technical University

Approved by the Examining Committee

Prof. Dr. Yusuf AYVAZ

Yıldız Technical University _____

Assoc. Prof. Dr. Serkan BEKİROĞLU, Member

Yıldız Technical University _____

Asst. Prof. Dr. Ahmet Utku YAZGAN, Member

Maltepe University _____

ACKNOWLEDGEMENTS

I owe a debt of gratitude to my respectful adviser Prof. Dr. Yusuf AYVAZ whose guidance was a key factor for the success of this study. I also appreciate to valuable members of the examining committee, Assoc. Prof. Dr. Serkan BEKİROĞLU and Asst. Prof. Dr. Ahmet Utku YAZGAN.

Beside my efforts, my family and especially my mother gave me a huge support during this study, and I gratefully acknowledge their support.

January, 2019

Sefa UZUN

TABLE OF CONTENTS

Page

LIST OF SYMBOLS vi

LIST OF ABBREVIATIONS vii

LIST OF FIGURES viii

LIST OF TABLES x

ABSTRACT xi

ÖZET xii

CHAPTER 1

INTRODUCTION 1

1.1 Literature Review 1
1.2 Objective of the Thesis 12
1.3 Hypothesis 13

CHAPTER 2

MODELING AND METHODOLOGY 14

CHAPTER 3

PARAMETRIC STUDY 18

3.1 Parameters in This Study 18
3.2 The Buried Box Culvert 20
3.3 Input Motion 21
3.4 Determination of Model Width Ratio 26
3.5 Numerical Analyses 28
3.6 Results and Discussion 28
3.6.1 Variation of the Normalized Absolute Maximum Internal Forces 28
3.6.2 Variation of the Bending Moments 42
3.6.3 Variation of the Drift Ratios 55
3.6.4 Variation of the Shear Strain Deformation Ratios 59

CHAPTER 4

CONCLUSIONS AND RECOMMENDATIONS 62

REFERENCES 65

CURRICULUM VITAE 71

LIST OF SYMBOLS

Δ_{ff}	The free-field shear deformation over the height of the buried box culvert
Δ_{st}	The shear deformation of the buried box culvert embedded in soil
A	Base area of the FEM model
C	Viscous damper coefficient
DR	Depth ratio
E	Elastic modulus of buried box culvert
FR	Flexibility ratio
f_s	Shear flexibility of the soil block with the same dimensions as the buried box culvert
f_{st}	Shear flexibility of the buried box culvert without soil interaction
G	Shear modulus of soil layer
h	Height of buried box culvert
H	Height of soil layer
I	Moment of inertia about the Z-axis of the wall or roof of buried box culvert
K	Stiffness of the roof or wall of buried box culvert
R	Shear strain deformation ratio
t	Thickness of buried box culvert
$V_{bedrock}$	Shear wave velocity of bedrock
V_s	Shear wave velocity of the soil medium
w	Width of buried box culvert
W	Width of soil layer
ν	Poisson's ratio of the soil layer
ρ	Mass density of bedrock
Ω	Model width ratio

LIST OF ABBREVIATIONS

2D	Two-dimensional
3D	Three-dimensional
BEM	Boundary Element Method
DOF	Degree of Freedom
FEM	Finite Element Model
FFT	Fast Fourier Transform
FLAC	Fast Lagrangian Analysis of Continua
MATLAB	Matrix Laboratory
OpenSEES	Open System for Earthquake Engineering Simulation
PBC	Periodic Boundary Condition
PGA	Peak Ground Acceleration
PGD	Peak Ground Displacement
PGV	Peak Ground Velocity
SDOF	Single Degree of Freedom
SSI	Soil-Structure Interaction

LIST OF FIGURES

Page

Figure 2.1 Dimensions and boundary conditions of the FEM model I 14
Figure 2.2 The dimensions and boundary conditions of the FEM model II 15
Figure 2.3 The dimensions of the FEM model III 16
Figure 2.4 Boundary conditions of the FEM model III 17
Figure 3.1 (a) 3D view and (b) dimensions of the buried box culvert 20
Figure 3.2 Displacement response spectrums of the real-time earthquakes and the Ricker wavelet I 22
Figure 3.3 Displacement response spectrums of the real-time earthquakes and the Ricker wavelet II 23
Figure 3.4 (a) Acceleration history, (b) velocity history and (c) FFT of acceleration history for the Ricker wavelet I 24
Figure 3.5 (a) Acceleration history, (b) velocity history and (c) FFT of acceleration history for the Ricker wavelet II 25
Figure 3.6 Convergence of the model width ratio for the soil deposit I 27
Figure 3.7 Convergence of the model width ratio for the soil deposit II 27
Figure 3.8 Variation of the normalized (a) axial forces, (b) shear forces, (c) bending moments of the buried box culvert for the depth ratio of 0.25 30
Figure 3.9 Variation of the normalized (a) axial forces, (b) shear forces, (c) bending moments of the buried box culvert for the depth ratio of 0.50 31
Figure 3.10 Variation of the normalized (a) axial forces, (b) shear forces, (c) bending moments of the buried box culvert for the depth ratio of 0.75 32
Figure 3.11 Variation of the normalized (a) axial forces, (b) shear forces, (c) bending moments of the buried box culvert for the depth ratio of 1.0 33
Figure 3.12 Variation of the normalized (a) axial forces, (b) shear forces, (c) bending moments for depth ratio of 1.50 35
Figure 3.13 Variation of the normalized (a) axial forces, (b) shear forces, (c) bending moments of the buried box culvert for the depth ratio of 2.00 36
Figure 3.14 Variation of the normalized (a) axial forces, (b) shear forces, (c) bending moments of the buried box culvert for the depth ratio of 2.50 37
Figure 3.15 Variation of the normalized (a) axial forces, (b) shear forces, (c) bending moments of the buried box culvert for the depth ratio of 3.00 38
Figure 3.16 Variation of the normalized (a) axial forces, (b) shear forces, (c) bending moments of the buried box culvert for the soil deposit I 40
Figure 3.17 Variation of the normalized (a) axial forces, (b) shear forces, (c) bending moments of the buried box culvert for the soil deposit II 41
Figure 3.18 The bending moment diagrams of the buried box culvert for the depth ratio of 0.25 for (a) FR=0.125, (b) FR=1.0, (c) FR=8.0, and FR=15.0 44

Figure 3.19 The bending moment diagrams of the buried box culvert for the depth ratio of 0.50 for (a) FR=0.125, (b) FR=1.0, (c) FR=8.0, and FR=15.0 45
Figure 3.20 The bending moment diagrams of the buried box culvert for the depth ratio of 0.75 for (a) FR=0.125, (b) FR=1.0, (c) FR=8.0, and FR=15.0 47
Figure 3.21 The bending moment diagrams of the buried box culvert for the depth ratio of 1.00 for (a) FR=0.125, (b) FR=1.0, (c) FR=8.0, and FR=15.0 48
Figure 3.22 The bending moment diagrams of the buried box culvert for the depth ratio of 1.50 for (a) FR=0.125, (b) FR=1.0, (c) FR=8.0, and FR=15.0 51
Figure 3.23 The bending moment diagrams of the buried box culvert for the depth ratio of 2.00 for (a) FR=0.125, (b) FR=1.0, (c) FR=8.0, and FR=15.0 52
Figure 3.24 The bending moment diagrams of the buried box culvert for the depth ratio of 2.50 for (a) FR=0.125, (b) FR=1.0, (c) FR=8.0, and FR=15.0 53
Figure 3.25 The bending moment diagrams of the buried box culvert for the depth ratio of 3.00 for (a) FR=0.125, (b) FR=1.0, (c) FR=8.0, and FR=15.0 54
Figure 3.26 The variation of the drift ratios for the soil deposits (a) I and (b) II 56
Figure 3.27 The variation of the drift ratios for the depth ratios of (a) 0.25, (b) 0.50, (c) 0.75, (d) 1.00, (e) 1.50, (f) 2.00, (g) 2.50, and (h) 3.00 57
Figure 3.28 The variation of the drift ratios for a constant value of the flexibility ratios for the soil deposits (a) I and (b) II 58
Figure 3.29 The shear strain deformation ratios for the soil deposits (a) I and (b) II ... 60
Figure 3.30 The comparison of the numerical and analytical shear strain deformation ratios 61

LIST OF TABLES

Page

Table 3.1 Mechanical properties of the soil deposits and bedrock 20
Table 3.2 Properties of the Ricker wavelets 22
Table 3.3 PGA, PGV, and PGD of the real-time earthquakes 23

ABSTRACT

INVESTIGATION OF BURIED STRUCTURES UNDER EARTHQUAKE LOADING

Sefa UZUN

Department of Civil Engineering

MSc. Thesis

Adviser: Prof. Dr. Yusuf AYVAZ

The purpose of this study is to investigate the effects of various parameters on the response (i.e., internal forces, drift ratios, and shear strain deformation ratios) of the buried structure under earthquake loading. These parameters are the ground types of the soil deposit, depth ratios, and flexibility ratios. In the analysis, the Finite Element Method is used. The finite element model consists of three parts. The first part is the soil deposit which is modelled with two dimensional plane-strain elements using elastic material. The second part is the buried box culvert which is modelled with frame elements using elastic material. The contact between the soil deposit and buried structure is assumed to be bonded type. The third part is the free-field columns which are modelled with two dimensional plane-strain elements using elastic material. Linear time history analyses are performed in Open System for Earthquake Engineering Simulation (OpenSEES).

The results are illustrated by using Matrix Laboratory (MATLAB) program. It can be concluded that the effects of ground types, depth ratio, and flexibility ratio on the response of the buried box culvert are significant.

Key words: Buried box culvert, buried structures, soil-structure interaction, flexibility ratio, seismic effect

ÖZET

DEPREM ETKİSİNDEKİ GÖMÜLÜ YAPILARIN İNCELENMESİ

Sefa UZUN

İnşaat Mühendisliği Anabilim Dalı

Yüksek Lisans Tezi

Tez Danışmanı: Prof. Dr. Yusuf AYVAZ

Bu çalışmanın amacı deprem etkisi altındaki gömülü yapılara ait iç kuvvetlerin, ötelenmelerin ve kesme gerilmesi deformasyonlarının çeşitli parametrelere göre değişimini incelemektir. İncelenen parametreler zemin tabakasının tipi, gömülü yapının gömülme derinliği ve gömülü yapının zemine göre esneklik oranıdır. Analizlerde Sonlu Elemanlar Yöntemi kullanılmıştır. Sonlu elemanlar modeli üç kısımdan oluşmaktadır; birinci kısım elastik malzeme kullanılarak iki boyutlu dörtgen elemanlar ile modellenen zemin tabakasıdır, ikinci kısım elastik malzeme kullanılarak çerçeve elemanlar ile modellenen gömülü yapıdır, üçüncü kısım ise elastik malzeme kullanılarak iki boyutlu dörtgen elemanlar ile modellenen serbest saha kolonlarıdır. Zemin tabakası ve gömülü yapı birbirlerine bağlı kabul edilerek modellenmiştir. Open System for Earthquake Engineering Simulation (OpenSEES) programı kullanılarak doğrusal dinamik analizler gerçekleştirilmiştir.

Analizler sonucu gömülü kutu menfeze ait elde edilen sonuçlar Matrix Laboratory (MATLAB) programı kullanılarak görselleştirilmiştir. Yapılan çalışma sonucunda zemin tipinin, gömülme derinliğinin ve esneklik oranın gömülü yapının sismik tepkileri üzerinde önemli bir etkiye sahip olduğu görülmektedir.

Anahtar Kelimeler: Gömülü kutu menfez, gömülü yapılar, yapı-zemin etkileşimi, esneklik oranı, sismik etki

CHAPTER 1

INTRODUCTION

1.1 Literature Review

Soil-structure interaction (SSI) is one of the major subjects in the structural and earthquake engineering disciplines. There are a large number of studies about the SSI in the literature.

Dai et al. [1] investigated the effect of SSI and base isolation on the dynamic characteristics of bridge. They used three-dimensional structural model with continuous mass along each member of the model. Also, they used transfer functions to investigate the dynamic behavior of the bridge. They compared the numerical results with real response of the bridge measured previous earthquakes. Their results show that the numerical results are in good agreement with the measured results from the bridge.

Cruz and Miranda [2] investigated the effect of SSI on the damping ratios of the fundamental period of multi-story buildings on an elastic-half space. Their results show that the SSI reduces the effective modal damping ratio of long period buildings, and the SSI increases the effective modal damping ratio of short or medium periods buildings.

Hassani et al. [3] investigated the effect of SSI on inelastic displacement ratios of structure. They used different hysteric models in the numerical analyses. They modeled a number of soil-structure model with different periods. They used a number of strong ground motions as input. Their results show that the SSI increases the inelastic displacement ratios.

Bolisetti et al. [4] investigated the effect of nonlinear SSI on nuclear structures. They performed a lot of numerical analyses in LS-DYNA [5]. They benchmarked nonlinear analyses (time-domain) against linear analyses (frequency-domain). Their results show that the nonlinear response is significantly different from the linear response.

Martakis et al. [6] investigated the effect of soil properties and structural parameters on the SSI. They carried out dynamic centrifuge tests. They compared the experimental results with the analytical results. Their results show that the negligence of the SSI might not be lie on the safe side.

Luco [7] investigated the effects of SSI on the performance of a nonlinear base isolation. He modeled superstructure as single degree of freedom (SDOF) system using elastic material in the analyses. He used nonlinear material to model base isolation. He performed a number of numerical analyses. His results show that SSI effect depends on the viscous damping in the isolator and magnitude of the input motion.

Ghandil and Behnamfar [8] investigated the nonlinear response of moment resisting frames. They considered the SSI effects. They modeled soil domain with equivalent linear model. They performed nonlinear time-history analyses with and without the SSI. They calculated drifts, shear forces, and ductility demands of structure. Their results show that the soil-structure increases the drifts and ductility demands of lower stories. And also, the SSI is playing an important role of calculation of nonlinear response of structures.

von Estorff and Firuziaan [9] investigated the nonlinear soil-structure using coupled Boundary Element Method (BEM)-Finite Element Method (FEM). They also investigated the dynamic inelastic response of structure.

Padrón et al. [10] investigated the dynamic SSI effects on piled structures. They modeled the soil medium with BEM using viscoelastic material. They also modeled the pile using FEM. And, they modeled the superstructure using linear elastic material. Their results show that the dynamic SSI is playing an important role for the calculation of the response of structure.

Abascal [11] investigated the SSI effects on shallow and deep foundations. He performed a number of analyses. His results show that consideration of nonlinear friction between the foundation and surrounding soil is important.

Guarracino et al. [12] investigated the SSI using simple coupled BEM-FEM methodology. They modeled the soil medium to be elastic half-space.

Karabalis [13] investigated the SSI using simple 3D BEM. He performed a number of linear elasto-dynamic analyses in the time domain. He compared his results with the results of previous studies. His results are in good agreement with the results of previous studies.

Galvin and Romero [14] developed a toolbox for investigation of SSI using MATLAB [15]. They used the 3D coupled FEM-BEM to model the soil medium.

Yeganeh et al. [16] investigated the response of high-rise buildings built near the deep excavation. They took the SSI into account.

Livaoğlu [17] investigated the dynamic response of tall slender structures such as chimneys. He also investigated the effects of pile foundation on response of the chimneys. He took the SSI in to account in the numerical analyses.

Rahnema et al. [18] investigated the SSI effects on reinforced concrete frames using scaled-boundary finite element method. They modeled the soil medium using nonlinear materials with different densities. They performed a number of analyses in the time-domain. Their results are verified with the results of previous studies.

Durmuş and Livaoğlu [19] investigated the dynamic response of a silo system considered the SSI. They performed a number of analyses using FEM. They compared the SDOF results with the FEM results. Their results show that the SSI does not affect the response of the squat silos considerably and for this reason the SSI is not necessary to be taken into account in the practice.

Kim et al. [20] proposed the boundary reaction method to investigate the nonlinear SSI. They also verified the boundary reaction method using equivalent linear analyses results including the SSI effects. They investigated the dynamic response of nuclear power plant using boundary reaction method. Their results show that the proposed method is very effective for the nonlinear SSI.

Li et al. [21] investigated the response of cable-stayed bridges in the different sites considering the SSI. Their results show that the soil-structure interaction affects the response of cable-stayed bridges.

Shakib and Fuladgar [22] investigated response of asymmetric buildings considering the SSI. They idealized the asymmetric buildings as a three-dimensional single-story structure. They modeled the soil medium and the superstructure using linear elastic materials. Their results show that the soil-structure effects reduce the lateral and torsional displacements.

Spyrakos et al. [23] investigated the base-isolated structures considering the SSI. They modeled the soil medium to be elastic half-space. They performed a number of analyses

in frequency domain. Their results show that effects of the SSI on system damping is very little. And also, the SSI affects the modal properties of the structure.

Burman et al. [24] investigated the effect of SSI on the response of the concrete gravity dam. They modeled the soil medium and the concrete dam using linear elastic material with two-dimensional plane-strain elements.

Liang et al. [25] investigated the effect of soil conditions on the SSI. They modeled domain with two-dimensional (2D) plain-strain elements. They compared the results of numerical analyses with the theorical results. Their results show that the numerical results are in good agreement with the theorical results.

Yazdchi et al. [26] investigated the response of structures considering the SSI. They performed a number of time history analyses with coupled FEM-BEM technique. They modeled the soil medium to be elastic half-space. Their results show that presence of foundation affects the response of structure.

Haroun and Temraz [27] investigated the response of elevated tanks considering the SSI. They evaluated the static, dynamic elastic, and dynamic inelastic response of the tanks.

Carbonari et al. [28] investigated reinforced concrete frames resting on monopile and double pile foundations. They took the SSI into account. They performed the numerical analyses using different nonlinear soil materials. Their results show that the reinforced concrete frames on the monopile foundation are strongly affected from the SSI.

Haiyang et al. [29] investigated the response of the base-isolated structures using shaking table tests. They took the SSI into account. Their results show that the SSI affects the damping ratio, rotation of foundation and acceleration magnification factor.

Sáez et al. [30] investigated the influence of SSI on the moment resisting frames. They modeled the soil medium and the structure using inelastic material. Their results show that the SSI affects the response of the structure.

Zangeneh et al. [31] investigated the response of a portal frame railway bridges. They carried out dynamic tests on the railway bridges. They used the test results to validate FEM model. They performed a number of finite element analyses. Their results show that the SSI effects are playing a crucial role on the response of the portal frame.

Seo et al. [32] developed five different three-dimensional infinite elements to consider SSI. Proposed elements can be used for the multi-wave propagation problem. They

performed a number of analyses to test the infinite elements. Their results show that proposed infinite elements are very effective.

Küçükarslan et al. [33] investigated inelastic pile-SSI. They modeled piles and structural elements as linear finite elements and they modeled the soil medium to be inelastic.

Koçak and Mengi [34] proposed a simple three-dimensional SSI model. They developed a general program code to analyze static SSI. They performed four examples and they compared their results with other methods. Result of comparison shows that proposed model can be used reliably in SSI.

As mentioned in the abstract, buried structures are investigated in this study. The buried structures are a major part of civil infrastructure. They serve as transportation facilities, storage places, water supply, waste water disposal systems, etc. Recent earthquakes denoted that the buried structures are under great earthquake induced risk. Those structures can be constructed at different depths. Design of buried structures is based on both static and dynamic loadings. Dynamic SSI should be considered to take the seismic effects into account. Thus, during Finite Element analyses, interactive models should be created. There are a large number of studies on design and analysis of buried structures.

Cilingir and Madabhushi [35] investigated the effects of input motion on seismic behavior of circular and square tunnels. They carried out dynamic centrifuge tests. They used input motions whose amplitude and frequency are different. They measured accelerations and earth pressures around the tunnel. Additionally, they performed finite element analyses with different input motions. Their results show that the magnitude of the input motion plays a crucial role on lining forces.

Chen et al. [36] investigated the effects of isolation layer around the tunnel and the cross-section of the tunnel on the bending moment. The isolation layer is consisting of a rubber wrapped around the tunnel. They carried out dynamic centrifuge tests. Their results show that the isolation layer decreases the dynamic bending moments on the lining. And also, the isolation layer prevents deformation of the lining. Nevertheless, when the cross-section of the tunnel increases, then the dynamic bending moments increase. Additionally, for the same isolation layer thickness, the tunnel which has the smaller cross-section is more effective for the reducing of structural response.

Ma et al. [37] investigated the effects of burial depth on seismic response of underground structures. They performed three dimensional (3D) finite element analyses. They used 3D

constitutive elasto-plastic soil model in finite element analyses. They took in consideration of the stresses around the underground structure and surrounding soil which are occurred before earthquakes in detail. They used multiple ground motions in finite element analyses. Their results show that when the buried depth increases, the seismic response of the underground structure decreases.

Sandoval and Bobet [38] investigated the effects of the input frequency and flexibility ratio on seismic response and distortion of the tunnels. They used Fast Lagrangian Analysis of Continua (FLAC) [39] to perform two-dimensional (2D) analyses. They used linear-elastic and nonlinear material for the analyses. Their results show that the input frequency does not affect the seismic response of the tunnel for both linear-elastic and nonlinear materials. Additionally, distortions of the tunnel increase with increasing flexibility ratio for both linear-elastic and nonlinear materials.

Shahrour et al. [40] investigated the effects of plasticity and soil dilatancy on seismic response of tunnels which are buried in soft soil. They modeled a circular tunnel with linear-elastic material properties. They modeled soil medium with two-dimensional eight-node elements. They used elastoplastic material for the soil medium. They used acceleration time history as input motion. The frequency of the input motion is close to the fundamental frequency of the soil medium. Their results show that the plastic deformations reduce seismic amplification. Thus, the reduction of the seismic amplification decreases the bending moment in the tunnel. Additionally, the soil dilatancy influences the vertical displacements in the soil medium but does not affect the bending moment.

Abdel-Motaal et al. [41] investigated seismic interaction between the tunnel and surrounding soil. Additionally, they investigated the effects of lining thickness and burial depth. The soil is granular dry soil. The relative density of the soil is varying from 25% to 90%. The diameter of the tunnel is varying from 6 m to 10 m. They modeled soil medium with two-dimensional plane-strain four-noded elements. They performed nonlinear dynamic analyses. They considered the full seismic interaction between tunnel and surrounding soil. They used artificial earthquake time histories as input motion. Their results show that the bending moments increase with increasing burial depth. Additionally, when the relative stiffness increases, then the bending moments in the lining section increase.

Tsinidis et al. [42] investigated the seismic response of the square tunnels which are embedded in sandy soil. They carried out the centrifuge tests and performed numerical analyses. They compared the numerical results with the experimental results. Then, they improved the numerical model according to the test results. They used different soils and soil-tunnel interface in the numerical analyses. They used the validated numerical model to investigate the effects of lining rigidity on the response of the tunnel. They performed 3D and 2D analyses to obtain optimal finite element model. After these analyses, they decided that the optimal model would be 2D finite element model. They used elastic and elasto-plastic properties for the soil medium. They modeled the lining with elastic-perfectly plastic material. Their results show that the racking distortion decreases with increasing lining rigidity. Additionally, properties of the soil-tunnel interface affect the dynamic axial force of the lining.

Tsinidis [43] investigated dynamic lining forces, the dynamic earth pressures, and the soil dynamic shear stresses developed around the rectangular tunnel. He used two different soil types in the analyses (i.e., Soil types B and C according to Eurocode 8 [44]). He used visco-elastic material for the soil medium and modeled with two-dimensional plane-strain quadrilateral elements. He used linear elastic material for the rectangular tunnel. He also used different burial depths and cross-sections of the rectangular tunnel in the analyses. He performed nonlinear finite element analyses. His results show that the racking ratios increase with increasing burial depth. And, the distribution of the dynamic earth pressures is different from each other for the elastic and elasto-plastic analyses. And also, the interface properties between the tunnel and surrounding soil affect the soil dynamic shear stresses and dynamic lining forces.

Tsinidis et al. [45] investigated the dynamic of the soil-tunnel systems. They carried out dynamic centrifuge tests. They used tests result to validate the finite element model. They used visco-elastic dry sand whose relative density is 70% as soil material. They used linear elastic material for the tunnel. They modeled the soil medium with two-dimensional plane-strain elements. They modeled the tunnel with beam elements. They performed time history analyses in ABAQUS [46]. Their results show that results obtained from the analyses are coincide the recorded results from the dynamic centrifuge tests.

Baziar et al. [47] investigated the effect of flexibility ratio of box-shaped tunnel on the ground surface acceleration. They carried out the dynamic centrifuge tests. They used the

tests results to validate numerical model. They used silicate sand whose relative density is 84%. They used Kobe and Northridge earthquakes as input motion for the dynamic centrifuge tests. They modeled the soil medium with two-dimensional plane-strain elements in the FLAC [39]. They modeled the tunnel with elastic beam elements. Additionally, they modeled the interface between the tunnel and surrounding using the interface elements with Mohr-Coulomb [48] failure criterion. They performed nonlinear analyses in the FLAC [39]. The response of the ground surface is dependent on the frequency content of the input motion. The amplification of acceleration at the ground surface decreases with increasing flexibility ratio.

Abuhajar et al. [49] investigated the seismic response of box culvert with experimentally and numerically. They carried out a number of centrifuge tests. They used earthquake records which have different amplitudes and frequencies in the centrifuge tests. They considered different thicknesses and relative densities in the tests. They presented experimental results in terms of comparisons of bending moments. They used tests results to validate numerical model. They used finite element model to investigate the effects of intensity and frequency of the earthquake, embedment depth, and thickness of the box culvert on the bending moment. They modeled the soil medium using two-dimensional plane-strain elements with nonlinear elastic-plastic material. They modeled the box culvert using frame elements with linear elastic material. Additionally, they modeled the interface between the box culvert and surrounding soil using interface elements in FLAC [39]. Subsequently, they performed a number of analyses in the FLAC [39]. Their results show that the bending moment increases with increasing peak ground acceleration (PGA) of the input motion and increasing thickness of the box culvert. The bending moment values are high at the edges of the top slab and corners of the side wall.

Liu and Song [50] investigated the effects of vertical earthquake motions and embedment depth on underground structures. They modeled the soil deposit using two-dimensional plane-strain quadrilateral elements with loose Nevada sand. They modeled the underground structures using Mindlin beam [51] element with linear elastic material. They performed a number of analyses in the finite element code DYNA Swandyne-II [52]. The numerical results show that the maximum internal forces at the structural members occurred at the connections, center columns and edges. And, the effect of vertical motion is depended on characteristic of the input motion. Additionally, when the embedment depth increases, then safety of the underground structure increases.

Ertugrul [53] investigated the dynamic behavior of the box culvert. He modeled the soil deposit using two-dimensional plane-strain quadrilateral elements with homogeneous isotropic elastic-plastic material. He modeled the box culvert using beam-column elements with linear elastic material. He validated the numerical model using previous dynamic centrifuge tests. He performed a number of analyses in FLAC [39]. The numerical results show that the dynamic forces decrease with increasing flexibility ratio.

Rahai [54] investigated the buried box culvert at different depths. He modeled the soil medium using two-dimensional plane-strain elements. He used Drucker-Prager [55] elasto-plastic model to study nonlinear behavior of the soil medium. He used three different sandy soil in the analyses. He performed linear and nonlinear analyses. His results show that tangential stresses on the top and bottom slab of the box culvert increase with decreasing rigidity of the box culvert. Additionally, the tangential stresses obtained from nonlinear analysis on the top slab of the box culvert is higher than the tangential stresses obtained from the linear analyses. Furthermore, the vertical pressures on the walls of the box culvert decrease with decreasing rigidity of the box culvert.

Hatzigeorgiou and Beskos [56] investigated inelastic response of the underground structures such as tunnels. He modeled the soil medium with finite element method. And also, he modeled concrete liner with boundary element method. He used soft rock material properties for the soil medium. And, he used fiber-reinforced concrete material properties for the concrete liner. His results show that the behaviors of the soil medium and underground structure are inelastic.

Akhlaghi and Nikkar [57] investigated the effect of propagation of vertical shear waves on the seismic behavior of circular tunnels. They performed dynamic nonlinear analyses in FLAC [39]. And also, they solved the problem with different analytical methods. They compared numerical results with analytical results. Their results show that the maximum bending moments are obtained from the numerical analyses. And, the differences of axial forces between the numerical analyses and analytical methods are less.

Katona [58] investigated the buried culverts and cut-and-cover culverts. He modeled the soil medium using two-dimensional plane-strain elements. He divided his study into two parts. In the first part, he investigated circular and rectangular culvert with linear-elastic material. He performed a number of analyses in CANDE-2007 [59]. And, he compared numerical results with closed-form solutions. In the second part, he investigated a

nonlinear reinforced box culvert. He used combination of static and seismic loading in the analyses. And also, he plotted internal forces obtained from the numerical analyses. Subsequently, he suggested a method to analyze and evaluate culverts.

Hushmand et al. [60] investigated the effects of structure stiffness and input motion properties on the seismic response of the buried structures. They performed three dynamic centrifuge tests. They used medium dense dry sand in the centrifuge tests. Their results show that the confining pressure in the soil and flexural rigidity affect the acceleration response of the buried box structure. And also, at the time of the maximum thrust, then dynamic bending moment increase with increasing flexural stiffness of the buried box structure.

Nam et al. [61] investigated the effects of stiffness and interface properties on the behavior of reinforced concrete underground structures. They used Ohsaki [62] soil model for modelling of the soil medium. And, they used elasto-plastic interface elements between the underground structure and surrounding soil. They performed a number of both static and dynamic analyses to investigate the behavior of the underground structure. Their results show that the shear capacity and the ductility of the reinforced concrete underground structures play an important role in the design of the underground structures.

Awwad et al. [63] investigated the behavior of the precast concrete box culvert under different loading conditions. They used different span lengths for culvert in the analyses. And also, they used different soil covers for culvert in the analyses. They modeled the culvert using shell elements. They performed a number of analyses in SAP2000 [64].

Pimentel et al. [65] investigated the behavior of the box culvert with numerical and experimental studies. They modeled the soil medium and interface to behave to be elasto-plastic. And, they modeled the box culvert using nonlinear reinforced concrete material. They presented that the numerical results are in good harmony with the experimental results. Their results show that soil pressures and nonlinear behavior of the box culvert are directly interconnected the design of the box culvert. And, the soil pressures and nonlinear behavior of the box culvert should be taken into consideration to achieve the economical and more rational design.

Tsinidis [66] investigated the effects of various parameters on the seismic response of the circular tunnels embedded in clayey soil near the urban areas. The parameters he investigated are burial depth of the circular tunnels, number of high-rise buildings and

their position relative to axis of the circular tunnels, and soil properties. He modeled the soil deposit using two-dimensional plane-strain quadrilateral elements with visco-elastic material. And, he also modeled the tunnel lining and high-rise buildings as linear-elastic. He performed a number of numerical simulations in ABAQUS [46]. The numerical results show that dynamic shear stresses and the dynamic lining forces increase with increasing flexibility ratio as well as with decreasing the burial depth of the tunnel. Additionally, the presence of the high-rise buildings increases the response of the tunnel.

Pitilakis et al. [67] investigated the seismic behavior of the circular tunnels with respect to various parameters. The parameters they investigated are soil to tunnel relative flexibility, tunnel dimensions, burial depth of the tunnels, and the soil nonlinearities. They used two different sandy soil deposits in the analyses. They modeled the soil deposits using two-dimensional plane-strain elements. And, they used linear visco-elastic and elasto-plastic material in the analyses. And also, they assumed that the tunnel and surrounding soil are linked with a solid connection. They used linear elastic material for modelling the tunnel and aboveground structures. They performed a number of analyses in ADINA [68]. They compared numerical results with closed-form solutions. The results indicate that the presence of the aboveground structures increases the response of the circular tunnels in terms of deformations and lining forces.

Seylabi et al. [69] investigated the capabilities of the equivalent soil model. They carried out the dynamic centrifuge tests. They used the dynamic centrifuge tests for validating the numerical model. And, they used equivalent linear soil model for modelling the soil deposits. They presented that the numerical results are in good harmony with the experimental results for the high amplitude base motion.

Abuhajar et al. [70] investigated the SSI between the culvert, soil, and the surface foundation. They performed the dynamic centrifuge tests. They used three input motions with different amplitude and frequency. They used the experimental results for calibrating the numerical model. They modeled the soil deposit using the plane-strain elements with the nonlinear elastic-plastic material. And, they modeled the tunnel using structural elements with the linear elastic material. They presented that the numerical results are in good harmony with the experimental results.

Penzien (2000) [71] suggested a formula to calculate shear strain deformation ratio. The shear strain deformation ratio, *R*, can be calculated by using the following equation.

$$R = \left[\frac{4(1-\nu)}{1+\frac{(3-4\nu)\, f_s}{f_{st}}} \right] \tag{1.1}$$

where, ν is the Poisson's ratio of the soil, f_{st} is the shear flexibility of the buried box culvert without soil interaction and f_s is the shear flexibility of the soil block with the same dimensions as the buried box culvert.

Nishioka and Unjoh (2002) [72] suggested a formula to calculate shear strain deformation ratio. The shear strain deformation ratio, *R*, can be calculated by using the following equation.

$$R = \frac{2FR}{FR+1} \tag{1.2}$$

where, *FR* is the flexibility ratio.

Wang (1993) [73] suggested a formula to calculate shear strain deformation ratio. The shear strain deformation ratio, *R*, can be calculated by using the following equation.

$$R = \frac{8FR(1-\nu)}{2FR+5-6\nu} \tag{1.3}$$

where, ν is the Poisson's ratio of the soil and *FR* is the flexibility ratio.

1.2 Objective of the Thesis

The purpose of the thesis is to investigate the effects of various parameters on the response of buried structure under earthquake loading. These parameters are the burial depth, ground type of soil deposit, and flexibility ratio. The investigated seismic response of buried structure are the internal forces, drift ratios, and shear-strain deformation ratios. A number of analyses are performed in Open System for Earthquake Engineering Simulation (OpenSEES) [74]. Analyses results are illustrated by using Matrix Laboratory (MATLAB) [15] program.

1.3 Hypothesis

It is impossible to model many systems as in the nature. Therefore, the assumptions are used to model the systems to be almost same with the nature. So, there are three assumptions made in this study. The first assumption is that the soil layer is assumed to be infinitely long in the horizontal direction. The second assumption is that the soil layer and buried box culvert are bonded together. Lastly, the mechanical properties of the soil layer are the same at any points of the soil medium.

There are many expected results in this study. Firstly, it is expected that the internal forces increase with increasing depth ratio. Secondly, it is expected that the bending moments decrease with increasing flexibility ratio. Thirdly, it is expected that the drift ratios increase with increasing depth ratio.

CHAPTER 2

MODELING AND METHODOLOGY

Different FEM models can be used to model the soil medium. The most used three FEM models will be explained in this chapter. Dimensions and boundary conditions of the FEM model I are given in Figure 2.1 [43]. As seen from Figure 2.1, nodes on the both sides of the FEM model share equal degree of freedoms (DOFs) in the X and Y directions. The nodes on the base of the FEM model share equal DOF with lower-left node of the FEM model in the X direction. The nodes on the base of the FEM model are fixed in the Y direction. A viscous damper (Lysmer-Kuhlemeyer dashpot) [75] is used between the nodes A and B. Velocity histories are used as input motions at the lower-left node of the FEM model (i.e., node B in Figure 2.1). As also seen from Figure 2.1, H and W represent height and width of the FEM model, respectively. Also, h and w represent the width and height of the buried structure, respectively.

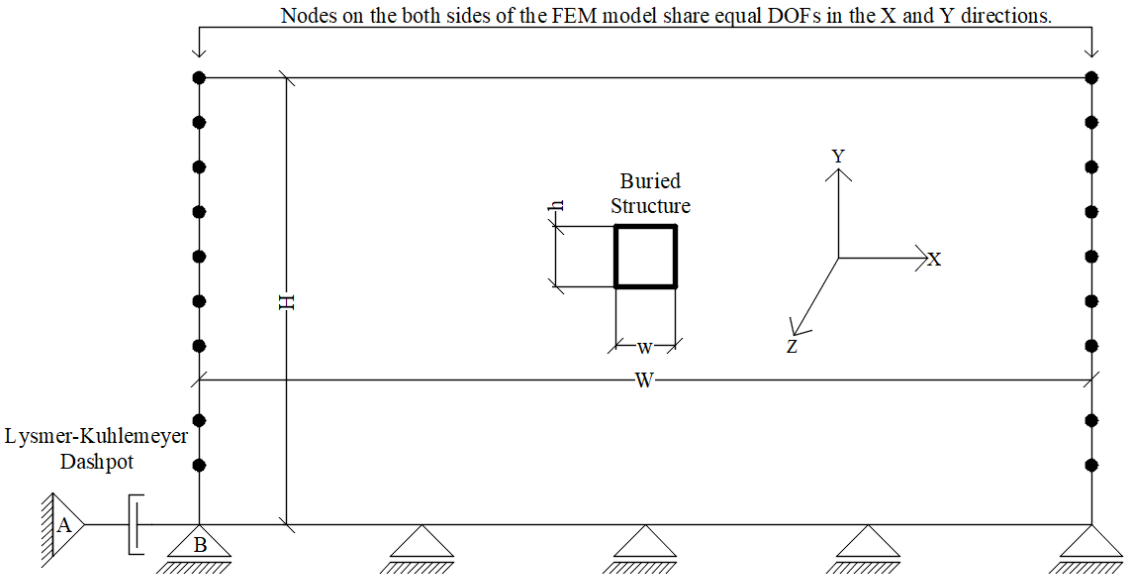


Figure 2.1 Dimensions and boundary conditions of the FEM model I

The dimensions and boundary conditions of the FEM model II are given in Figure 2.2 [24]. As seen from Figure 2.2, the viscous dampers (Lysmer-Kuhlemeyer dashpot) [75] are used on the left-hand and the right-hand sides of the FEM model. The nodes on the base of the FEM model share equal DOF with lower-left node of the FEM model in the X direction. The nodes on the base of the FEM model are fixed in the Y direction. Velocity histories are used as input motions at the lower-left node of the FEM model (i.e., node A in Figure 2.2). As also seen from Figure 2.2, H and W represent height and width of the FEM model, respectively. Also, h and w represent the width and height of the buried structure, respectively.

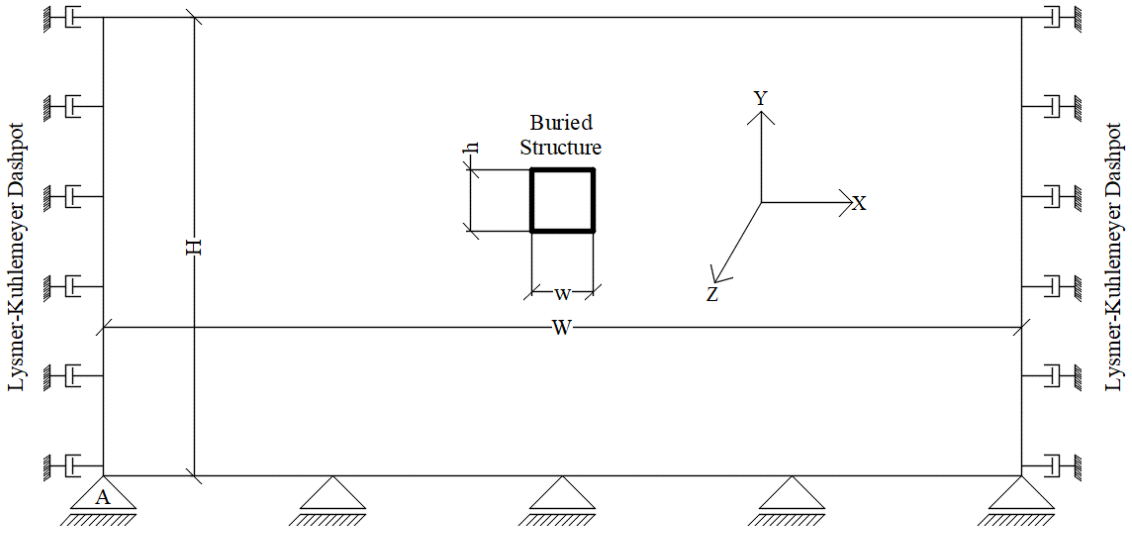


Figure 2.2 The dimensions and boundary conditions of the FEM model II

The dimensions of the FEM model III are given in Figure 2.3 [76]. The FEM model is consisting of three parts. The first part is the soil deposit which is modeled using the two-dimensional plane-strain quadrilateral elements. The second part is the buried box culvert which is modeled by using frame elements. Contact properties between soil and frame elements are assumed to be bonded type. The bonded contact between the soil and the buried box culvert is modeled using equal DOF in OpenSEES. The third part is the free-field columns which are modeled using the two-dimensional plane-strain quadrilateral elements. The free-field columns are added to the left-hand and the right-hand sides of the FEM model to assure periodic boundary conditions (PBC). PBCs are used for modeling infinite media as finite media.

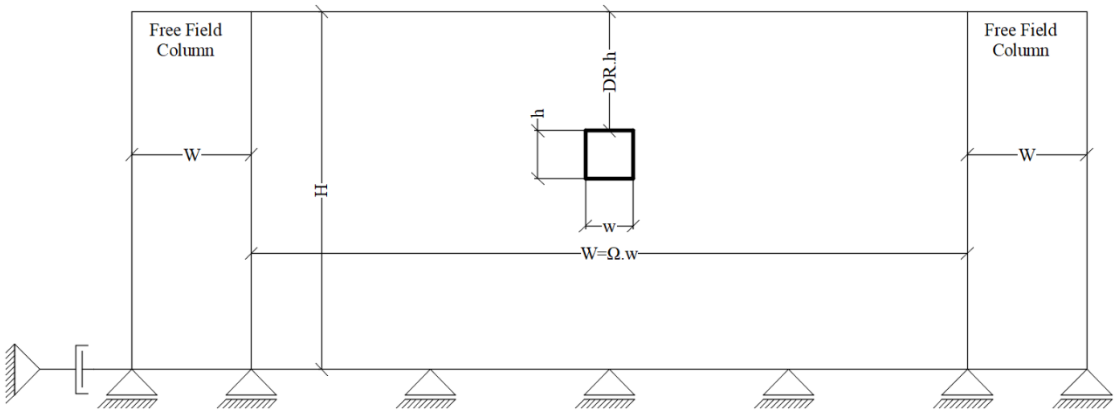


Figure 2.3 The dimensions of the FEM model III

The width of the soil deposit is calculated by using Equation 2.1 as follows;

$$W = \Omega.w \tag{2.1}$$

where, *W*, Ω, and *w* are the width of the soil deposit, model width ratio, and width of the buried box culvert, respectively. As seen from Figure 2.3, H represents the height of the soil deposit. It is assumed that the width of the free-field columns is the same the width of the soil deposit.

The model width ratio, Ω, is determined as a result of lots of analyses performed in OpenSEES. Firstly, the initial value for the model width ratio has to be selected. The initial value can be selected as 10 or greater. Then, the FEM model created by using the selected model width ratio is analyzed in OpenSEES. This process is repeated for increasing values of the model width ratio. Graphs of the model width ratio and absolute maximum ground surface displacement are drawn by using analyses results. Changes in absolute maximum surface displacement are negligible after a certain value of the model width ratio. This value can be selected as the model width ratio.

Boundary conditions of the FEM model are shown in Figure 2.4 [77]. Nodes on both sides of the free-field columns except the nodes on the base of the FEM model share equal DOF in the X and Y directions. The nodes at the base of the FEM model share equal DOF in the X direction with lower-left node of the FEM model (node 1, see in Figure 2.4). The node 1, node A and node B are in the same location. The node A is fixed in the X and Y directions.

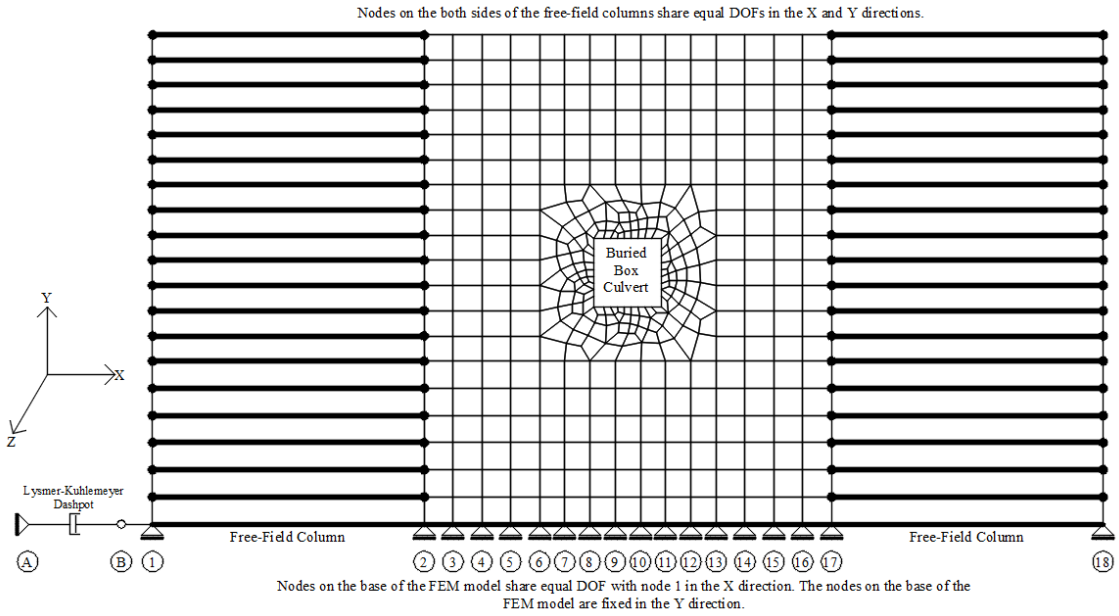


Figure 2.4 Boundary conditions of the FEM model III

Also, the node A share equal DOF with node 1 in the X and Y directions. A viscous damper (Lysmer-Kuhlemeyer dashpot) [75] is used between the node A and the node B. The viscous damper coefficient can be calculated by using Equation 2.2 as follows;

$$C = \rho.A.V_{bedrock} \tag{2.2}$$

where A is the base area of the FEM model, $V_{bedrock}$ is the shear velocity of the bedrock, ρ is the mass density of the bedrock.

Velocity histories are used as input motions at the lower-left node of the left free-field column of the FEM model (i.e., node 1 in Figure 2.4). The FEM model III is used as FEM model in this study.

CHAPTER 3

PARAMETRIC STUDY

3.1 Parameters in This Study

Three parameters are used in this study. The first parameter is the depth ratio which is the ratio of the cover depth of the buried box culvert to the height of the buried box culvert. The depth ratios that are used in the analyses are 0.25, 0.50, 0.75, 1.00, 1.50, 2.00, 2.50 and 3.0.

The second parameter is the flexibility ratio which is the ratio of the shear flexibility of the buried box culvert without soil interaction to the shear flexibility of soil block with the same dimensions as the buried box culvert. The flexibility ratio, *FR*, can be calculated by using the following equation [78].

$$FR = \frac{f_{st}}{f_s} \tag{3.1}$$

where, f_{st} is the shear flexibility of the buried box culvert without soil interaction and f_s is the shear flexibility of the soil block with the same dimensions as the buried box culvert. The shear flexibility of the square buried box culvert without soil interaction, f_{st}, can be calculated by using the following equation [78].

$$f_{st} = \frac{h^2}{12K} \tag{3.2}$$

where, h is the height of the buried box culvert (see Figure 2.3) and *K* is the stiffness of the wall or roof of the buried box culvert. *K* can be calculated by using the following equation [78].

$$K = \frac{EI}{h} \tag{3.3}$$

where E is the Young's Modulus of the buried box culvert and I is the moment of inertia about the Z-axis (see Figure 2.3) of the wall or roof of the buried box culvert.

The shear flexibility of the soil block with the same dimensions as the buried box culvert, f_s, can be calculated by using the following equation [78].

$$f_s = \frac{h}{wG} \tag{3.4}$$

where w is the width of the soil block and G is the shear modulus of the soil block. If Equation (3.4) is substituted into Equation (3.1), Equation (3.1) can be re-written in the following form.

$$FR = \frac{f_{st}}{f_s} = \frac{wGh^2}{12EI} \tag{3.5}$$

The modulus of elasticity of the buried box culvert can be calculated by arithmetic manipulation from Equation (3.5), it can be calculated by using the following equation [38, 78].

$$E = \frac{wGh^2}{12IFR} \tag{3.6}$$

If the flexibility ratio is smaller than 1, the buried box culvert will be stiffer than the soil deposit. If the flexibility ratio is 1.0, the stiffness of the buried box culvert is the same with the stiffness of the soil deposit. On the other hand, if the flexibility ratio is greater than 1.0, the buried box culvert is more flexible than the soil deposit. The flexibility ratios that are used in the analyses are 0.125, 0.25, 0.50, 1, 2, 3, 4, 5, 6, 7, 8, 9, 10, 11, 12, 13, 14, and 15.

The third parameter is the ground type of the soil deposit. Two soil deposits are investigated in this study. The first soil deposit which is assumed to be soil type B according to Eurocode 8 [44]. The second soil deposit which is assumed to be soil type C according to Eurocode 8 [44]. Mechanical properties of the investigated soil deposits and bedrock are given in Table 3.1 [79]. It is also assumed that the height of the FEM model is to be 40 m [79]. The first fundamental frequencies of the investigated soil deposits are 2.50 Hz and 1.5625 Hz, respectively [80, 81].

Table 3.1 Mechanical properties of the soil deposits and bedrock

	Shear Wave Velocity, Vs (m/sec)	Poisson's Ratio (ν)	Mass Density, ρ (ton/m^3)
Soil Deposit I (Soil Type B)	400	0.3	1.90
Soil Deposit II (Soil Type C)	250	0.3	1.80
Bedrock	1000	0.3	2.20

The maximum edge lengths of the quadrilateral elements are 2 meters and 1 meter for the soil deposit I and II, respectively. The maximum edge length of the quadrilateral elements is determined according to the frequency content of the input motion and the shear wave velocity of the soil deposit.

3.2 The Buried Box Culvert

The square buried box culvert is used in the analyses. The dimensions of the buried box culvert used in the analyses are illustrated in Figure 3.1. As seen from Figure 3.1 as also mentioned before, h, w, and t represent the height of the buried box culvert, the width of the buried box culvert and the thickness of the buried box culvert, respectively. The height of the buried box culvert is equal to the width of the buried box culvert in this study. The height and width of the buried box culvert are 5 meters and the thickness of the buried box culvert is 0.50 meters [78]. As also seen from Figure 3.1, the corners of the buried box culvert are represented by the letter A, B, C, and D, respectively.

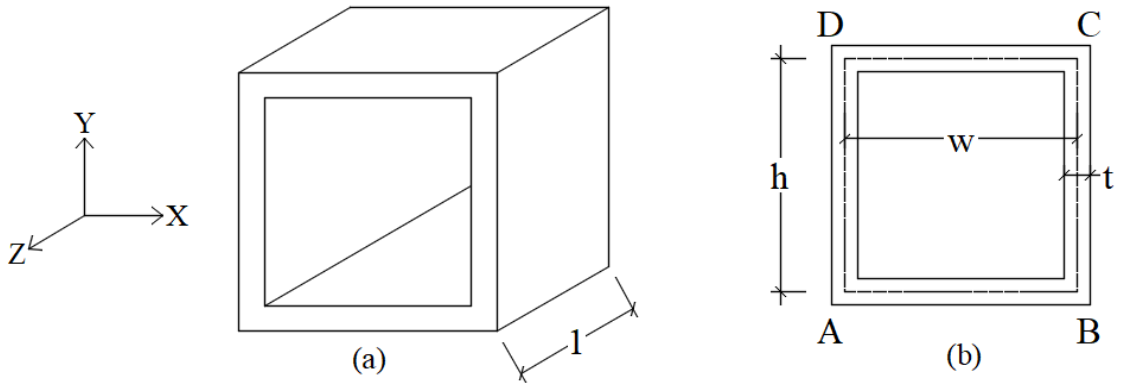


Figure 3.1 (a) 3D view and (b) dimensions of the buried box culvert

The buried box culvert is modeled with frame elements. The length of a frame element is 0.50 meters. The moment of inertia of the frame elements about the Z axis is 0.01042 m^4. The cross-section area of the frame elements is 0.50 m^2. The mass density of the frame elements is 2.50 ton/m^3. The elastic modulus of the frames elements is calculated by using Equation 3.6.

3.3 Input Motion

The input motions must be generated for numerical analyses (i.e., the determination of the model width ratio). Velocity histories are used as input motion. Ricker wavelet formula is used for the generation of the velocity histories. The velocity histories are generated in two steps. In the first step, the acceleration histories are generated with the Ricker wavelet formula. Subsequently, the velocity histories are derived from the acceleration histories. Two acceleration histories are generated with Ricker wavelet formula for the determination of the model width ratio. Time steps of the Ricker wavelets are 0.005 seconds [76]. And, the durations of the Ricker wavelets are 2 seconds. And also, the amplitude of the Ricker wavelets is selected to be 0.3 g [67]. On the other hand, the dominant frequencies of the Ricker wavelets are different. The dominant frequencies of the Ricker wavelets are selected to be equal to the fundamental frequencies of the soil deposits, because resonance occurs in the soil deposits. Thus, the maximum effects may be observed from the analyses. The properties of the Ricker wavelets are given in Table 3.2. The Ricker wavelet I is used to determining the width of the soil deposit I. And, the Ricker wavelet II is used to determine the width of the soil deposit II. The reason for the selection of the Ricker wavelet is to avoid dependency of a real-time history. Displacement response spectrums of the real-time accelerograms and the displacement response spectrum of the Ricker wavelet I are shown in Figure 3.2. As seen from Figure 3.2, Loma Prieta earthquake has the maximum displacement response spectrum. The displacement response spectrums of the real-time accelerograms and the displacement response spectrum of the Ricker wavelet II are shown in Figure 3.3. As seen from Figure 3.3, the Loma Prieta earthquake has the maximum displacement response spectrum. The peak ground acceleration (PGA), peak ground velocity (PGV), and peak ground displacement (PGD) of the real-time earthquakes which are used for calculation of the displacement response spectrums are given in Table 3.3. The peak ground acceleration (PGA) of the real-time earthquake records are normalized to be 0.30 g [67].

Table 3.2 Properties of the Ricker wavelets

Motion	Amplitude	Dominant Frequency (Hz)	Time Step (sec)	Duration (sec)
Ricker wavelet I	0.3g	2.50	0.005	2
Ricker wavelet II	0.3g	1.5625	0.005	2

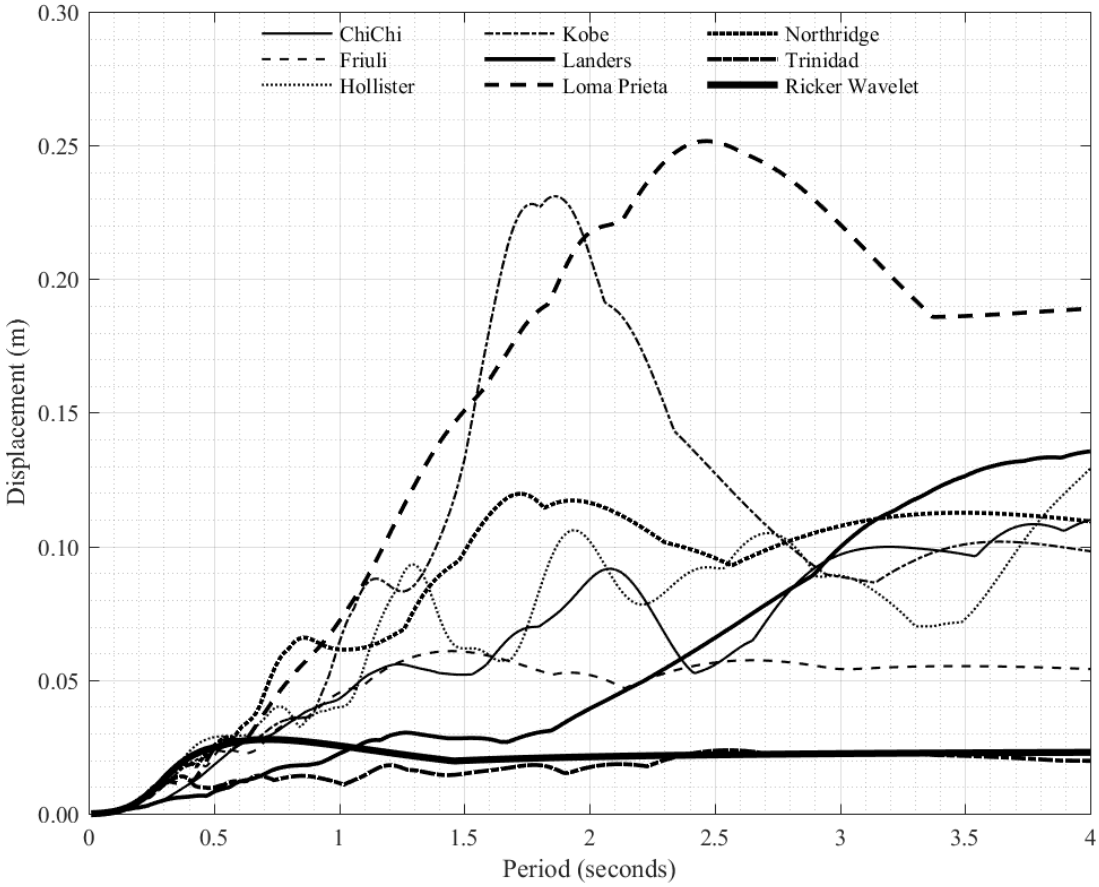


Figure 3.2 Displacement response spectrums of the real-time earthquakes and the Ricker wavelet I

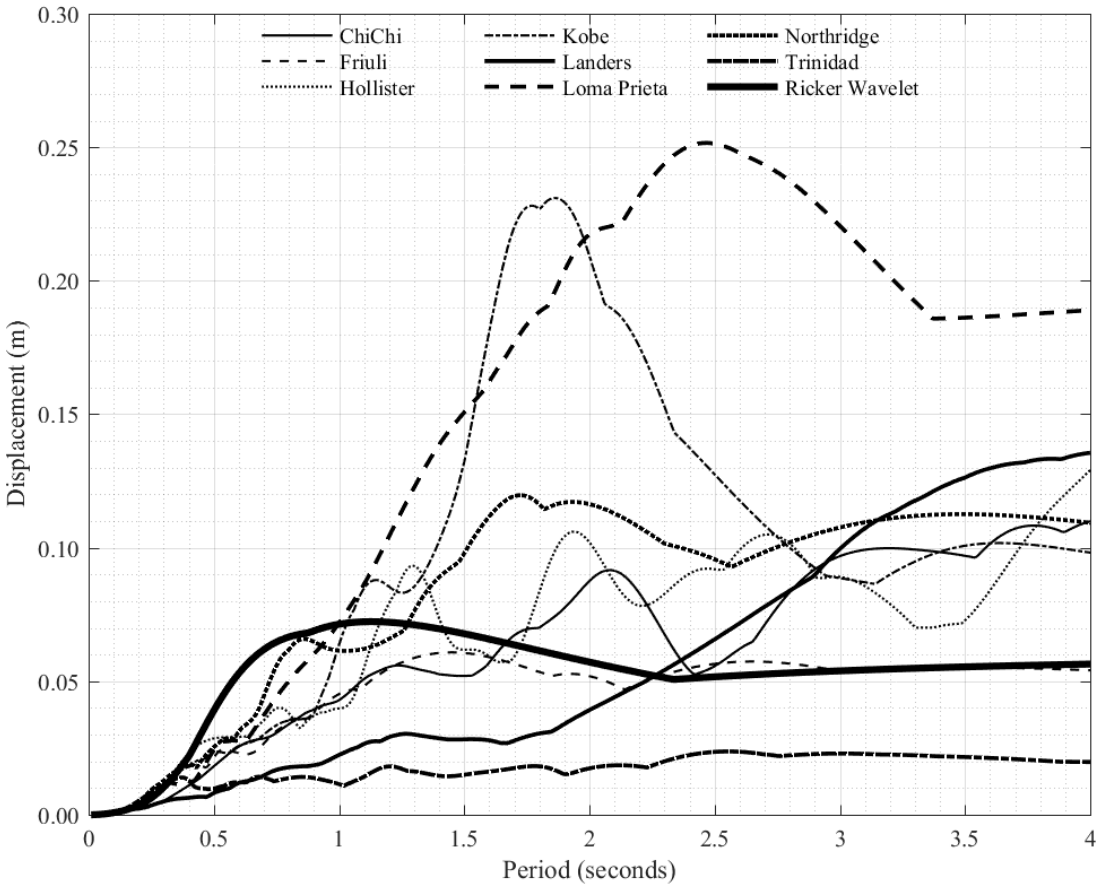


Figure 3.3 Displacement response spectrums of the real-time earthquakes and the Ricker wavelet II

Table 3.3 PGA, PGV, and PGD of the real-time earthquakes

Earthquake	**PGA (g)**	**PGV (m/sec)**	**PGD (m)**
Chi Chi	0.361	0.215	0.219
Friuli	0.351	0.220	0.041
Hollister	0.195	0.124	0.043
Kobe	0.345	0.277	0.097
Landers	0.780	0.316	0.165
Loma Prieta	0.367	0.447	0.196
Northridge	0.568	0.518	0.090
Trinidad	0.194	0.085	0.009
Maximum	**0.780**	**0.518**	**0.219**

Acceleration history, velocity history and Fast Fourier Transform (FFT) of the acceleration history for the Ricker wavelet I and the Ricker wavelet II are illustrated in Figure 3.4 and in Figure 3.5, respectively.

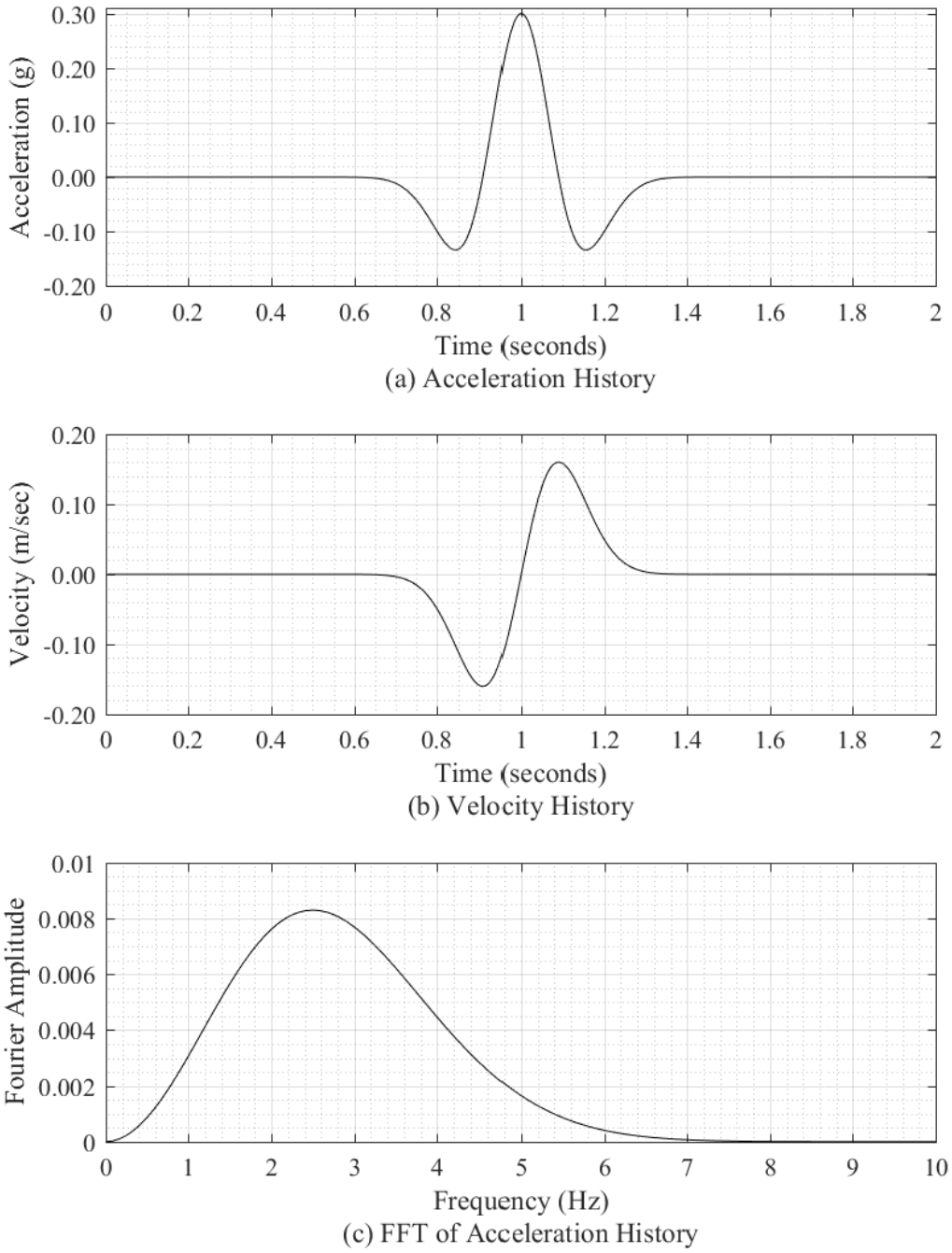


Figure 3.4 (a) Acceleration history, (b) velocity history and (c) FFT of acceleration history for the Ricker wavelet I

As seen from Figure 3.4, the maximum and minimum accelerations observed from the acceleration history are 0.3g and -0.13g, respectively. The acceleration history is symmetric and peak acceleration is observed at 1 sec. of the motion. And, the maximum and minimum velocities observed from the velocity history are 0.16 m/sec and -0.16

m/sec. The peak velocity is observed between 1 and 1.2 seconds of the motion. And also, observed maximum frequency is almost 7 Hz. When the frequency is 2.5 Hz, the maximum Fourier amplitude is observed.

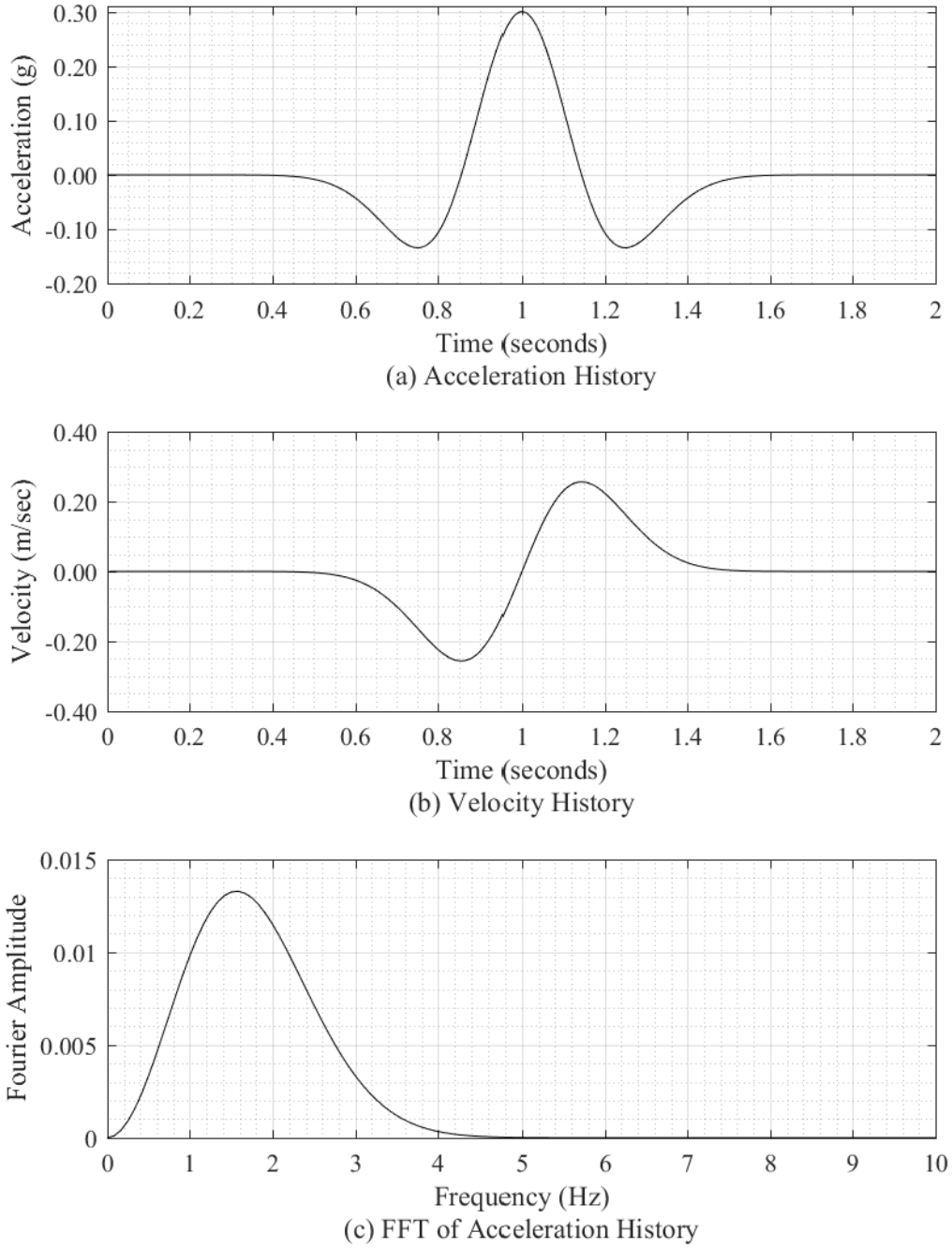


Figure 3.5 (a) Acceleration history, (b) velocity history and (c) FFT of acceleration history for the Ricker wavelet II

As seen from Figure 3.5, the maximum and minimum accelerations observed from the acceleration history are 0.3g and -0.13g, respectively. The acceleration history is symmetric and peak acceleration is observed at 1 second of the motion. And, the maximum and minimum velocities observed from the velocity history are 0.26 m/sec and

-0.26 m/sec. The peak velocity is observed between 1 and 1.2 seconds of the motion. And also, observed maximum frequency is almost 5 Hz. When the frequency is 1.5625 Hz, the maximum Fourier amplitude is observed.

3.4 Determination of Model Width Ratio

After introducing the soil deposits and the buried box culvert, the model width ratio must be determined for the calculation of the widths of the soil deposits. The length of the buried box culvert and the soil deposit along the Z axis is constant and it is 1 meter (i.e., analyses performed for unit length). It should be noted that contact properties between soil and frame elements are assumed to be bonded (i.e., welded) type. Rayleigh damping is utilized in this study by assuming 5% viscous damping [79].

For each of the soil deposits I and II, 72 (i.e., 9 different model width ratios, 4 different flexibility ratios and, 2 different depth ratios) different analyses are performed in OpenSEES to determine the model width ratio for the soil deposits I and II. The width ratio values used are 10, 25, 50, 75, 100, 150, 200, 250, and 300. The flexibility ratio values used are 0 (without box culvert), 0.125, 1, and 15. The depth ratio values used are 0.25 and 3. Convergences of the model width ratio for the soil deposits I and II are illustrated in Figure 3.6 and Figure 3.7. As seen from Figure 3.6 and Figure 3.7, when the model width ratio is equal to or greater than 50, the change in the maximum absolute peak displacement at the ground surface is negligible. Therefore, in order to minimize the computational time, but to obtain more realistic results, the model width ratio (Ω) is used to be 100. After introducing the value of the model width ratio (Ω), the width of the soil deposits I and II can be calculated as 500 meters.

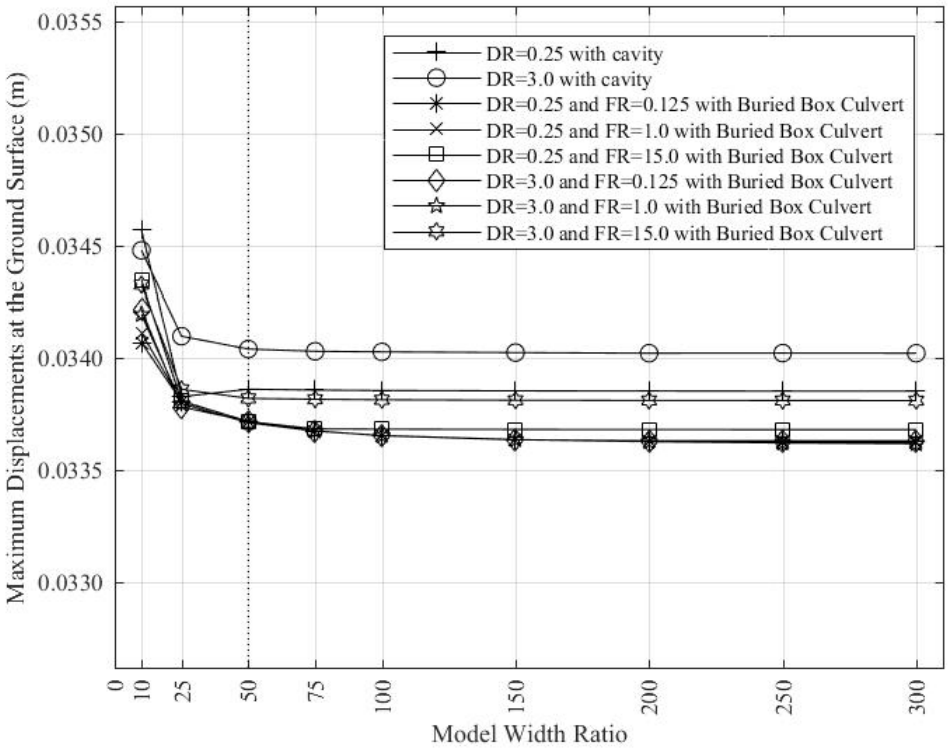


Figure 3.6 Convergence of the model width ratio for the soil deposit I

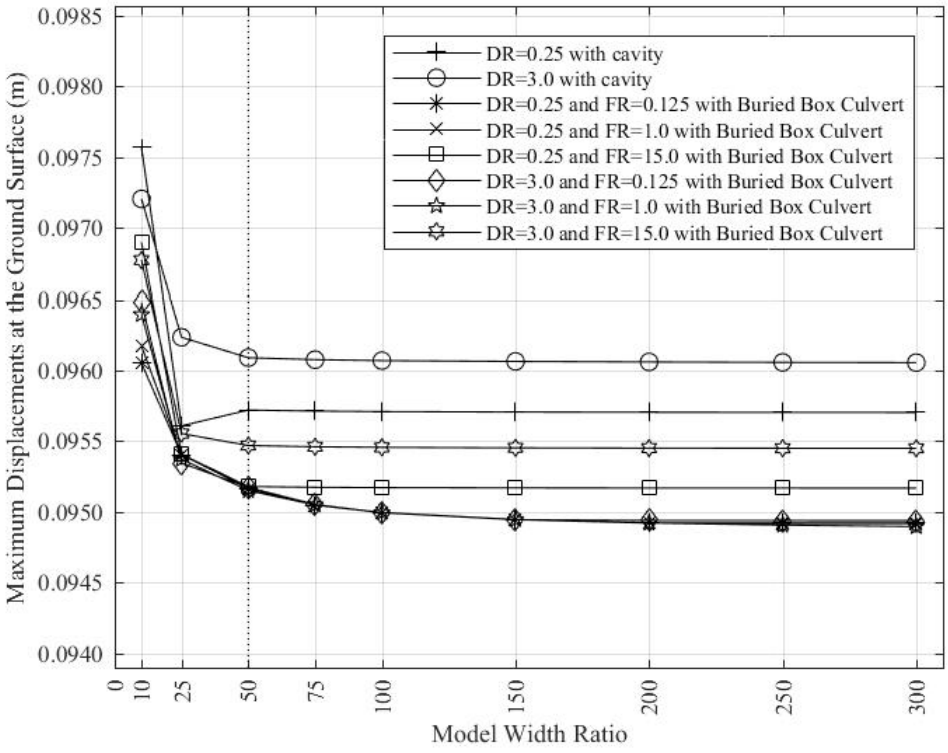


Figure 3.7 Convergence of the model width ratio for the soil deposit II

3.5 Numerical Analyses

After determining the widths of the soil deposits, a number of analyses are performed in OpenSEES to observe the effects of the depth ratio and the flexibility ratio on the internal forces, drift ratios and the shear strain deformation ratios. For each of the soil deposits I and II, 144 analyses (i.e., 8 different depth ratios and 18 different flexibility ratios) are performed in OpenSEES. The depth ratio values used are 0.25, 0.50, 0.75, 1.0, 1.50, 2.0, 2.50, and 3. The flexibility ratio values used are 0.125, 0.25, 0.50, 1, 2, 3, 4, 5, 6, 7, 8, 9, 10, 11, 12, 13, 14, and 15. The Ricker wavelet II is used in all analyses. Then, analyses results are separated into three different groups. These groups are internal forces (i.e., bending moments, shear forces and normal forces), drift ratios and shear strain deformation ratios.

3.6 Results and Discussion

3.6.1 Variation of the Normalized Absolute Maximum Internal Forces

Variations of the absolute maximum internal forces of the buried box culvert obtained from the analyses are illustrated. The maximum absolute internal forces are normalized. The axial forces, the shear forces, the bending moments are normalized by the value of 500 kN/m, 750 kN/m, and 1700 kNm/m, respectively. These values are obtained to be the absolute maximum values of the all analyses results.

Variations of the normalized absolute maximum internal forces for depth ratio of 0.25 are illustrated in Figure 3.8 for the soil deposits I and II. As seen from Figure 3.8, the normalized axial forces are almost constant with increasing flexibility ratio, but the normalized shear forces and the normalized bending moments decrease with increasing flexibility ratio. This decrease is much higher for the smaller values of the flexibility ratios than for the larger values of the flexibility ratios. The changes in the normalized internal forces are negligible after a value of the flexibility ratio, depending on the internal forces. The maximum values of the normalized axial force is obtained for the maximum flexibility ratio considered, but the maximum values of the normalized shear force and bending moment are obtained for the smallest flexibility ratio considered.

Variations of the normalized absolute maximum internal forces for depth ratio of 0.50 are illustrated in Figure 3.9 for the soil deposits I and II. As seen from Figure 3.9, the normalized axial forces are almost constant with increasing flexibility ratio, but the normalized shear forces and the normalized bending moments decrease with increasing flexibility ratio. This decrease is much higher for the smaller values of the flexibility ratios than for the larger values of the flexibility ratios. The changes in the normalized internal forces are negligible after a value of the flexibility ratio, depending on the internal forces. The maximum values of the normalized axial force is obtained for the maximum flexibility ratio considered, but the maximum values of the normalized shear force and bending moment are obtained for the smallest flexibility ratio considered.

Variations of the normalized absolute maximum internal forces for depth ratio of 0.75 are illustrated in Figure 3.10 for the soil deposits I and II. As seen from Figure 3.10, the normalized axial forces are almost constant with increasing flexibility ratio, but the normalized shear forces and the normalized bending moments decrease with increasing flexibility ratio. This decrease is much higher for the smaller values of the flexibility ratios than for the larger values of the flexibility ratios. The changes in the normalized internal forces are negligible after a value of the flexibility ratio, depending on the internal forces. The maximum values of the normalized axial force is obtained for the maximum flexibility ratio considered, but the maximum values of the normalized shear force and bending moment are obtained for the smallest flexibility ratio considered.

Variations of the normalized absolute maximum internal forces for depth ratio of 1.00 are illustrated in Figure 3.11 for the soil deposits I and II. As seen from Figure 3.11, the normalized axial forces are almost constant with increasing flexibility ratio, but the normalized shear forces and the normalized bending moments decrease with increasing flexibility ratio. This decrease is much higher for the smaller values of the flexibility ratios than for the larger values of the flexibility ratios. The changes in the normalized internal forces are negligible after a value of the flexibility ratio, depending on the internal forces. The maximum values of the normalized axial force is obtained for the maximum flexibility ratio considered, but the maximum values of the normalized shear force and bending moment are obtained for the smallest flexibility ratio considered.

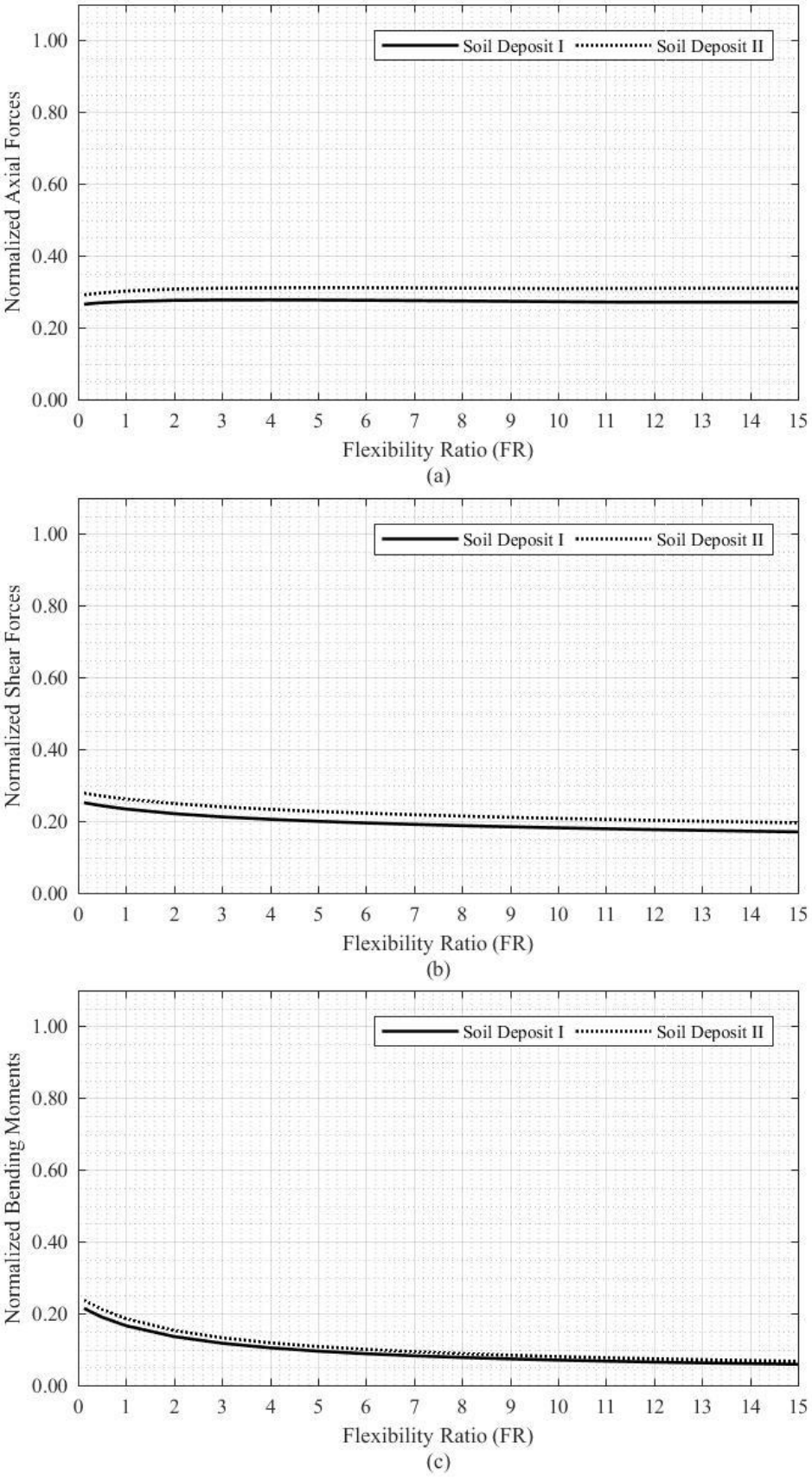


Figure 3.8 Variation of the normalized (a) axial forces, (b) shear forces, (c) bending moments of the buried box culvert for the depth ratio of 0.25

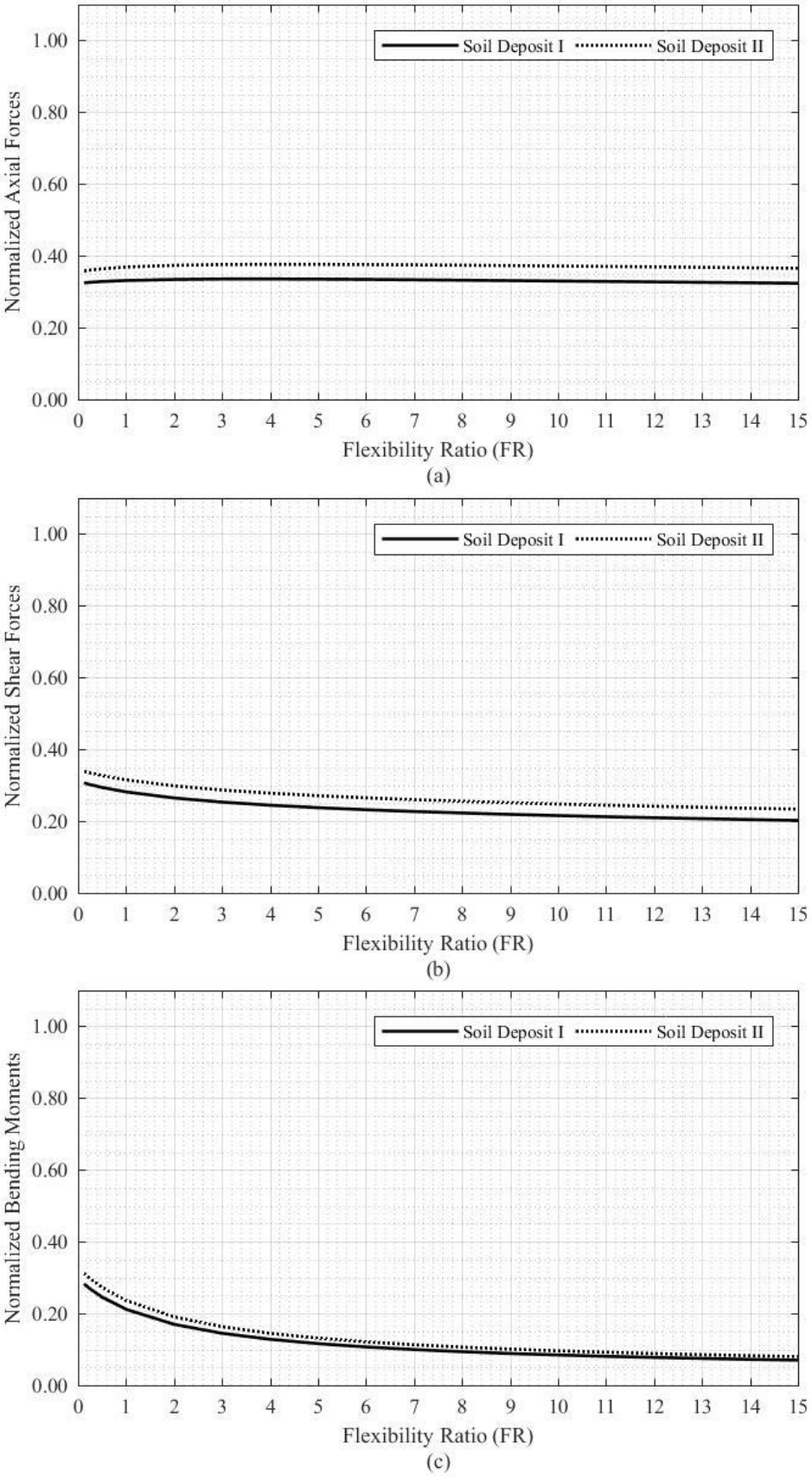


Figure 3.9 Variation of the normalized (a) axial forces, (b) shear forces, (c) bending moments of the buried box culvert for the depth ratio of 0.50

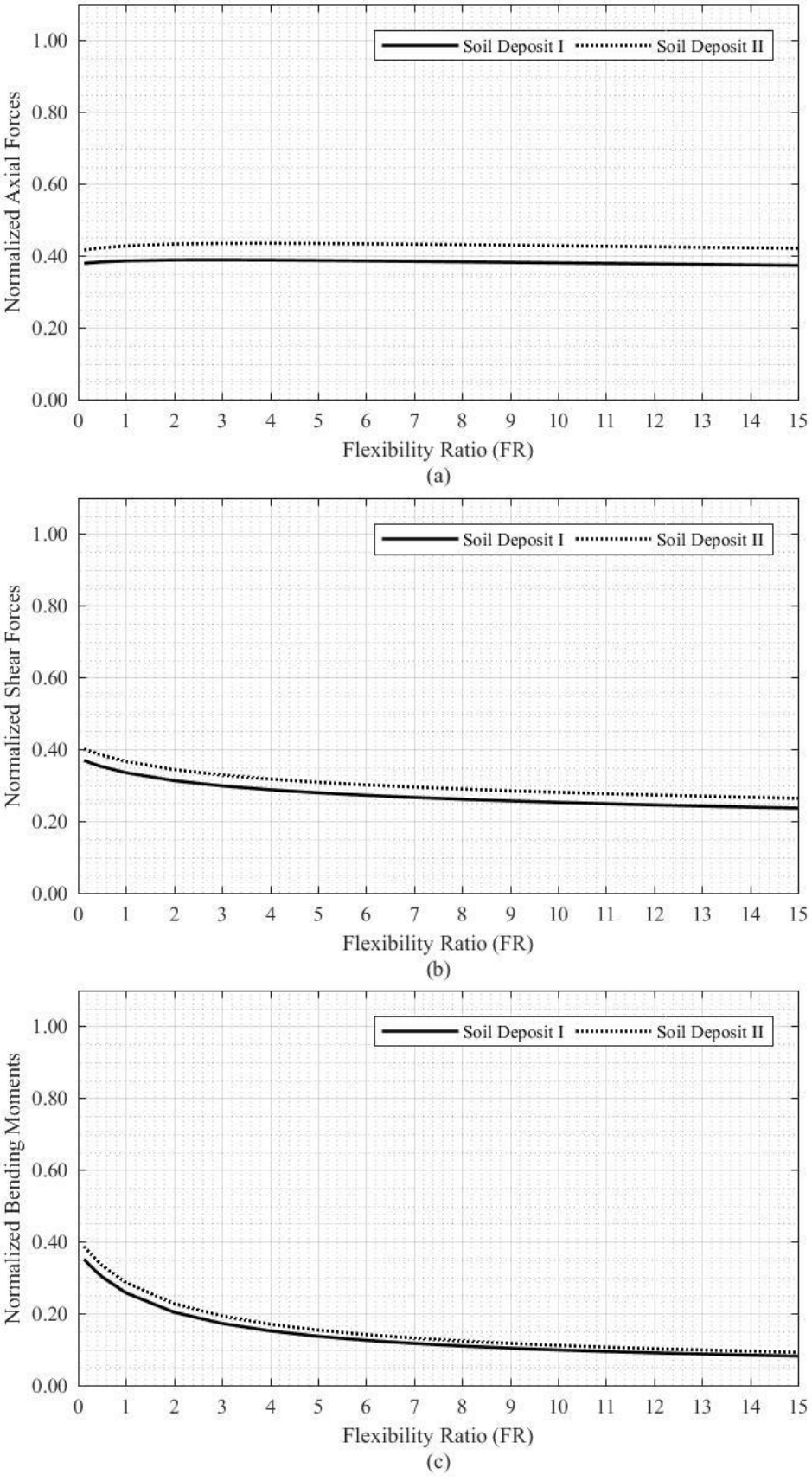
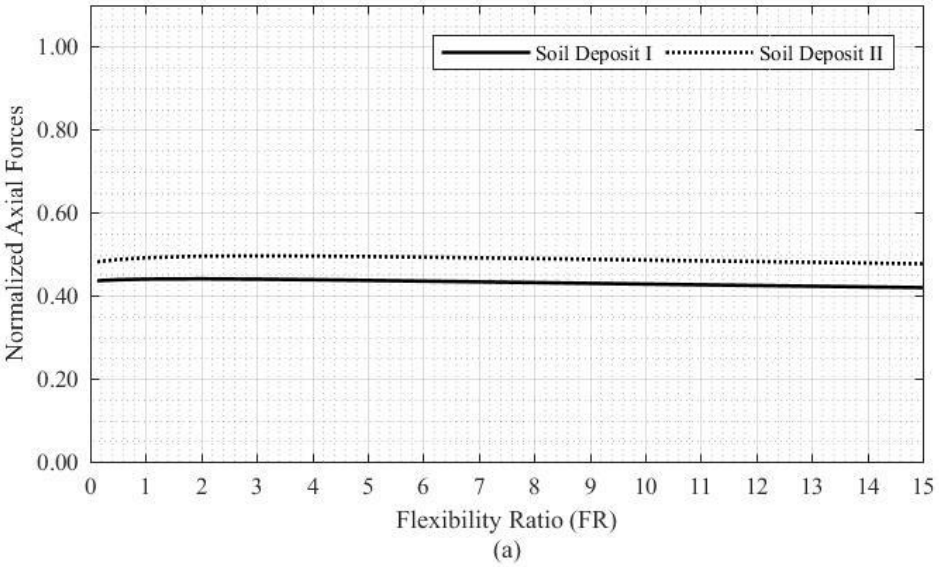
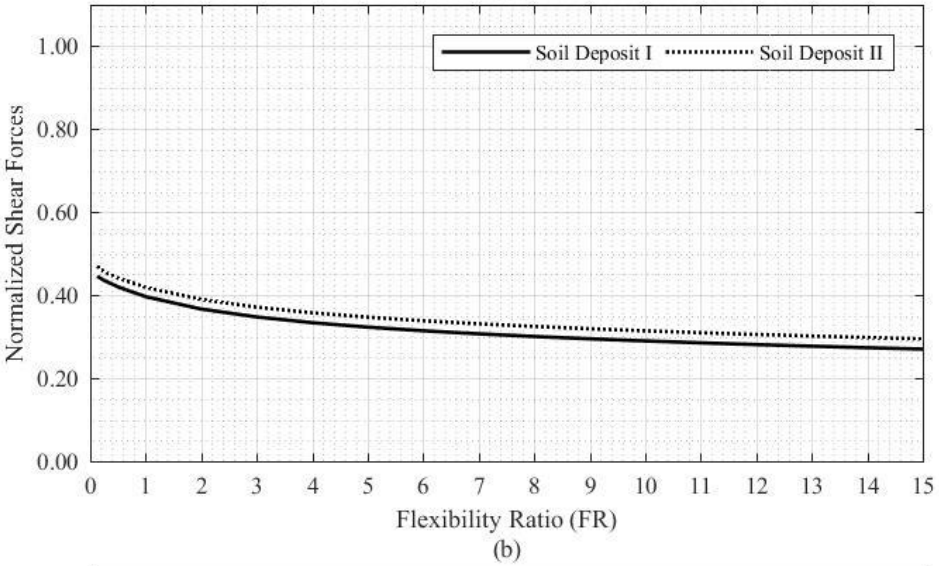


Figure 3.10 Variation of the normalized (a) axial forces, (b) shear forces, (c) bending moments of the buried box culvert for the depth ratio of 0.75





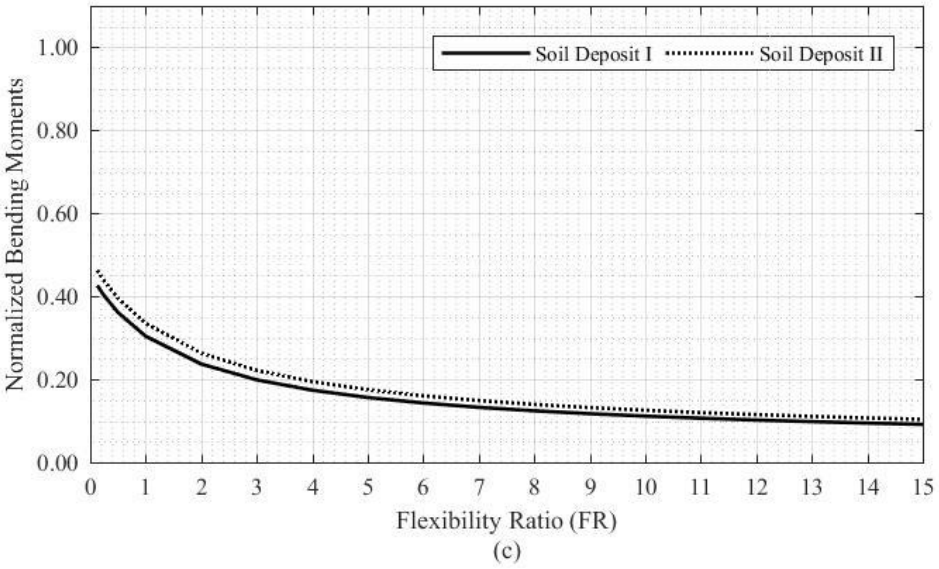


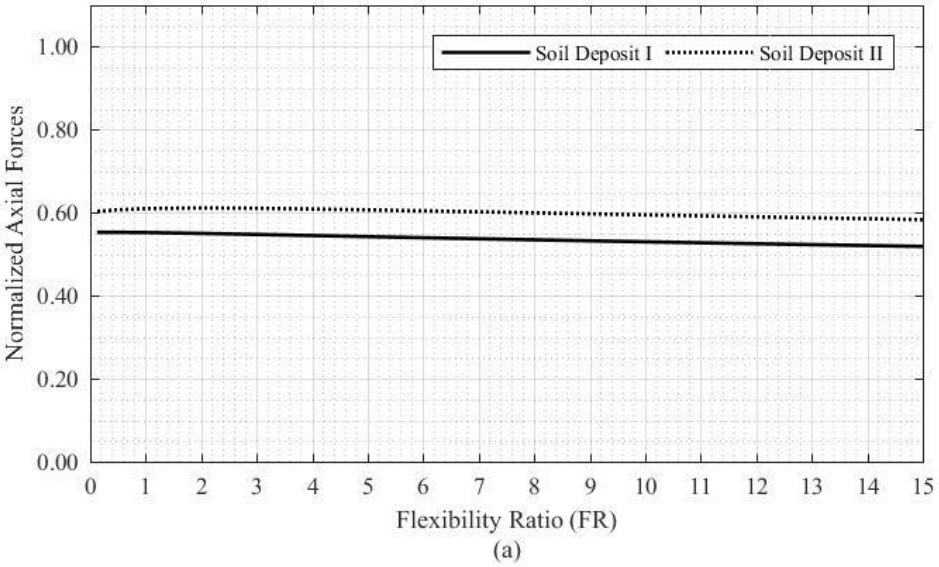
Figure 3.11 Variation of the normalized (a) axial forces, (b) shear forces, (c) bending moments of the buried box culvert for the depth ratio of 1.0

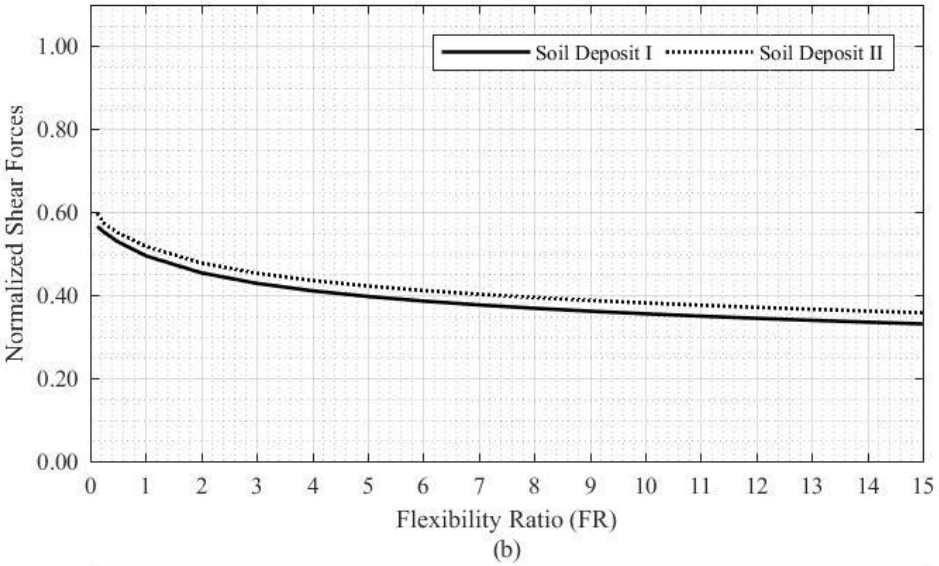
Variations of the normalized absolute maximum internal forces for depth ratio of 1.50 are illustrated in Figure 3.12 for the soil deposits I and II. As seen from Figure 3.12, the normalized axial forces decrease with increasing flexibility ratio. As also seen from Figure 3.12, the normalized shear forces and the normalized bending moments decrease with increasing flexibility ratio. This decrease for the normalized shear forces and the normalized bending moments is much higher for the smaller values of the flexibility ratios than for the larger values of the flexibility ratios. The maximum values of the normalized internal forces are obtained for the smallest flexibility ratio considered.

Variations of the normalized absolute maximum internal forces for depth ratio of 2.00 are illustrated in Figure 3.13 for the soil deposits I and II. As seen from Figure 3.13, the normalized axial forces decrease with increasing flexibility ratio. As also seen from Figure 3.13, the normalized shear forces and the normalized bending moments decrease with increasing flexibility ratio. This decrease for the normalized shear forces and the normalized bending moments is much higher for the smaller values of the flexibility ratios than for the larger values of the flexibility ratios. The maximum values of the normalized internal forces are obtained for the smallest flexibility ratio considered.

Variations of the normalized absolute maximum internal forces for depth ratio of 2.50 are illustrated in Figure 3.14 for the soil deposits I and II. As seen from Figure 3.14, the normalized axial forces decrease with increasing flexibility ratio. As also seen from Figure 3.14, the normalized shear forces and the normalized bending moments decrease with increasing flexibility ratio. This decrease for the normalized shear forces and the normalized bending moments is much higher for the smaller values of the flexibility ratios than for the larger values of the flexibility ratios. The maximum values of the normalized internal forces are obtained for the smallest flexibility ratio considered.

Variations of the normalized absolute maximum internal forces for depth ratio of 3.00 are illustrated in Figure 3.15 for the soil deposits I and II. As seen from Figure 3.15, the normalized axial forces decrease with increasing flexibility ratio. As also seen from Figure 3.15, the normalized shear forces and the normalized bending moments decrease with increasing flexibility ratio. This decrease for the normalized shear forces and the normalized bending moments is much higher for the smaller values of the flexibility ratios than for the larger values of the flexibility ratios. The maximum values of the normalized internal forces are obtained for the smallest flexibility ratio considered.





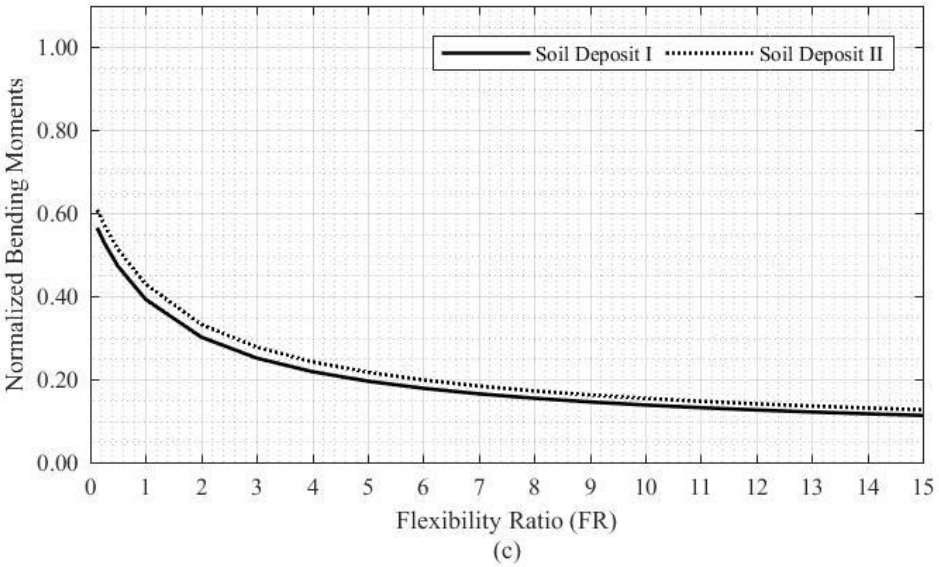
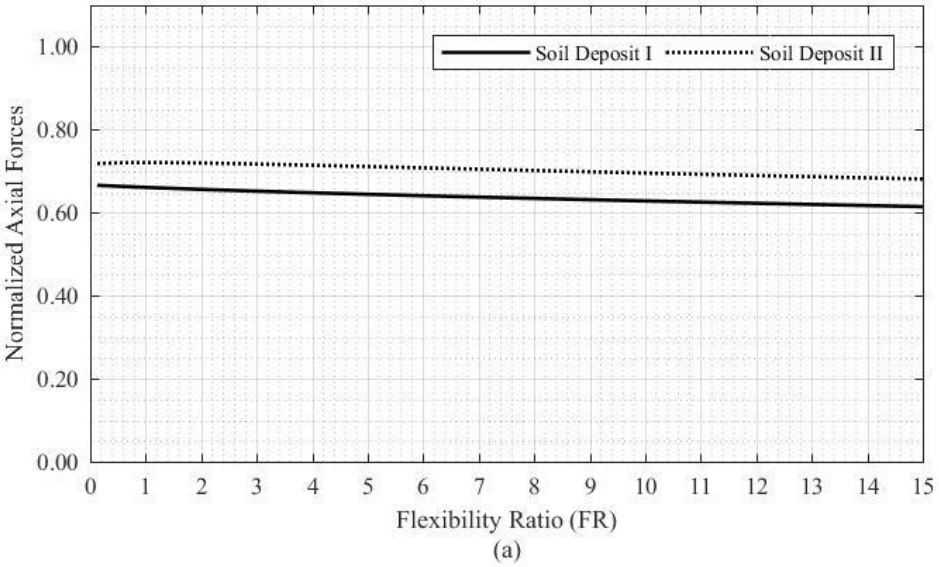
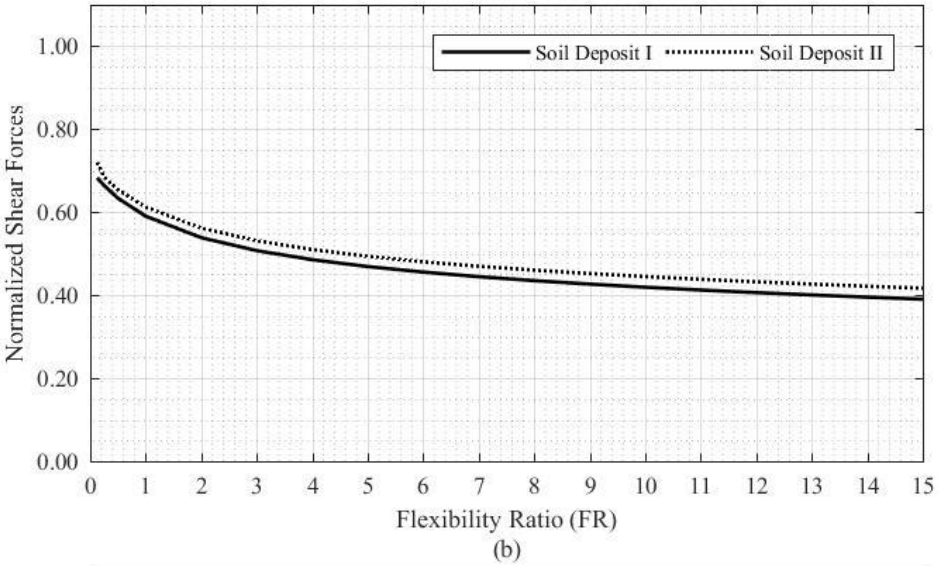


Figure 3.12 Variation of the normalized (a) axial forces, (b) shear forces, (c) bending moments for depth ratio of 1.50





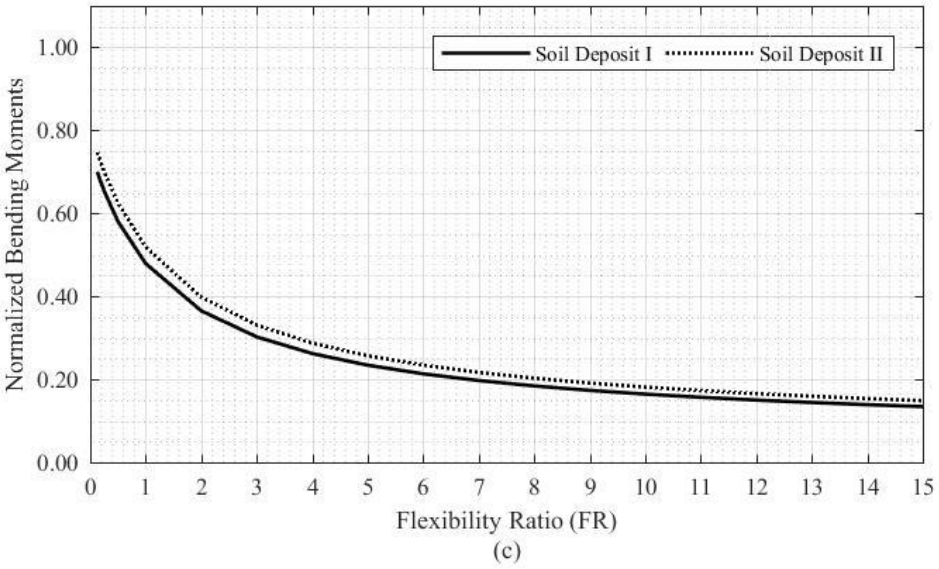
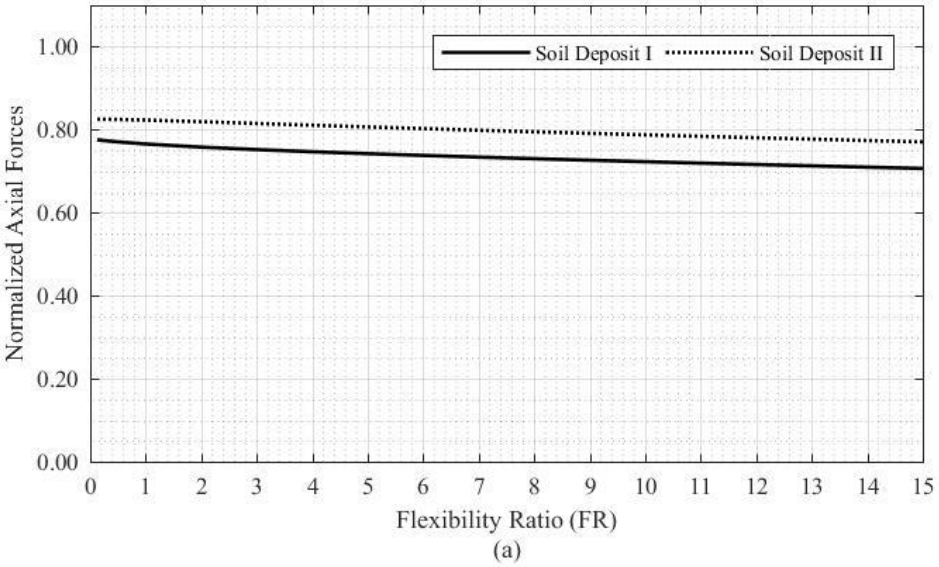
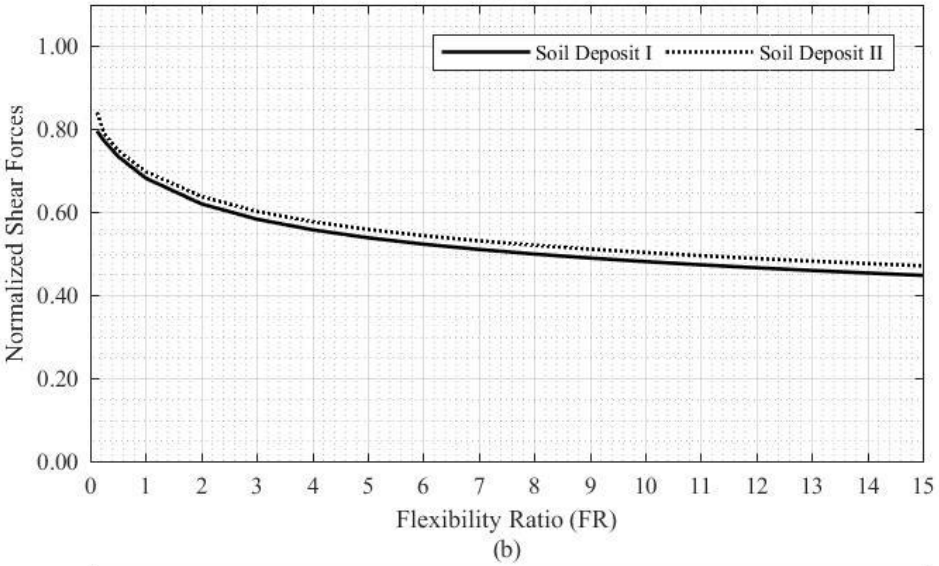


Figure 3.13 Variation of the normalized (a) axial forces, (b) shear forces, (c) bending moments of the buried box culvert for the depth ratio of 2.00





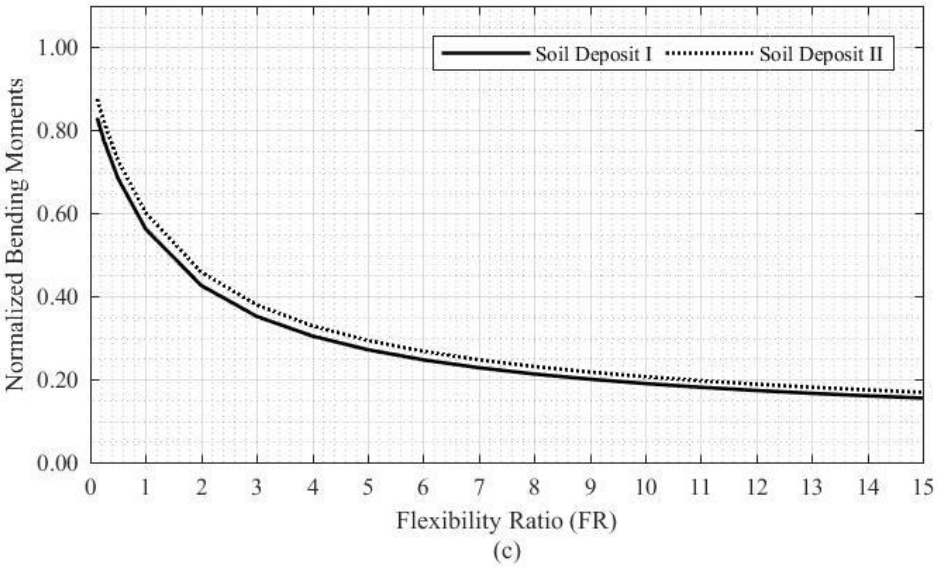


Figure 3.14 Variation of the normalized (a) axial forces, (b) shear forces, (c) bending moments of the buried box culvert for the depth ratio of 2.50

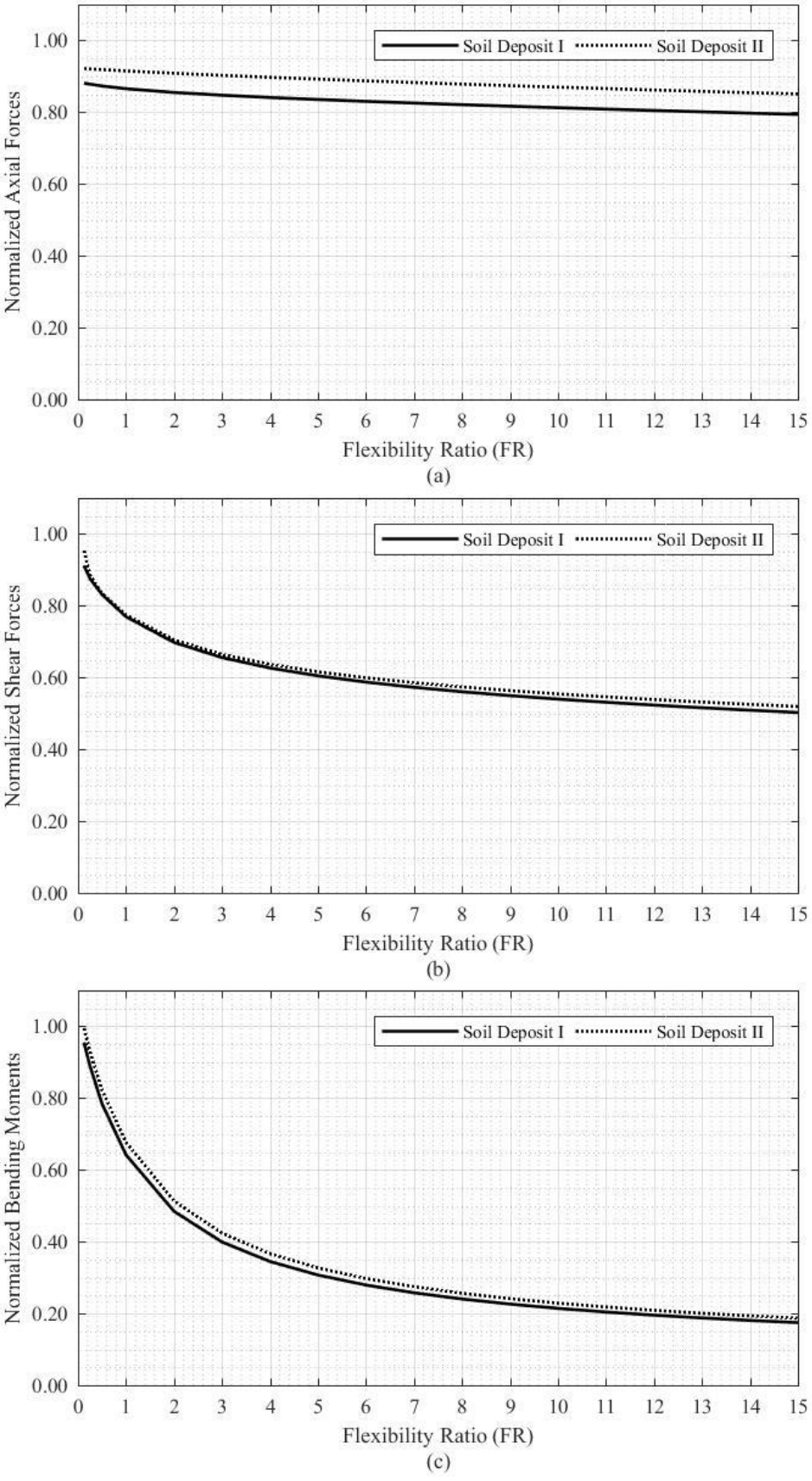
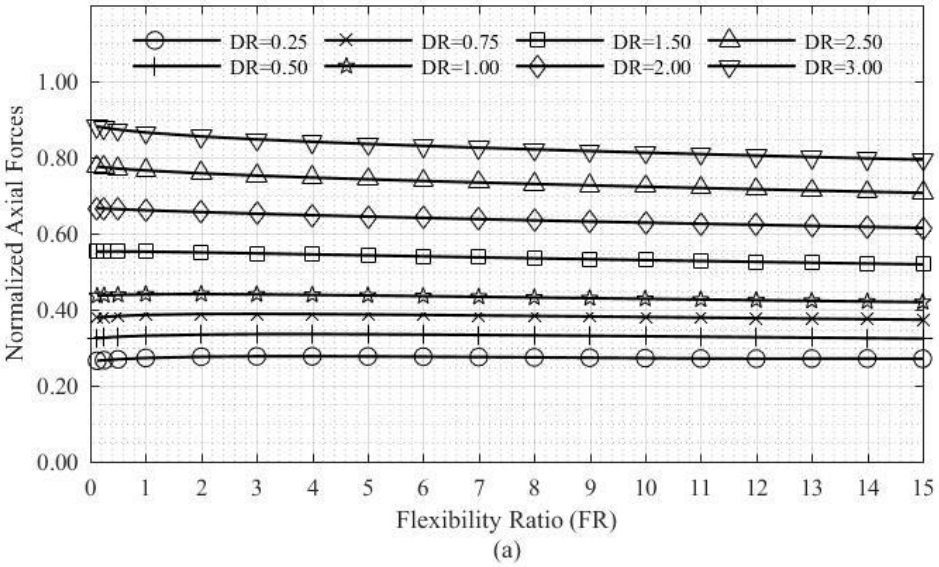
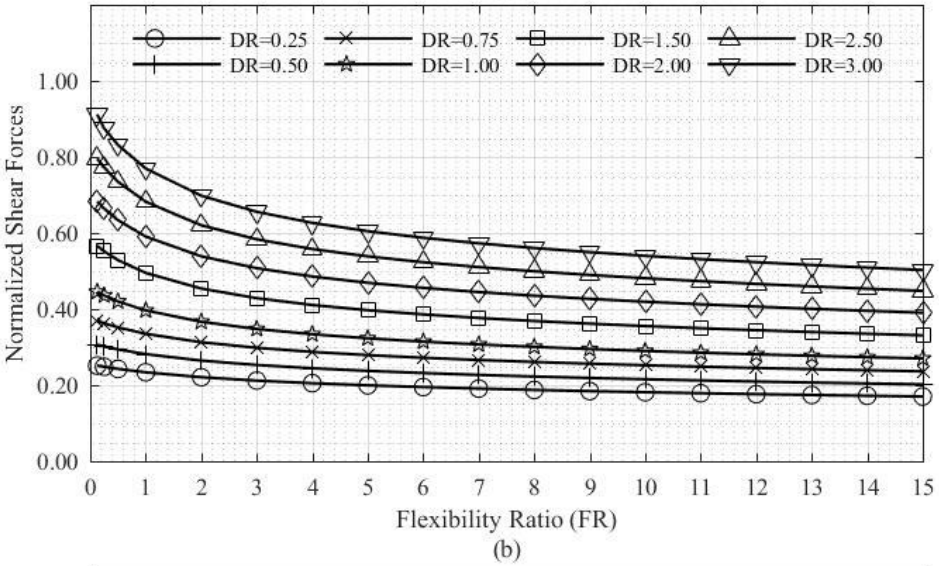


Figure 3.15 Variation of the normalized (a) axial forces, (b) shear forces, (c) bending moments of the buried box culvert for the depth ratio of 3.00

Variations of the normalized absolute maximum internal forces for the soil deposits I and II are illustrated in Figure 3.16 and Figure 3.17, respectively. As seen from Figure 3.16 and Figure 3.17, the normalized axial forces are almost constant with increasing flexibility ratio for depth ratios of 0.25, 0.50, 0.75, and 1.00. And also, the normalized axial forces decrease with increasing flexibility ratio for depth ratios of 1.50, 2.00, 2.50, and 3.00. As also seen from Figure 3.16 and Figure 3.17, the normalized shear forces and the normalized bending moments decrease with increasing flexibility ratio for a constant value of the depth ratio. This decrease for the normalized shear forces and the normalized bending moments is much higher for the smaller values of the flexibility ratios than for the larger values of the flexibility ratios. And also, the normalized shear forces and the normalized bending moments increase with increasing depth ratio for a constant value of the flexibility ratio. This increase for the normalized shear forces and the normalized bending moments is much higher for the smaller values of the flexibility ratios than for the larger values of the flexibility ratios. In addition, the maximum values of the normalized internal forces are obtained for the smallest flexibility ratio considered.

As also seen from Figure 3.8 to Figure 3.17, if the depth ratio is equal to or less than 1.0, the normalized axial forces are almost constant with increasing flexibility ratio. If the depth ratio is greater than 1.0, the normalized axial forces decrease with increasing flexibility ratio. The normalized shear forces and the normalized bending moments decrease with increasing flexibility ratio for a constant value of depth ratio. This decrease is much higher for the smaller values of the flexibility ratios than for the larger values of the flexibility ratios. The normalized internal forces increase with increasing depth ratio for a constant value of the flexibility ratio. The differences among the normalized axial forces are almost constant with increasing depth ratio for the soil deposits I and II, but the differences among the normalized shear forces decrease with increasing depth ratio for the soil deposits I and II. In addition, the differences among the normalized bending moments are almost constant with increasing depth ratio for the soil deposits I and II. The maximum values of the normalized internal forces are obtained for the smallest flexibility ratio and the maximum depth ratio.





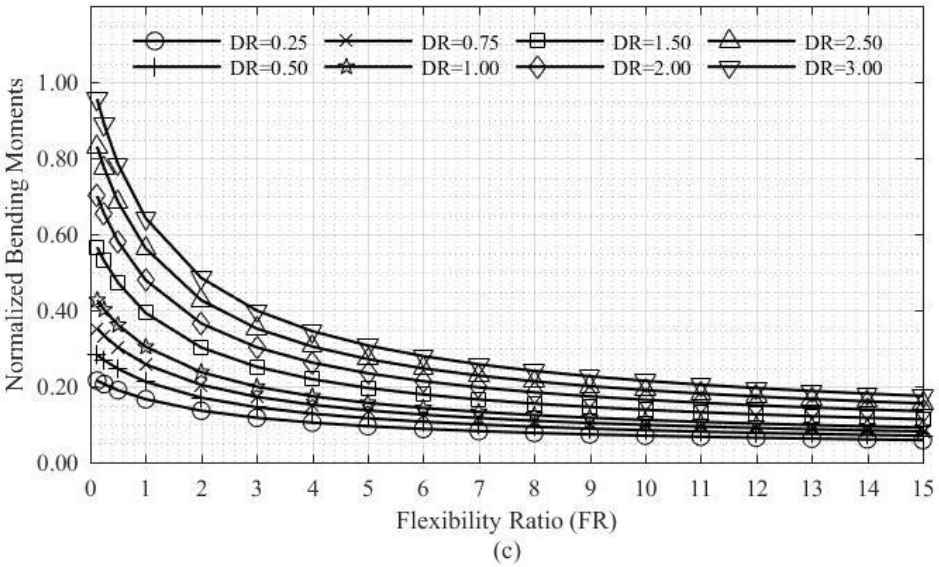
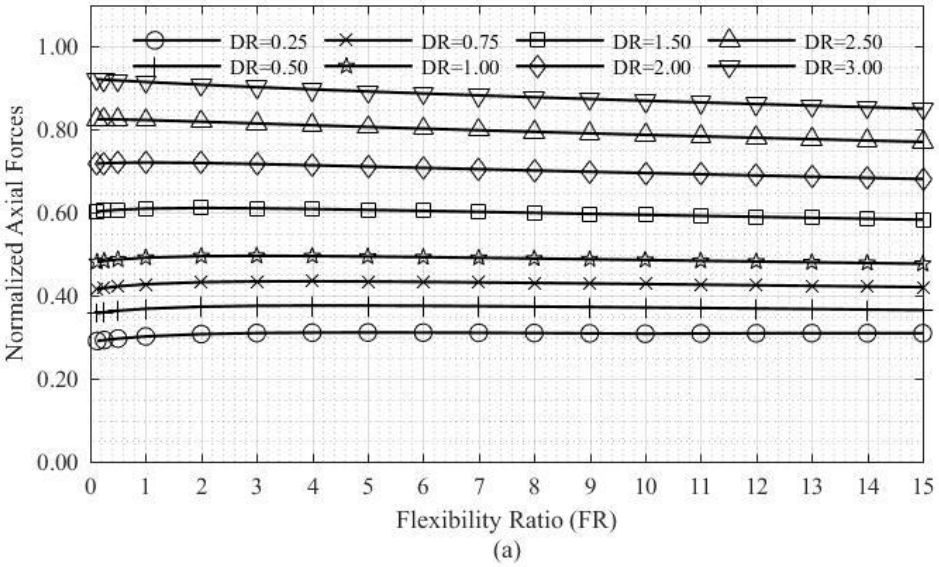
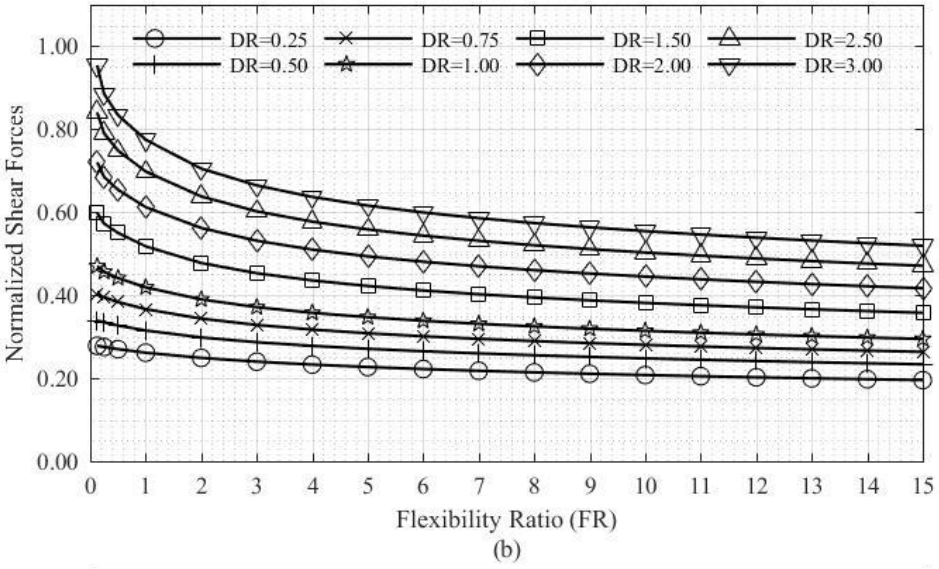


Figure 3.16 Variation of the normalized (a) axial forces, (b) shear forces, (c) bending moments of the buried box culvert for the soil deposit I





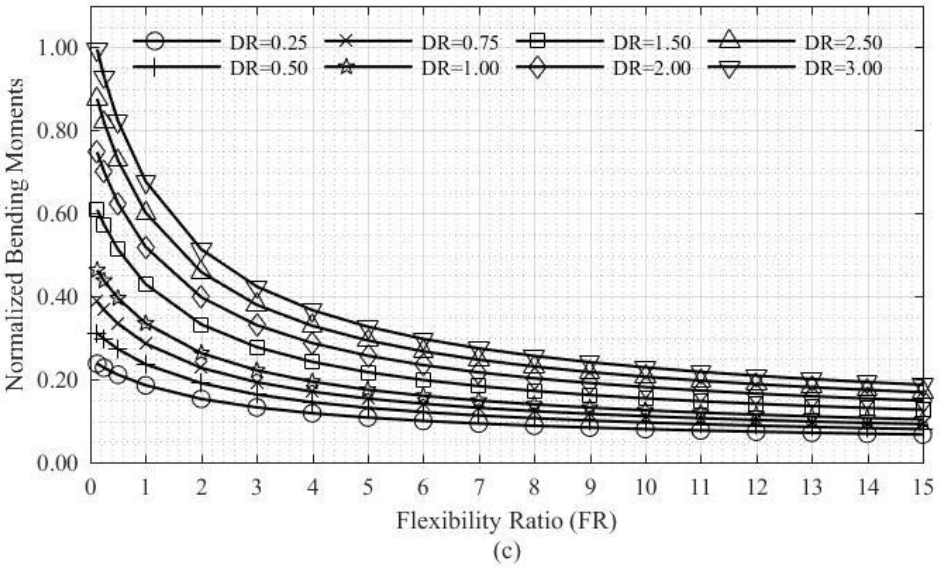


Figure 3.17 Variation of the normalized (a) axial forces, (b) shear forces, (c) bending moments of the buried box culvert for the soil deposit II

3.6.2 Variation of the Bending Moments

Variation of bending moments on the sides of the buried box culvert is illustrated with respect to the depth ratio and flexibility ratio. Four flexibility ratios are used to draw the bending moment diagrams. These ratios are 0.125, 1, 8, and 15. Each of these values represents different cases. If the flexibility ratio is 0.125, the buried box culvert is stiffer than the soil deposit. If the flexibility ratio is 1.0, the stiffness of the buried box culvert is equal to the stiffness of the soil deposits. If the flexibility ratios 8.0 and 15.0, the buried box culvert is more flexible than the soil deposit. The reason for choosing these values is to observe different cases. The bending moment diagrams marked to be A-B, B-C, C-D, and D-A represent the bending moments on the bottom slab, right-side wall, top slab, and left-side wall, respectively.

The bending moment diagrams for the depth ratio of 0.25 are illustrated in Figure 3.18 for the soil deposits I and II. As seen from Figure 3.18, the bending moment diagrams for the soil deposit I are almost the same with the bending moment diagram for the soil deposit II for all of the flexibility ratios considered. For flexibility ratios of 0.125 and 1.0, the bending moment diagram is almost linear between A-B, B-C, C-D, and D-A. For all values of the flexibility ratios considered in this study, the maximum bending moment is obtained at the corner A of the buried box culverts, and the minimum bending moment is obtained at the corner B of the buried box culvert. As also seen from Figure 3.18, if the flexibility ratio increases, the bending moment decreases for both soil deposit I and II. The reason for this is that if the flexibility ratio increases, the buried box culvert becomes more flexible than the soil deposit. Therefore, the maximum bending moment value is obtained to be 365 kNm/m for the flexibility ratio of 0.125. As also seen from Figure 3.18, the difference between the bending moments values of the soil deposit I and II decreases with increasing flexibility ratio, and the curves of the bending moment values of the both soil deposits almost coincide. In addition, the variation of the bending moment values is not linear for the larger flexibility ratios.

The bending moment diagrams for the depth ratio of 0.50 are illustrated in Figure 3.19 for the soil deposits I and II. As seen from Figure 3.19, the bending moment diagrams for the soil deposit I are almost the same with the bending moment diagram for the soil deposit II for all of the flexibility ratios considered. For flexibility ratios of 0.125 and 1.0, the bending moment diagram is almost linear between A-B, B-C, C-D, and D-A. For all values of the flexibility ratios considered in this study, the maximum bending moment is

obtained at the corner A of the buried box culverts, and the minimum bending moment is obtained at the corner B of the buried box culvert. As also seen from Figure 3.19, if the flexibility ratio increases, the bending moment decreases for both soil deposit I and II. The reason for this is that if the flexibility ratio increases, the buried box culvert becomes more flexible than the soil deposit. Therefore, the maximum bending moment value is obtained to be 480 kNm/m for the flexibility ratio of 0.125. As also seen from Figure 3.19, the difference between the bending moments values of the soil deposit I and II decreases with increasing flexibility ratio, and the curves of the bending moment values of the both soil deposits almost coincide. In addition, the variation of the bending moment values is not linear for the larger flexibility ratios.

The bending moment diagrams for the depth ratio of 0.75 are illustrated in Figure 3.20 for the soil deposits I and II. As seen from Figure 3.20, the bending moment diagrams for the soil deposit I are almost the same with the bending moment diagram for the soil deposit II for all of the flexibility ratios considered. For flexibility ratios of 0.125 and 1.0, the bending moment diagram is almost linear between A-B, B-C, C-D, and D-A. For all values of the flexibility ratios considered in this study, the maximum bending moment is obtained at the corner A of the buried box culverts, and the minimum bending moment is obtained at the corner B of the buried box culvert. As also seen from Figure 3.20, if the flexibility ratio increases, the bending moment decreases for both soil deposit I and II. The reason for this is that if the flexibility ratio increases, the buried box culvert becomes more flexible than the soil deposit. Therefore, the maximum bending moment value is obtained to be 600 kNm/m for the flexibility ratio of 0.125. As also seen from Figure 3.20, the difference between the bending moments values of the soil deposit I and II decreases with increasing flexibility ratio, and the curves of the bending moment values of the both soil deposits almost coincide. In addition, the variation of the bending moment values is not linear for the larger flexibility ratios.

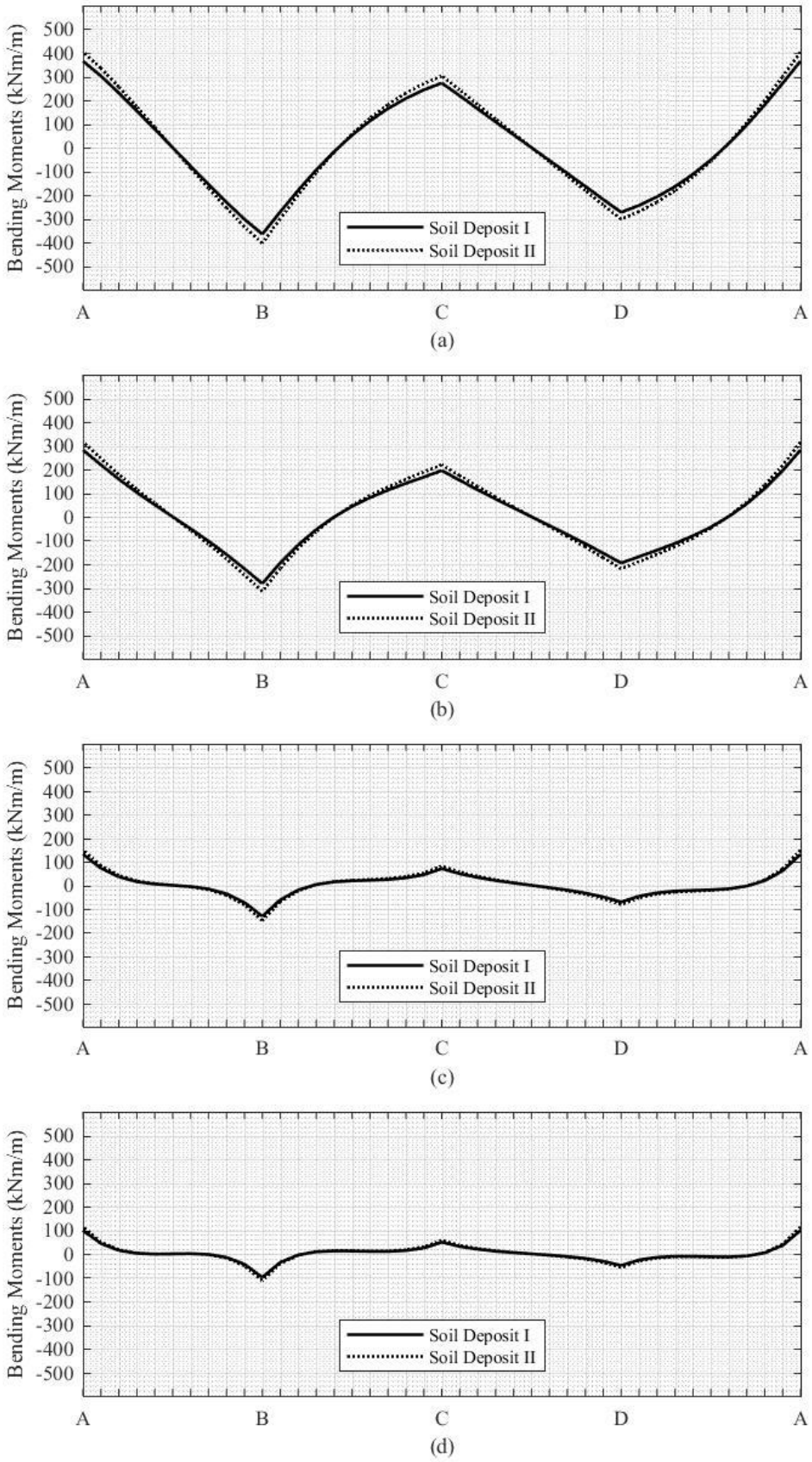


Figure 3.18 The bending moment diagrams of the buried box culvert for the depth ratio of 0.25 for (a) FR=0.125, (b) FR=1.0, (c) FR=8.0, and FR=15.0

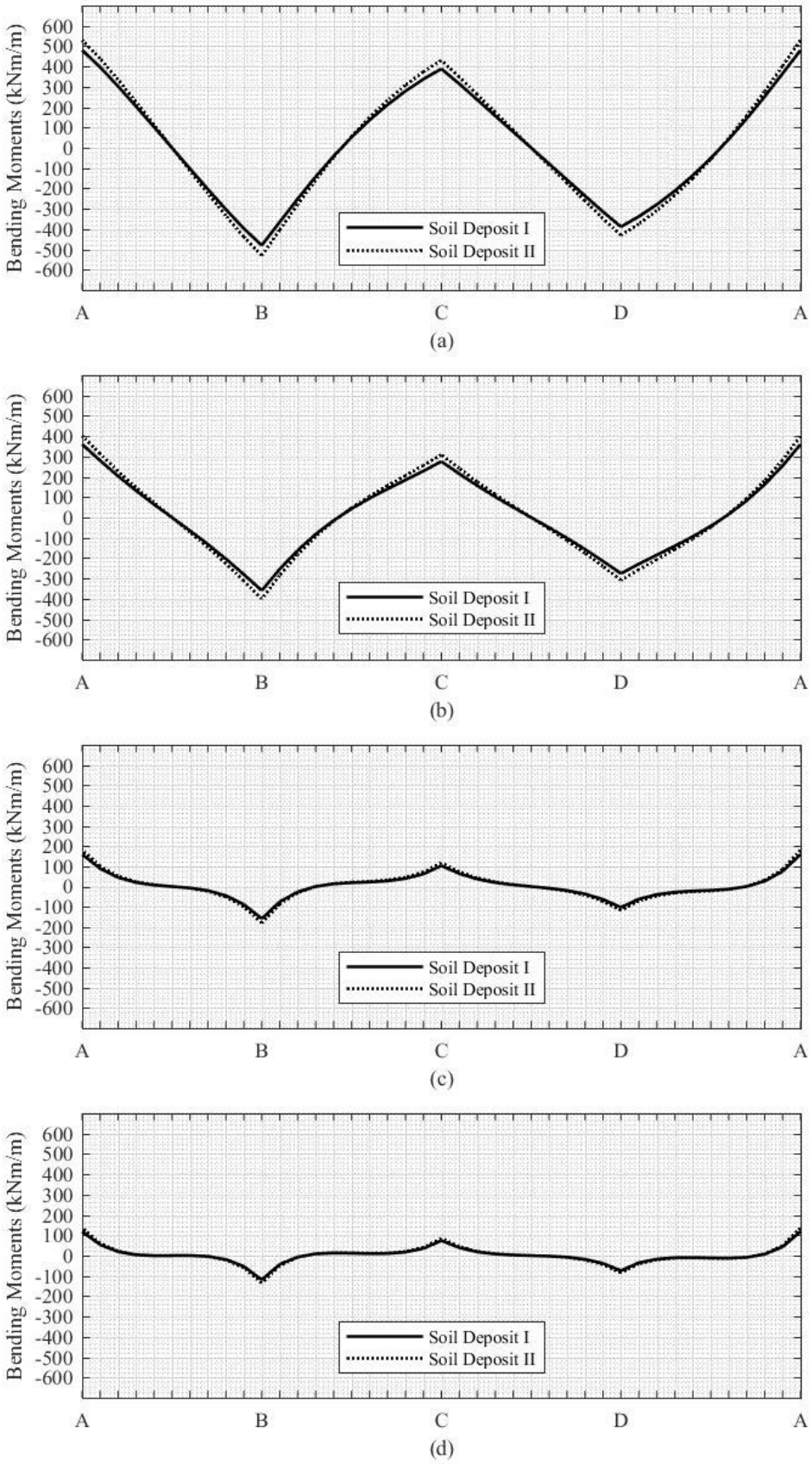


Figure 3.19 The bending moment diagrams of the buried box culvert for the depth ratio of 0.50 for (a) FR=0.125, (b) FR=1.0, (c) FR=8.0, and FR=15.0

The bending moment diagrams for the depth ratio of 1.00 are illustrated in Figure 3.21 for the soil deposits I and II. As seen from Figure 3.21, the bending moment diagrams for the soil deposit I are almost the same with the bending moment diagram for the soil deposit II for all of the flexibility ratios considered. For flexibility ratios of 0.125 and 1.0, the bending moment diagram is almost linear between A-B, B-C, C-D, and D-A. For all values of the flexibility ratios considered in this study, the maximum bending moment is obtained at the corner A of the buried box culverts, and the minimum bending moment is obtained at the corner B of the buried box culvert. As also seen from Figure 3.21, if the flexibility ratio increases, the bending moment decreases for both soil deposit I and II. The reason for this is that if the flexibility ratio increases, the buried box culvert becomes more flexible than the soil deposit. Therefore, the maximum bending moment value is obtained to be 725 kNm/m for the flexibility ratio of 0.125. As also seen from Figure 3.21, the difference between the bending moments values of the soil deposit I and II decreases with increasing flexibility ratio, and the curves of the bending moment values of the both soil deposits almost coincide. In addition, the variation of the bending moment values is not linear for the larger flexibility ratios.

The bending moment diagrams for the depth ratio of 1.50 are illustrated in Figure 3.22 for the soil deposits I and II. As seen from Figure 3.22, the bending moment diagrams for the soil deposit I are almost the same with the bending moment diagram for the soil deposit II for all of the flexibility ratios considered. For flexibility ratios of 0.125 and 1.0, the bending moment diagram is almost linear between A-B, B-C, C-D, and D-A. For all values of the flexibility ratios considered in this study, the maximum bending moment is obtained at the corner A of the buried box culverts, and the minimum bending moment is obtained at the corner B of the buried box culvert. As also seen from Figure 3.22, if the flexibility ratio increases, the bending moment decreases for both soil deposit I and II. The reason for this is that if the flexibility ratio increases, the buried box culvert becomes more flexible than the soil deposit. Therefore, the maximum bending moment value is obtained to be 960 kNm/m for the flexibility ratio of 0.125. As also seen from Figure 3.22, the difference between the bending moments values of the soil deposit I and II decreases with increasing flexibility ratio, and the curves of the bending moment values of the both soil deposits almost coincide. In addition, the variation of the bending moment values is not linear for the larger flexibility ratios.

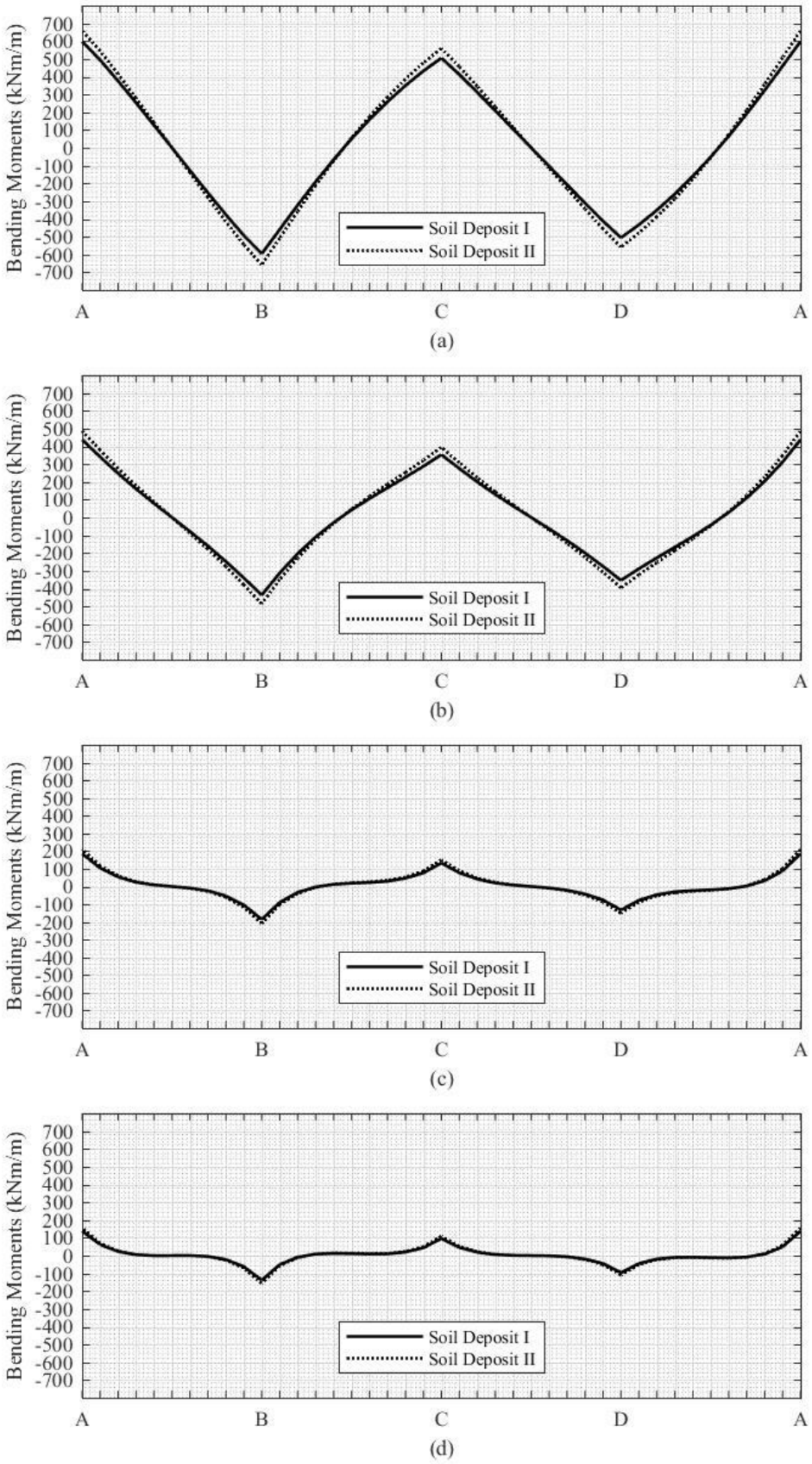


Figure 3.20 The bending moment diagrams of the buried box culvert for the depth ratio of 0.75 for (a) FR=0.125, (b) FR=1.0, (c) FR=8.0, and FR=15.0

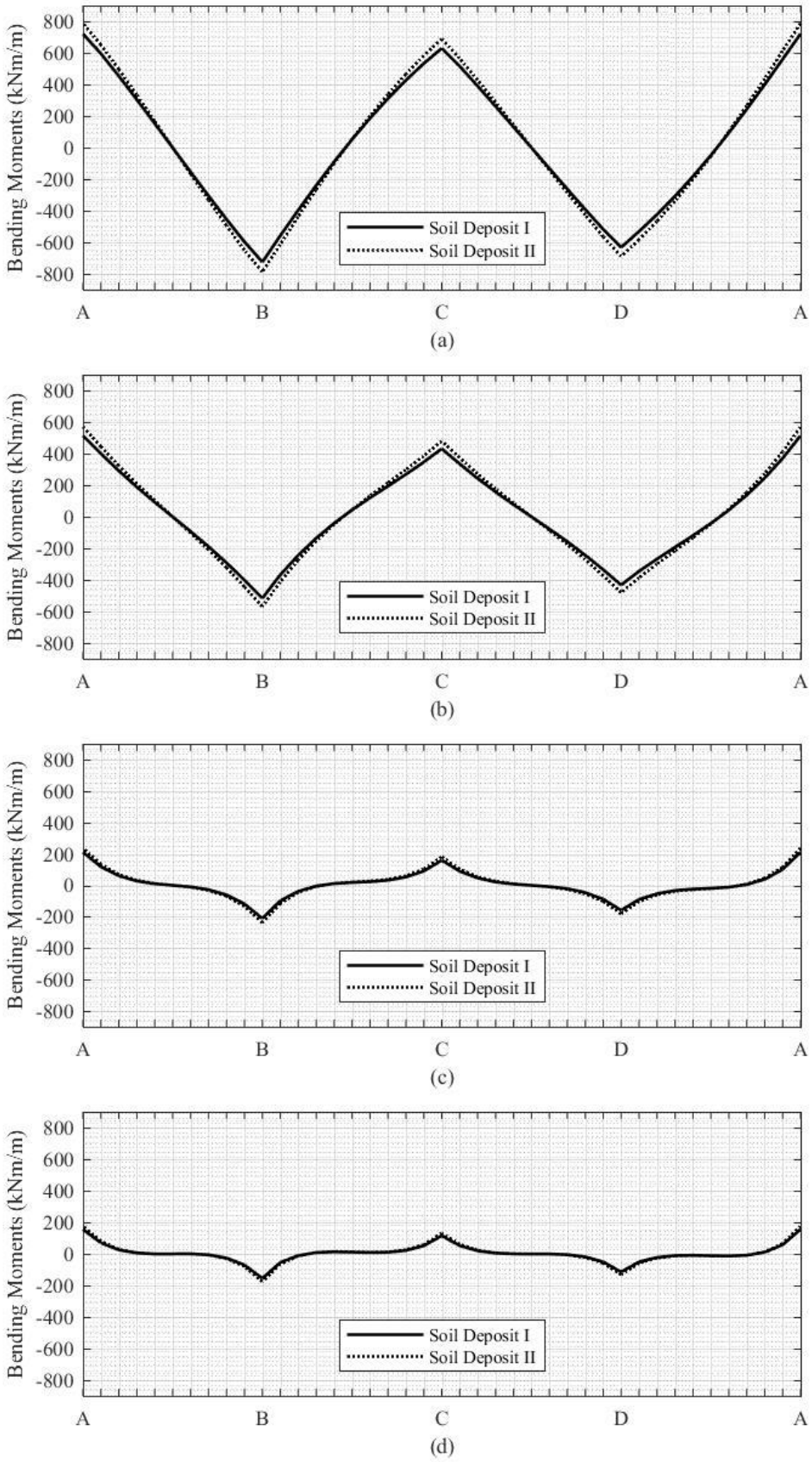


Figure 3.21 The bending moment diagrams of the buried box culvert for the depth ratio of 1.00 for (a) FR=0.125, (b) FR=1.0, (c) FR=8.0, and FR=15.0

The bending moment diagrams for the depth ratio of 2.00 are illustrated in Figure 3.23 for the soil deposits I and II. As seen from Figure 3.23, the bending moment diagrams for the soil deposit I are almost the same with the bending moment diagram for the soil deposit II for all of the flexibility ratios considered. For flexibility ratios of 0.125 and 1.0, the bending moment diagram is almost linear between A-B, B-C, C-D, and D-A. For all values of the flexibility ratios considered in this study, the maximum bending moment is obtained at the corner A of the buried box culverts, and the minimum bending moment is obtained at the corner B of the buried box culvert. As also seen from Figure 3.23, if the flexibility ratio increases, the bending moment decreases for both soil deposit I and II. The reason for this is that if the flexibility ratio increases, the buried box culvert becomes more flexible than the soil deposit. Therefore, the maximum bending moment value is obtained to be 1190 kNm/m for the flexibility ratio of 0.125. As also seen from Figure 3.23, the difference between the bending moments values of the soil deposit I and II decreases with increasing flexibility ratio, and the curves of the bending moment values of the both soil deposits almost coincide. In addition, the variation of the bending moment values is not linear for the larger flexibility ratios.

The bending moment diagrams for the depth ratio of 2.50 are illustrated in Figure 3.24 for the soil deposits I and II. As seen from Figure 3.24, the bending moment diagrams for the soil deposit I are the same with the bending moment diagram for the soil deposit II for all of the flexibility ratios considered. For flexibility ratios of 0.125 and 1.0, the bending moment diagram is almost linear between A-B, B-C, C-D, and D-A. For all values of the flexibility ratios considered in this study, the maximum bending moment is obtained at the corner A of the buried box culverts, and the minimum bending moment is obtained at the corner B of the buried box culvert. As also seen from Figure 3.24, if the flexibility ratio increases, the bending moment decreases for both soil deposit I and II. The reason for this is that if the flexibility ratio increases, the buried box culvert becomes more flexible than the soil deposit. Therefore, the maximum bending moment value is obtained to be 1410 kNm/m for the flexibility ratio of 0.125. As also seen from Figure 3.24, the variation of the bending moment values is not linear for the larger flexibility ratios.

The bending moment diagrams for the depth ratio of 3.00 are illustrated in Figure 3.25 for the soil deposits I and II. As seen from Figure 3.25, the bending moment diagrams for the soil deposit I are the same with the bending moment diagram for the soil deposit II

for all of the flexibility ratios considered. For flexibility ratios of 0.125 and 1.0, the bending moment diagram is almost linear between A-B, B-C, C-D, and D-A. For all values of the flexibility ratios considered in this study, the maximum bending moment is obtained at the corner A of the buried box culverts, and the minimum bending moment is obtained at the corner B of the buried box culvert. As also seen from Figure 3.25, if the flexibility ratio increases, the bending moment decreases for both soil deposit I and II. The reason for this is that if the flexibility ratio increases, the buried box culvert becomes more flexible than the soil deposit. Therefore, the maximum bending moment value is obtained to be 1625 kNm/m for the flexibility ratio of 0.125. As also seen from Figure 3.25, the variation of the bending moment values is not linear for the larger flexibility ratios.

As also seen from Figure 3.18 to Figure 3.25, the bending moment diagrams for the soil deposit I are almost the same with the bending moment diagram for the soil deposit II for all of the flexibility ratios considered. For flexibility ratios of 0.125 and 1.0, the bending moment diagram is almost linear between A-B, B-C, C-D, and D-A. For all values of the flexibility ratios considered in this study, the maximum bending moment is obtained at the corner A of the buried box culverts, and the minimum bending moment is obtained at the corner B of the buried box culvert. As also seen from Figure 3.18 to Figure 3.25, the bending moments increase with increasing depth ratio for a constant value of the flexibility ratio, but the bending moments decrease with increasing flexibility ratio for a constant value of the depth ratio. The reason for this is that if the flexibility ratio increases, the buried box culvert becomes more flexible than the soil deposit. The maximum values of the bending moment for the soil deposits I and II are obtained for the smallest flexibility ratio and the maximum depth ratio.

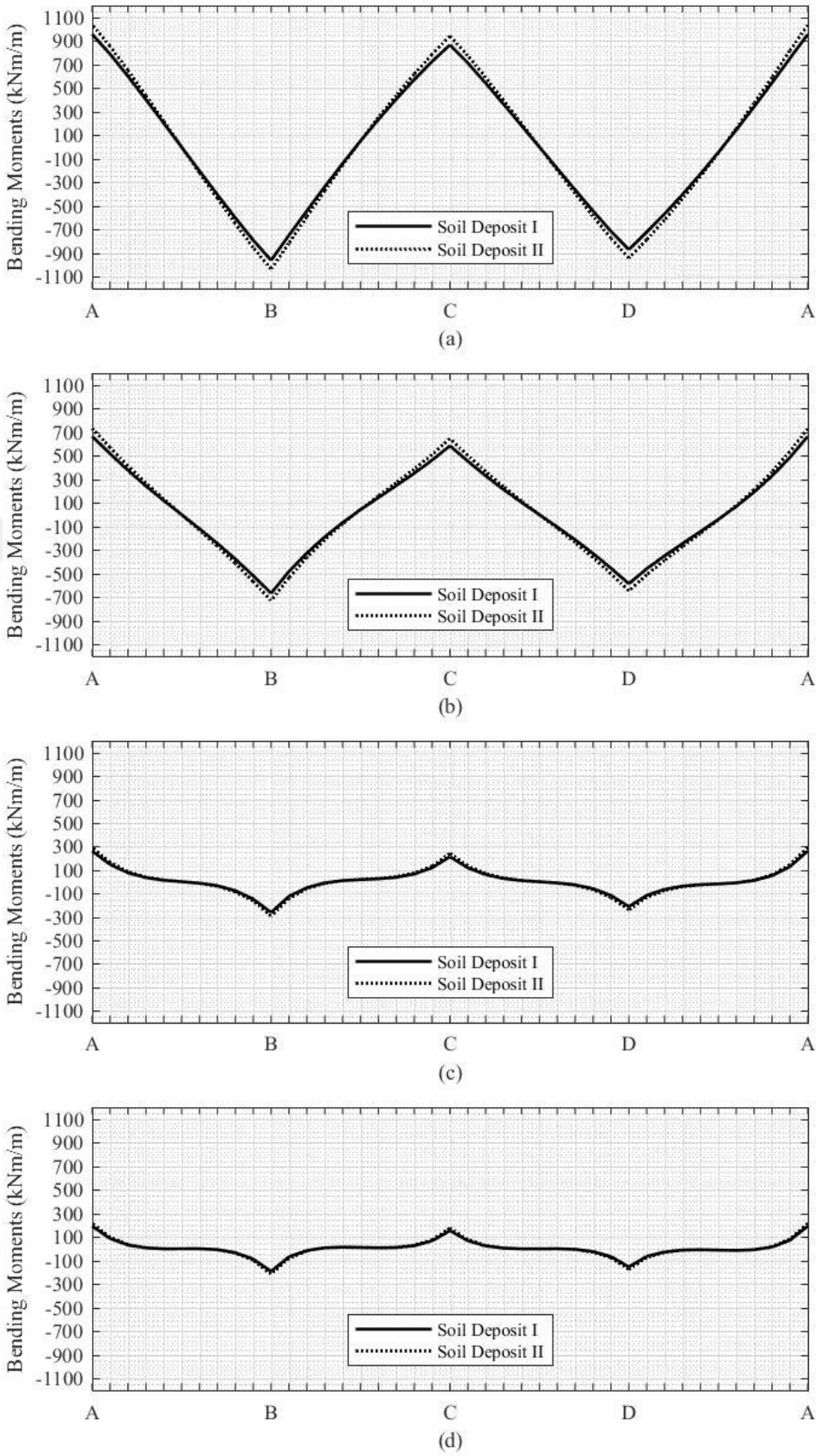


Figure 3.22 The bending moment diagrams of the buried box culvert for the depth ratio of 1.50 for (a) FR=0.125, (b) FR=1.0, (c) FR=8.0, and FR=15.0

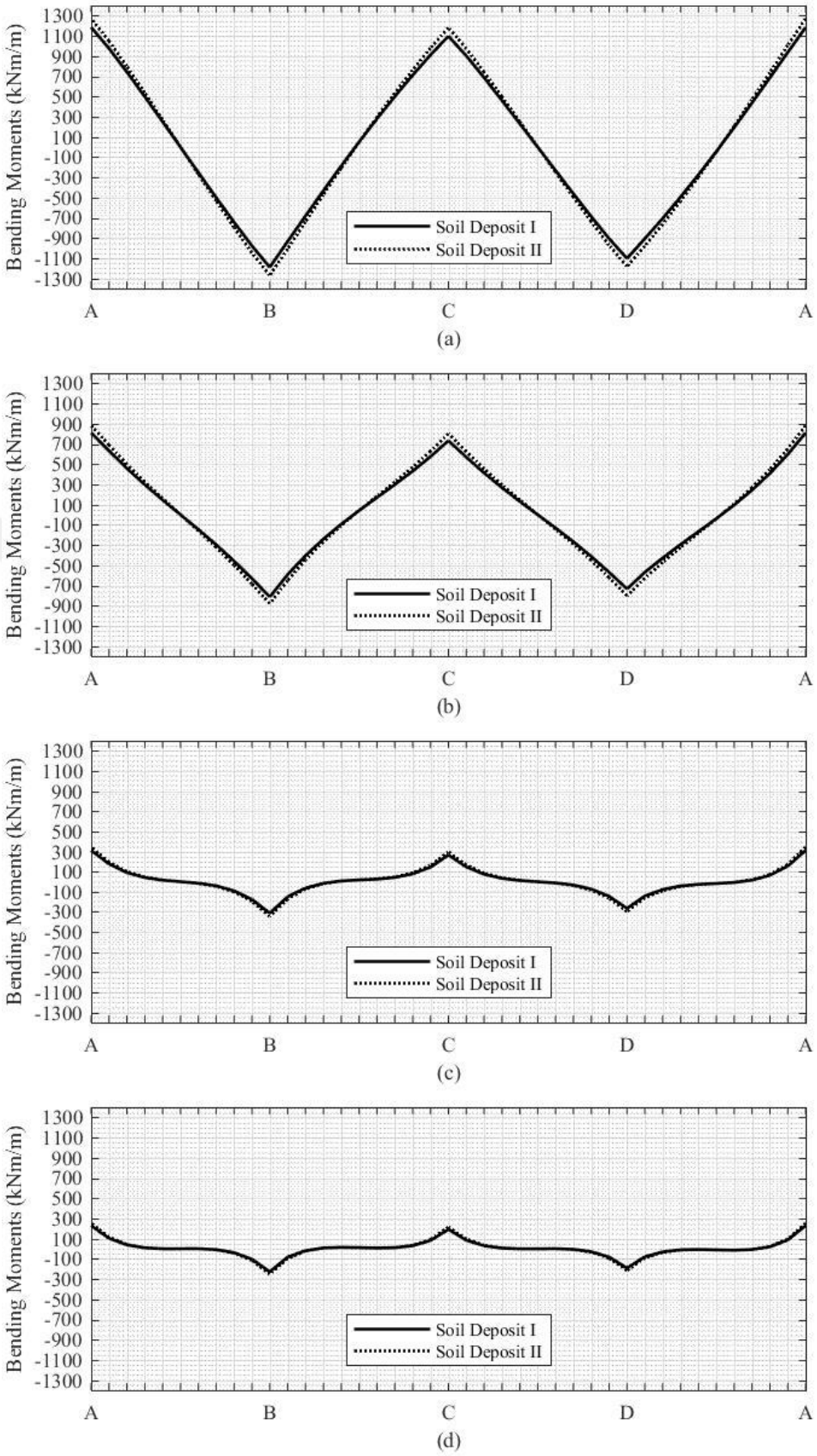


Figure 3.23 The bending moment diagrams of the buried box culvert for the depth ratio of 2.00 for (a) FR=0.125, (b) FR=1.0, (c) FR=8.0, and FR=15.0

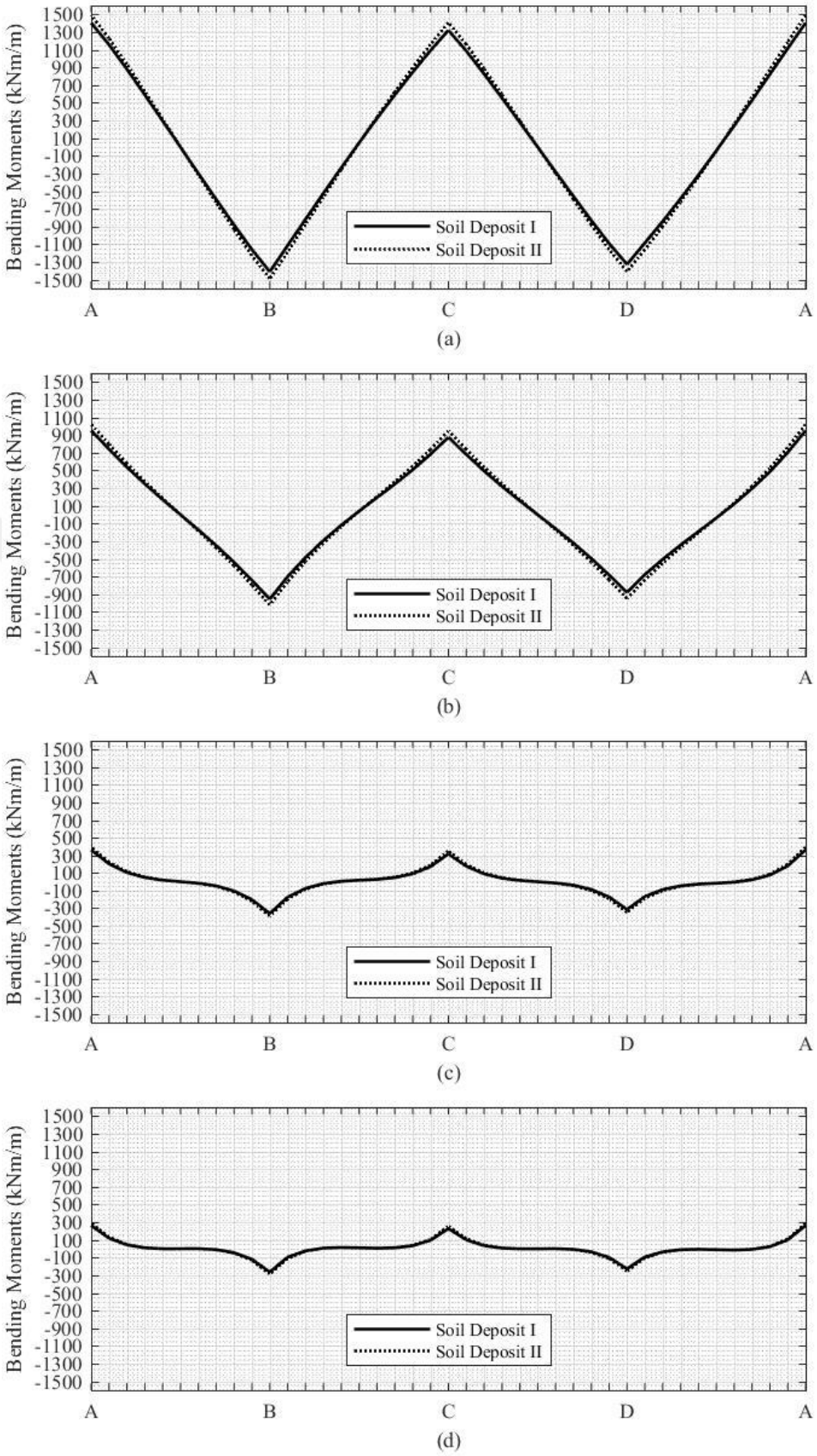


Figure 3.24 The bending moment diagrams of the buried box culvert for the depth ratio of 2.50 for (a) FR=0.125, (b) FR=1.0, (c) FR=8.0, and FR=15.0

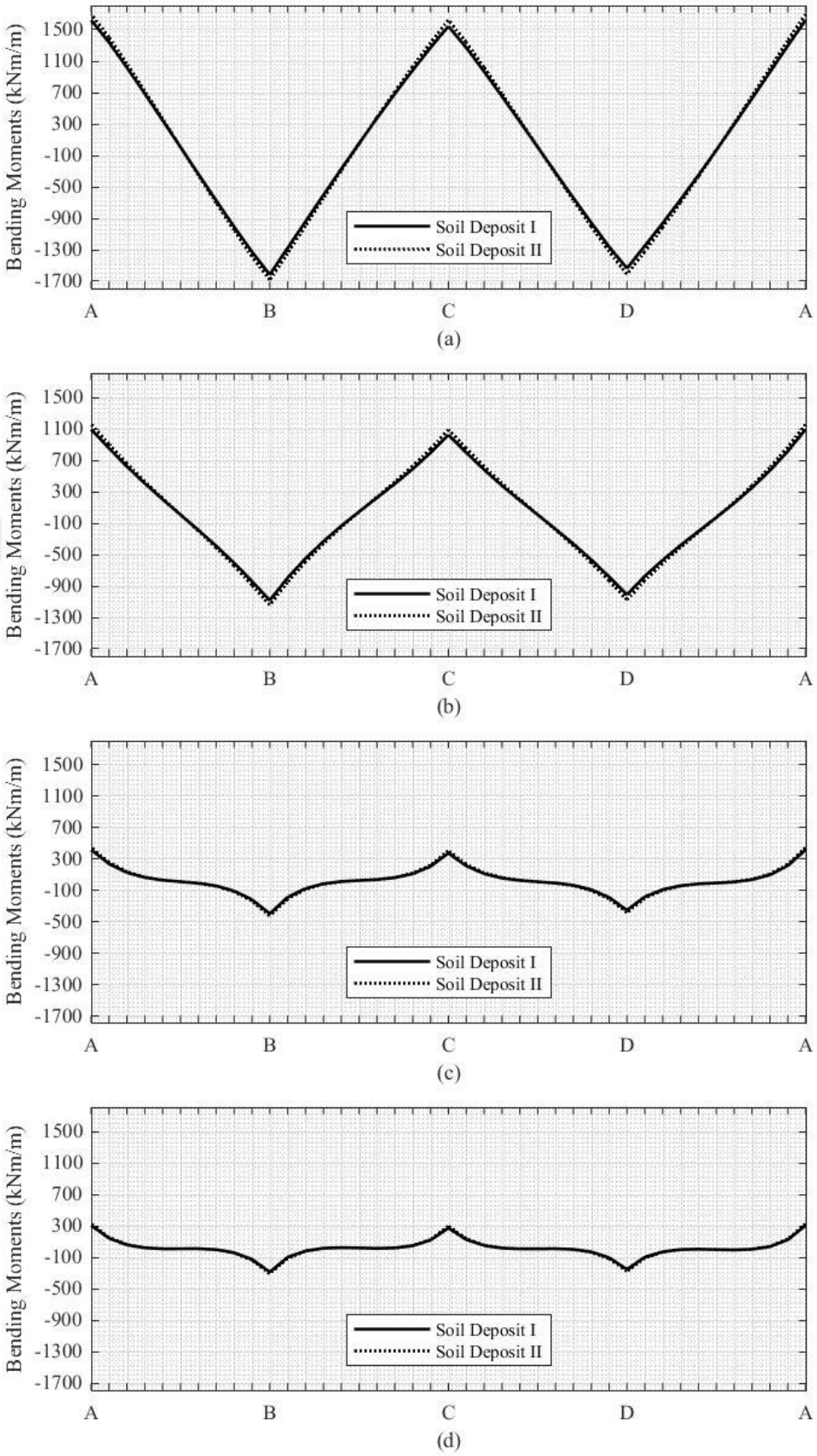


Figure 3.25 The bending moment diagrams of the buried box culvert for the depth ratio of 3.00 for (a) FR=0.125, (b) FR=1.0, (c) FR=8.0, and FR=15.0

3.6.3 Variation of the Drift Ratios

As mentioned before, the drift ratio is the ratio of the difference in the displacements of the lower-left (point A in Figure 3.1b) and upper-left corners (point D in Figure 3.1b) of the buried box culvert to the height of the buried box culvert. The variation of the drift ratios with the flexibility and depth ratios for the soil deposits I and II are given in Figure 3.26. As seen from Figure 3.26a, the drift ratios increase with increasing flexibility ratio for a constant value of the depth ratio. The drift ratios also increase with increasing depth ratio for a constant value of the flexibility ratio. The change in the drift ratios with increasing flexibility ratio for a constant depth ratio is higher for the smaller values of the flexibility ratios than for the larger values of the flexibility ratios. The change in the drift ratio with increasing depth ratio for a constant flexibility ratio is less for the smaller values of the depth ratio than for the larger values of the depth ratio. The maximum drift ratio is obtained for the largest depth and flexibility ratios considered. As seen from Figure 3.26b, the drift ratios increase with increasing flexibility ratio for a constant value of the depth ratio. The drift ratios also increase with increasing depth ratio for a constant value of the flexibility ratio. The change in the drift ratios with increasing flexibility ratio for a constant depth ratio is higher for the smaller values of the flexibility ratios than for the larger values of the flexibility ratios. The change in the drift ratio with increasing depth ratio for a constant flexibility ratio is less for the smaller values of the depth ratio than for the larger values of the depth ratio. The maximum drift ratio is obtained for the largest depth and flexibility ratios considered.

The drift ratios for soil deposits I and II are given in Figure 3.27 for depth ratios of 0.25, 0.50, 0.75, 1.00, 1.50, 2.00, 2.50, and 3.00. As seen from Figure 3.27, the drift ratio increases with increasing flexibility ratio for a constant values of depth ratio for soil deposits I and II. The change in this increase is larger for the smaller values of the flexibility ratio than for the larger values of the flexibility ratio for soil deposits I and II.

The variation of the drift ratios for a constant value of the flexibility ratios for the soil deposits I and II are given in Figure 3.28. As seen from Figure 3.28, the drift ratios increase with increasing depth ratio for a constant value of the flexibility ratio. The drift ratios also increase with increasing flexibility ratio for a constant value of the depth ratio. The maximum drift ratio is obtained for the largest depth and flexibility ratios considered.

As also seen from Figure 3.26 to Figure 3.28, the drift ratios increase with increasing flexibility ratio for the soil deposits I and II. If the depth ratio increases, the difference among the drift ratios increase for the soil deposits I and II.

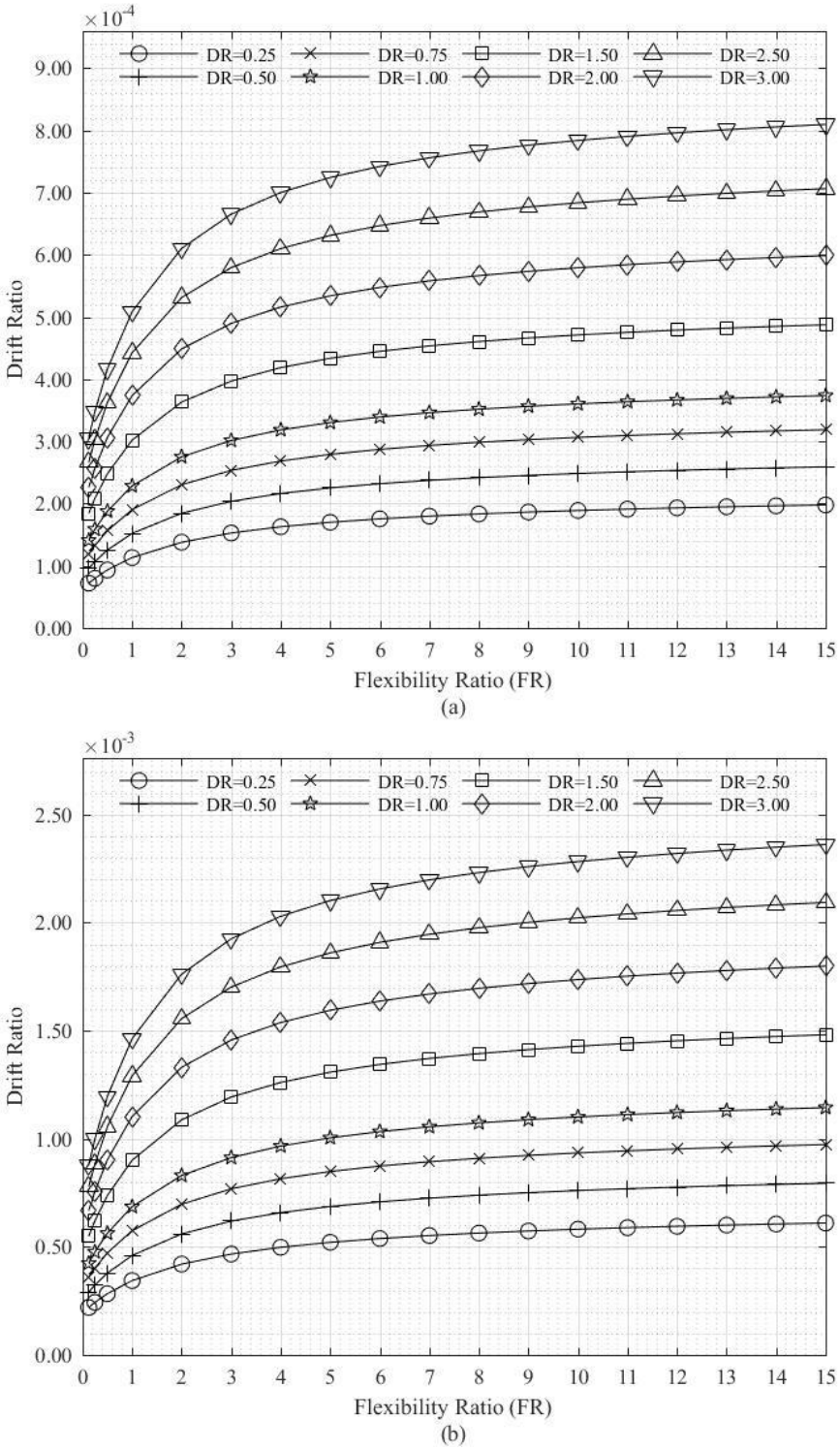


Figure 3.26 The variation of the drift ratios for the soil deposits (a) I and (b) II

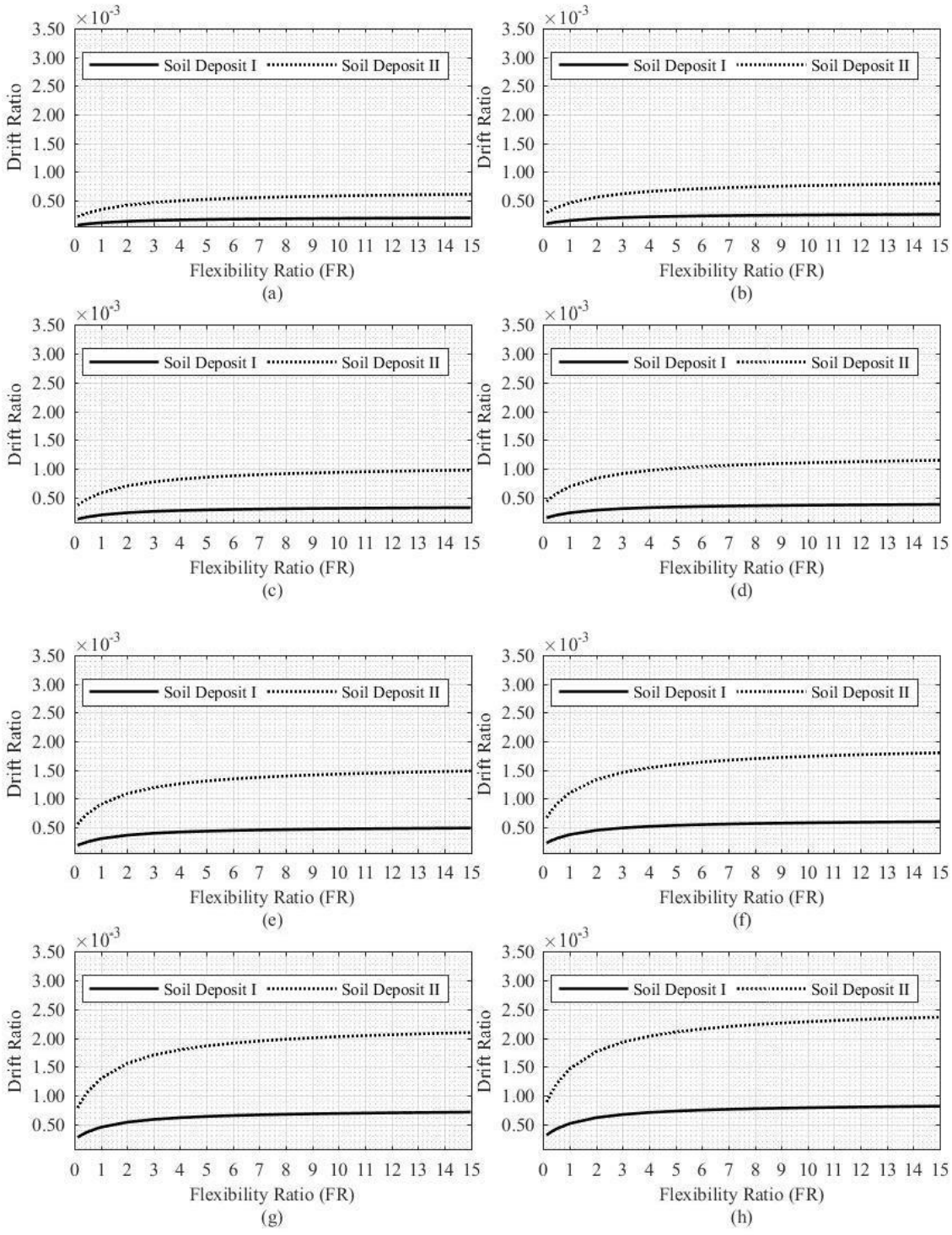


Figure 3.27 The variation of the drift ratios for the depth ratios of (a) 0.25, (b) 0.50, (c) 0.75, (d) 1.00, (e) 1.50, (f) 2.00, (g) 2.50, and (h) 3.00

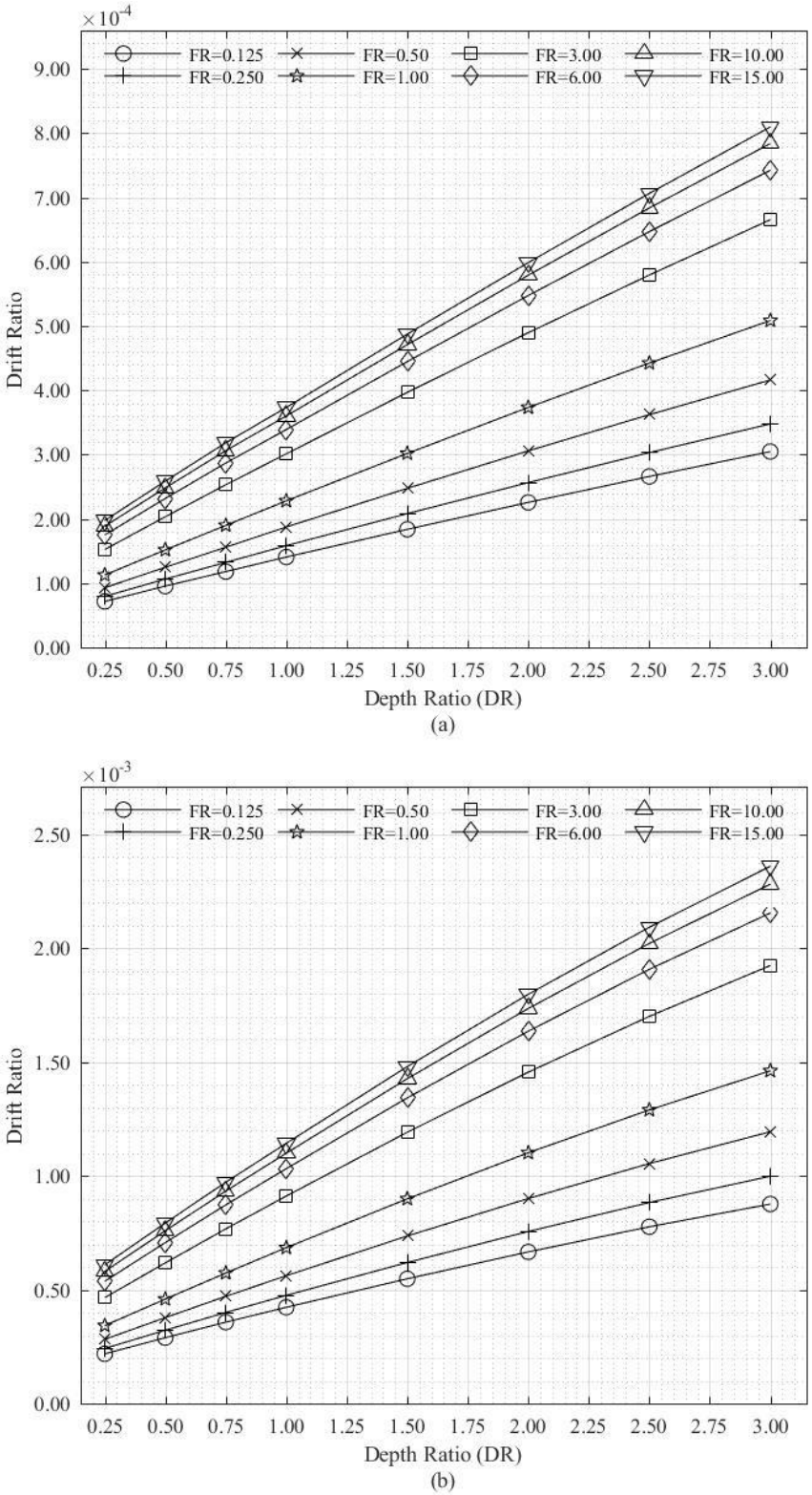


Figure 3.28 The variation of the drift ratios for a constant value of the flexibility ratios for the soil deposits (a) I and (b) II

3.6.4 Variation of the Shear Strain Deformation Ratios

The shear strain deformation ratio is the ratio of the shear deformation of the buried box culvert embedded in the soil to free-field shear deformation over the height of the buried box culvert. The shear strain deformation ratio, *R*, can be calculated by using the following equation.

$$R = \frac{\Delta_{st}}{\Delta_{ff}} \tag{3.7}$$

where, Δ_{st} is the shear deformation of the buried box culvert embedded in soil and Δ_{ff} is the free-field shear deformation over the height of the buried box culvert.

The shear strain deformation ratio curves with respect to depth ratios for the soil deposits I and II are given in Figure 3.29. As seen from Figure 3.29, the shear strain deformation ratio is almost the same up to the flexibility ratio of 3 for all of the depth ratios. After the flexibility values of 3, the shear strain deformation ratios differ from each other for the depth ratios considered. As also seen from Figure 3.29, the shear strain deformation ratio increases with increasing flexibility ratio for any values of the depth ratio. The shear strain deformation ratio value for a constant value of the flexibility ratio decrease with increasing depth ratio, after the flexibility ratio of 3. This decrease is less for the smaller values of the flexibility ratios than for the larger values of the flexibility ratios. It is possible to say that after a value of the flexibility ratios, the change in the shear strain deformation ratio is negligible for any values of the depth ratios considered in this study.

A number of formulas for a relation between the shear strain deformation and flexibility ratios are suggested by the researchers. Penzien (2000) [71] suggested a formula for a relation between the shear strain deformation and flexibility ratios. This formula is dependent on Poisson's ratio of the soil layer and flexibility ratio. And, Wang (1993) [72] suggested another formula. This formula is derived from results of the finite element analyses. On the other hand, this formula is dependent on Poisson's ratio of the soil layer and flexibility ratio. Nishioka and Unjoh (2002) [73] suggested a formula for a relation between the shear strain deformation and flexibility ratios. This formula is only dependent on the flexibility ratio. As mentioned above 3 formulas are independent of the depth ratio. The shear strain deformations are calculated according to the aforementioned 3 formulas. Nevertheless, mean values of the shear strain deformation for the soil deposits I and II are calculated.

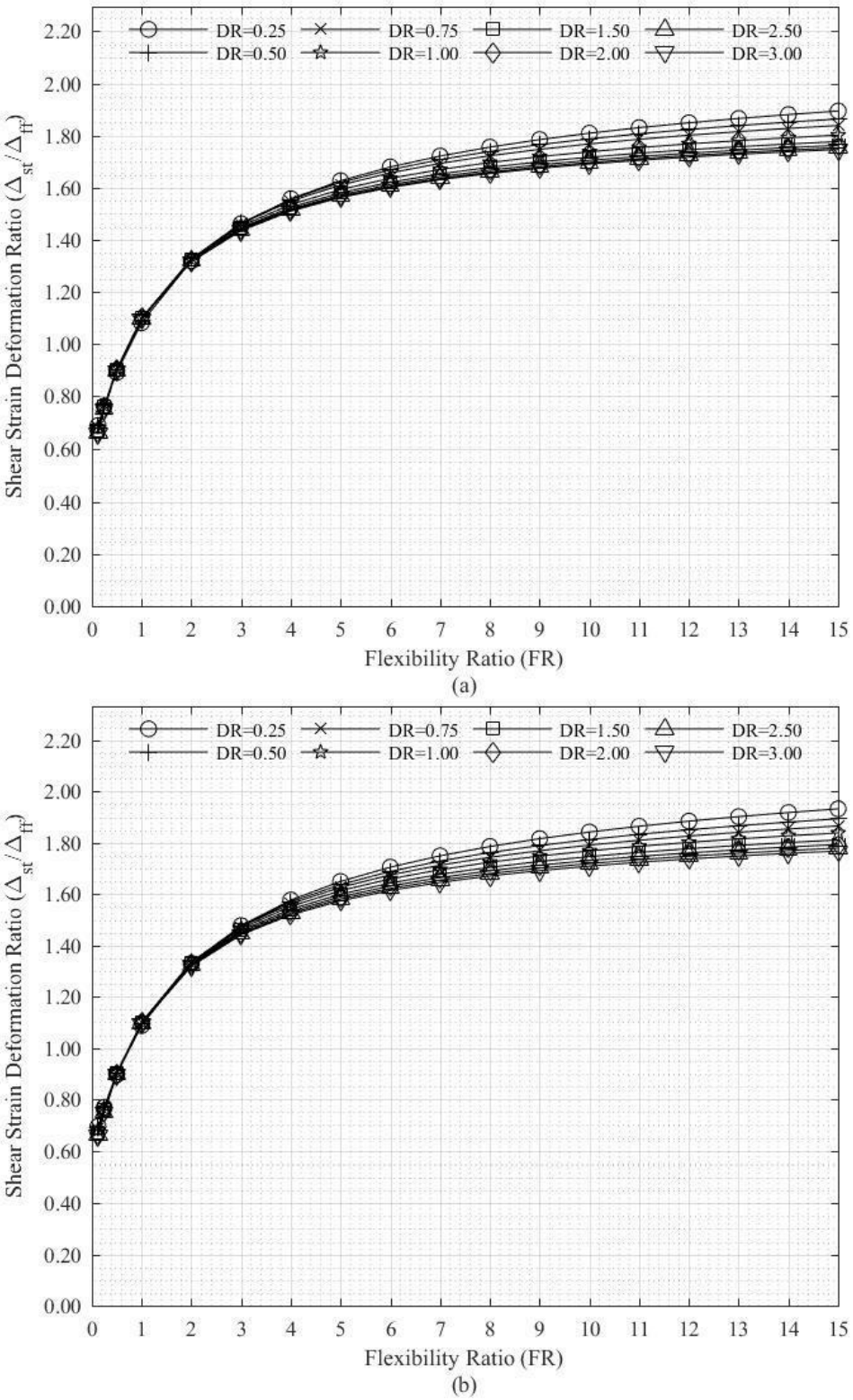


Figure 3.29 The shear strain deformation ratios for the soil deposits (a) I and (b) II

The comparison of the numerical and analytical shear strain deformation ratios is given in Figure 3.30. As seen from Figure 3.30, the shear strain deformation ratio curves follow the exact same path up to flexibility ratio of 2.0 for soil deposits I and II. When the flexibility ratio is greater than 2.0, the shear strain deformation ratio curves follow the almost same path for soil deposit I, soil deposit II and results of Nishioka and Unjoh (2002) [73]. And also, the shear strain deformation ratio curves follow the almost same path for results of Penzien (2000) [71] and Wang (1993) [72].

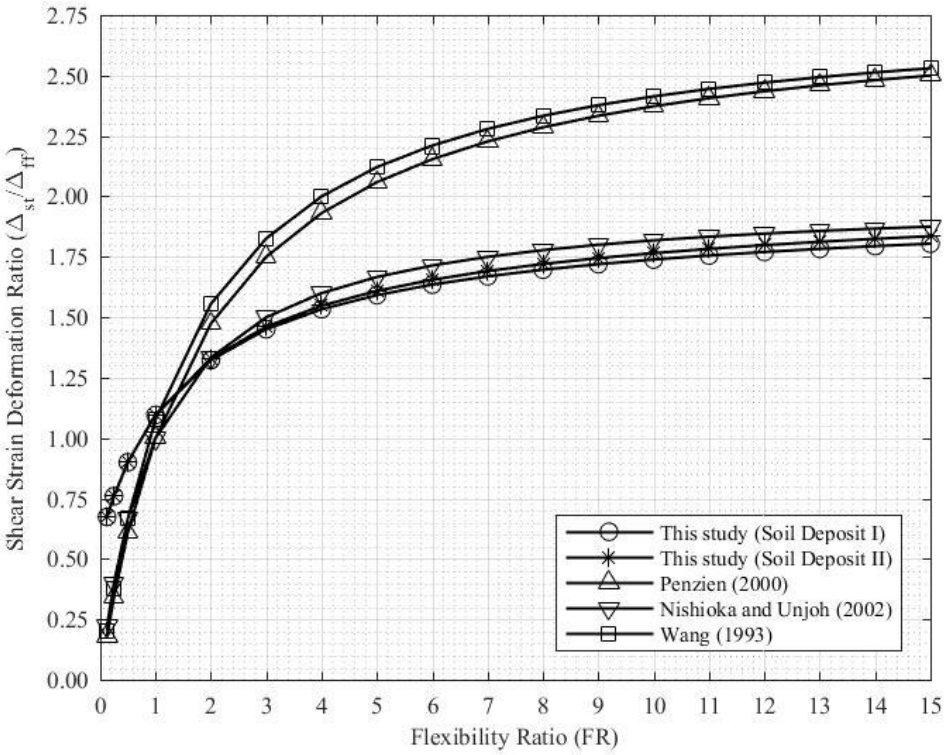


Figure 3.30 The comparison of the numerical and analytical shear strain deformation ratios

CHAPTER 4

CONCLUSIONS AND RECOMMENDATIONS

In this study, the effects of various parameters on the seismic response (i.e., internal forces, drift ratios, and shear strain deformation) of the buried box culvert are investigated. These parameters are ground type of the soil deposits, depth ratios, and flexibility ratios. Ground types B and C are used in this study. The depth ratio values used are 0.25, 0.50, 0.75, 1.00, 1.50, 2.00, 2.50, and 3.00. The flexibility ratio values used are 0.125, 0.25, 0.50, 1, 2, 3, 4, 5, 6, 7, 8, 9, 10, 11, 12, 13, 14, and 15. The FEM model is consisting of three parts. The first part is soil deposit which is modeled using two-dimensional plane-strain quadrilateral elements with elastic material. The second part is buried box culvert which is modeled using frame elements with elastic material. Contact properties between soil and frame elements are assumed to be bonded type. The third part is free-field columns which are modeled using two-dimensional plane-strain quadrilateral elements with elastic material. The free-field columns are added to assure PBCs at the left-hand and the right-hand sides of the FEM model. Rayleigh damping is utilized in this study by assuming 5% viscous damping. Velocity histories are used as input motion. A number of analyses are performed in the OpenSEES. The conclusions drawn from the results obtained in this study are given below.

If the depth ratio is equal to or less than 1.0, the normalized axial forces are almost constant with increasing flexibility ratio. If the depth ratio is greater than 1.0, the normalized axial forces decrease with increasing flexibility ratio. The normalized shear forces and the normalized bending moments decrease with increasing flexibility ratio for a constant value of the depth ratio. This decrease is much higher for the smaller values of the flexibility ratios than for the larger values of the flexibility ratios. The normalized internal forces increase with increasing depth ratio for a constant value of the flexibility ratio. The differences among the normalized axial forces are almost constant with

increasing depth ratio for the soil deposits I and II, but the differences among the normalized shear forces decrease with increasing depth ratio for the soil deposits I and II. In addition, the differences among the normalized bending moments are almost constant with increasing depth ratio for the soil deposits I and II. The maximum values of the normalized internal forces are obtained for the smallest flexibility ratio and the maximum depth ratio.

The maximum bending moment increases with increasing depth ratio for a constant value of the flexibility ratio, but the maximum bending moment decreases with increasing flexibility ratio for a constant value of the depth ratio. For the flexibility ratios of 0.125 and 1.0, the bending moment diagram is almost linear. For all values of the flexibility ratios considered in this study, the maximum bending moment is obtained at the corner A of the buried box culverts, and the minimum bending moment is obtained at the corner B of the buried box culvert. The difference between the bending moments values of the soil deposit I and II decreases with increasing flexibility ratio, and the curves of the bending moment values of the both soil deposits almost coincide. In addition, the variation of the bending moment values is not linear for the larger flexibility ratios. For the flexibility ratios of 8.0 and 15.0, the maximum bending moments occur at the corners of the buried box culvert. The maximum values of the bending moment for the soil deposits I and II are obtained for the smallest flexibility ratio and the maximum depth ratio.

The drift ratios increase with increasing flexibility ratio for a constant value of the depth ratio. The drift ratios also increase with increasing depth ratio for a constant value of the flexibility ratio. The change in the drift ratios with increasing flexibility ratio for a constant depth ratio is higher for the smaller values of the flexibility ratios than for the larger values of the flexibility ratios. The change in the drift ratio with increasing depth ratio for a constant flexibility ratio is less for the smaller values of the depth ratio than for the larger values of the depth ratio. The maximum drift ratio is obtained for the largest depth and flexibility ratios considered.

The shear strain deformation ratio is almost the same up to the flexibility ratio of 3 for all of the depth ratios. After the flexibility values of 3, the shear strain deformation ratios differ from each other for the depth ratios considered. The shear strain deformation ratio increases with increasing flexibility ratio for any values of the depth ratio. The shear strain deformation value for a constant value of the flexibility ratio decrease with increasing

depth ratio, after the flexibility ratio of 3. This decrease is less for the smaller values of the flexibility ratios than for the larger values of the flexibility ratios. It is possible to say that after a value of the flexibility ratios, the change in the shear strain deformation ratio is negligible for any values of the depth ratios considered in this study.

The following researches can be done for the future studies. Nonlinear materials may be used to model the soil medium and the buried structure. Different types of buried structures (i.e., multi-barrel or multi-story) may be used. Different contact types between the soil medium and the buried structure may be used. The effects of the buried structure on the response of the ground surface may be investigated. In addition, the interaction between the buried structure and the aboveground structure may be investigated.

REFERENCES

[1] Dai, W., Rojas, F., Shi, C., and Tan, Y. (2018). “Effect of soil structure interaction on the dynamic responses of base isolated bridges and comparison to experimental results”, Soil Dynamics and Earthquake Engineering, 114:242–252.

[2] Cruz, C., and Miranda, E. (2017). “Evaluation of soil-structure interaction effects on the damping ratios of buildings subjected to earthquakes”, Soil Dynamics and Earthquake Engineering, 100:183–195.

[3] Hassani, N., Bararnia, M., and Amiri, G. G. (2018). “Effect of soil-structure interaction on inelastic displacement ratios of degrading structures”, Soil Dynamics and Earthquake Engineering, 104:75–87.

[4] Bolisetti, C., Whittaker, A. S., and Coleman, J. L. (2018). “Linear and nonlinear soil-structure interaction analysis of buildings and safety-related nuclear structures”, Soil Dynamics and Earthquake Engineering, 107:218–233.

[5] LS-DYNA keyword user's manual - version R 7.0, Livermore Software Technology Corporation, Livermore, California (2013)

[6] Martakis, P., Taeseri, D., Chatzi, E., and Laue, J. (2017). “A centrifuge-based experimental verification of Soil-Structure Interaction effects”, Soil Dynamics and Earthquake Engineering, 103:1–14.

[7] Luco, J. E. (2014). “Effects of soil–structure interaction on seismic base isolation”, Soil Dynamics and Earthquake Engineering, 66:167–177.

[8] Ghandil, M., and Behnamfar, F. (2017). “Ductility demands of MRF structures on soft soils considering soil-structure interaction”, Soil Dynamics and Earthquake Engineering, 92:203–214.

[9] von Estorff, O., and Firuziaan, M. (2000). “Coupled BEM/FEM approach for nonlinear soil/structure interaction”, Engineering Analysis with Boundary Elements, 24(10):715–725.

[10] Padrón, L. A., Aznárez, J. J., and Maeso, O. (2009). “Dynamic structure–soil–structure interaction between nearby piled buildings under seismic excitation by BEM–FEM model”, Soil Dynamics and Earthquake Engineering, 29(6):1084–1096.

[11] Abascal, R. (1995). “2D transient dynamic friction contact problems. II. Applications to soil-structure interaction problems”, Engineering Analysis with Boundary Elements, 16(3):235–243.

[12] Guarracino, F., Minutolo, V., and Nunziante, L. (1992). “A simple analysis of soil-structure interaction by BEM-FEM coupling”, Engineering Analysis with Boundary Elements, 10(4):283–289.

[13] Karabalis, D. L. (1991). “A simplified 3-D time domain BEM for dynamic soil-structure interaction problems”, Engineering Analysis with Boundary Elements, 8(3):139–145.

[14] Galvín, P., and Romero, A. (2014). “A MATLAB toolbox for soil–structure interaction analysis with finite and boundary elements”, Soil Dynamics and Earthquake Engineering, 57:10–14.

[15] MATLAB, The Language of Technical Computing (R2010a), The MathWorks Inc.

[16] Yeganeh, N., Bazaz, J. B., and Akhtarpour, A. (2015). “Seismic analysis of the soil–structure interaction for a high rise building adjacent to deep excavation”, Soil Dynamics and Earthquake Engineering, 79:149–170.

[17] Livaoglu, R. (2014). “The numerical and empirical evaluation of chimneys considering soil structure interaction and high-temperature effects”, Soil Dynamics and Earthquake Engineering, 66:178–190.

[18] Rahnema, H., Mohasseb, S., and JavidSharifi, B. (2016). “2-D soil-structure interaction in time domain by the SBFEM and two non-linear soil models”, Soil Dynamics and Earthquake Engineering, 88:152–175.

[19] Durmuş, A., and Livaoglu, R. (2015). “A simplified 3 D.O.F. model of A FEM model for seismic analysis of a silo containing elastic material accounting for soil–structure interaction”, Soil Dynamics and Earthquake Engineering, 77:1–14.

[20] Kim, J., Lee, E., and Lee, S. (2016). “Boundary reaction method for nonlinear analysis of soil–structure interaction under earthquake loads”, Soil Dynamics and Earthquake Engineering, 89:85–90.

[21] Li, S., Zhang, F., Wang, J., Alam, M. S., and Zhang, J. (2017). “Seismic responses of super-span cable-stayed bridges induced by ground motions in different sites relative to fault rupture considering soil-structure interaction”, Soil Dynamics and Earthquake Engineering, 101:295–310.

[22] Shakib, H., and Fuladgar, A. (2004). “Dynamic soil–structure interaction effects on the seismic response of asymmetric buildings”, Soil Dynamics and Earthquake Engineering, 24(5):379–388.

[23] Spyrakos, C. C., Koutromanos, I. A., and Maniatakis, C. A. (2009). “Seismic response of base-isolated buildings including soil–structure interaction”, Soil Dynamics and Earthquake Engineering, 29(4):658–668.

[24] Burman, A., Nayak, P., Agrawal, P., and Maity, D. (2012). “Coupled gravity dam–foundation analysis using a simplified direct method of soil–structure interaction”, Soil Dynamics and Earthquake Engineering, 34(1):62–68.

[25] Liang, J., Fu, J., Todorovska, M. I., and Trifunac, M. D. (2013). “Effects of site dynamic characteristics on soil–structure interaction (II): Incident P and SV waves”, Soil Dynamics and Earthquake Engineering, 51:58–76.

[26] Yazdchi, M., Khalili, N., and Valliappan, S. (1999). “Dynamic soil–structure interaction analysis via coupled finite-element–boundary-element method”, Soil Dynamics and Earthquake Engineering, 18(7):499–517.

[27] Haroun, M. A., and Temraz, M. K. (1992). “Effects of soil-structure interaction on seismic response of elevated tanks”, Soil Dynamics and Earthquake Engineering, 11(2):73–86.

[28] Carbonari, S., Dezi, F., Gara, F., and Leoni, G. (2014). “Seismic response of reinforced concrete frames on monopile foundations”, Soil Dynamics and Earthquake Engineering, 67:326–344.

[29] Haiyang, Z., Xu, Y., Chao, Z., and Dandan, J. (2014). “Shaking table tests for the seismic response of a base-isolated structure with the SSI effect”, Soil Dynamics and Earthquake Engineering, 67:208–218.

[30] Sáez, E., Lopez-Caballero, F., and Modaressi-Farahmand-Razavi, A. (2013). “Inelastic dynamic soil–structure interaction effects on moment-resisting frame buildings”, Engineering Structures, 51:166–177.

[31] Zangeneh, A., Svedholm, C., Andersson, A., Pacoste, C., and Karoumi, R. (2018). “Identification of soil-structure interaction effect in a portal frame railway bridge through full-scale dynamic testing”, Engineering Structures, 159:299–309.

[32] Seo, C.-G., Yun, C.-B., & Kim, J.-M. (2007). “Three-dimensional frequency-dependent infinite elements for soil–structure interaction”, Engineering Structures, 29(11):3106–3120.

[33] Küçükarslan, S., Banerjee, P. K., and Bildik, N. (2003). “Inelastic analysis of pile soil structure interaction”, Engineering Structures, 25(9):1231–1239.

[34] Kocak, S., and Mengi, Y. (2000). “A simple soil–structure interaction model”, Applied Mathematical Modelling, 24(8):607–635.

[35] Cilingir, U., and Madabhushi, S. P. G. (2011). “A model study on effects of input motion on the seismic behavior of tunnels”, Soil Dynamics and Earthquake Engineering, 31(3):452–462.

[36] Chen, Z., Liang, S., Shen, H., and He, C. (2018). “Dynamic centrifuge tests on the effects of isolation layer and cross-section dimensions on shield tunnels”, Soil Dynamics and Earthquake Engineering, 109:173–187.

[37] Ma, C., Lu, D., Du, X., and Qi, C. (2018). “Effect of buried depth on seismic response of rectangular underground structures considering the influence of ground loss”, Soil Dynamics and Earthquake Engineering, 106:278-297.

[38] Sandoval, E., and Bobet, A. (2017). “Effect of frequency and flexibility ratio on the seismic response of deep tunnels”, Underground Space, 2(2):125–133.

[39] Itasca (2011a). “FLAC Fast Lagrangian analysis of continua”, ver. 8.0.

[40] Shahrour, I., Khoshnoudian, F., Sadek, M., and Mroueh, H. (2010). “Elastoplastic analysis of the seismic response of tunnels in soft soils”, Tunneling and Underground Space Technology, 25(4):478–482.

[41] Abdel-Motaal, M. A., El-Nahhas, F. M., and Khiry, A. T. (2014). “Mutual seismic interaction between tunnels and the surrounding granular soil”, HBRC Journal, 10(3):265–278.

[42] Tsinidis, G., Pitilakis, K., and Madabhushi, G. (2016). “On the dynamic response of square tunnels in sand”, Engineering Structures, 125:419–437.

[43] Tsinidis, G. (2017). “Response characteristics of rectangular tunnels in soft soil subjected to transversal ground shaking”, Tunneling and Underground Space Technology, 62:1–22.

[44] BS EN 1998-1, (2004). Eurocode 8: Design of structures for earthquake resistance, BS.

[45] Tsinidis, G., Rovithis, E., Pitilakis, K., and Chazelas, J. L. (2016). “Seismic response of box-type tunnels in soft soil: Experimental and numerical investigation”, Tunneling and Underground Space Technology, 59:199–214.

[46] ABAQUS: theory and analysis user’s manual, version 6.12. Dassault Systèmes SIMULIA, Providence, RI, USA; 2012.

[47] Baziar, M. H., Moghadam, M. R., Choo, Y. W., and Kim, D. S. (2016). “Tunnel flexibility effect on the ground surface acceleration response”, Journal of Earthquake Engineering and Engineering Vibration, 15(3):457–476.

[48] Labuz, J. F., and Zang, A. (2012). “Mohr–Coulomb Failure Criterion”, Rock Mechanics and Rock Engineering, 45(6):975-979.

[49] Abuhajar, O., Naggar, H. El, and Newson, T. (2015). “Seismic soil – culvert interaction”, NRC Research Press, 1667(April):1649–1667.

[50] Liu, H., and Song, E. (2005). “Seismic response of large underground structures in liquefiable soils subjected to horizontal and vertical earthquake excitations”, Computers and Geotechnics, 32(4):223–244.

[51] Mindlin, R.D., (1951). “Influence of rotatory inertia and shear in flexural motions of isotropic elastic plates”, Journal of Applied Mechanics 18:31–38.

[52] Chan AHC (1993) DIANA-SWANDYNE II Manual, (Part 1-14), Department of Civil Engineering, Birmingham University, England.

[53] Ertugrul, O. L. (2016). “Numerical modeling of the seismic racking behavior of box culverts in dry cohesionless soils”, KSCE Journal of Civil Engineering, 20(5):1737–1746.

[54] Rahai, A. R. (1996). “Investigation of Earthquake Effect on Buried Box Culverts”, 11 WCEE: Eleventh World Conference on Earthquake Engineering, 23-28 June 1996, Acapulco, Mexico

[55] Loret, B., and Prevost, J. (1986). “Accurate numerical solutions for Drucker-Prager elastic-plastic models”, Computer Methods in Applied Mechanics and Engineering, 54:259–277.

[56] Hatzigeorgiou, G. D., and Beskos, D. E. (2001). “Inelastic response of 3-D underground structures in rock under seismic loading”, Advances in Earthquake Engineering, 9:599–608.

[57] Akhlaghi, T., and Nikkar, A. (2014). “Effect of vertically propagating shear waves on seismic behavior of circular tunnels”, The Scientific World Journal, 2014.

[58] Katona., M. G. (2010). “Seismic Design and Analysis of Buried Culverts and Structures”, Journal of Pipeline Systems Engineering and Practice, 1(3):111–119.

[59] Katona, M.G. and Smith, J.M. (1976). CANDE User and System Manuals, Federal Highway Administration Report No. FHWA-RD-77-6, October 1976.

[60] Hushmand, A., Dashti, S., Davis, C., and Hushmand, B. (2016). “Seismic Performance of Underground Reservoir Structures: Insight from Centrifuge Modeling on the Influence of Structure Stiffness”, Journal of Geotechnical and Geoenvironmental Engineering, 142(7).

[61] Nam, S. H., Song, H. W., Byun, K. J., and Maekawa, K. (2006). “Seismic analysis of underground reinforced concrete structures considering elasto-plastic interface element with thickness”, Engineering Structures, 28(8):1122–1131.

[62] Ohsaki Y. (1982). “Dynamic nonlinear model and one-dimensional nonlinear response of soil deposits”, Research Report 82-02. Dept. of Architecture, University of Tokyo

[63] Awwad, E., Mabsout, M., Sadek, and S., Tarhini, K. (2000). “Finite Element Analysis of Concrete Box Culverts”, Computing in Civil and Building Engineering.

[64] CSI, “SAP2000 Integrated Software for Structural Analysis and Design,” Computers and Structures Inc., Berkeley, California.

[65] Pimentel, M., Costa, P., Felix, C., and Figueiras, J. (2009). “Behavior of Reinforced Concrete Box Culverts under High Embankments”, Journal of Structural Engineering, 135(4):366–375.

[66] Tsinidis, G. (2018). “Response of urban single and twin circular tunnels subjected to transversal ground seismic shaking” Tunnelling and Underground Space Technology, 76(March):177–193.

[67] Pitilakis, K., Tsinidis, G., Leanza, A., and Maugeri, M. (2014). “Seismic behavior of circular tunnels accounting for above ground structures interaction effects”, Soil Dynamics and Earthquake Engineering, 67:1–15.

[68] ADINA. Automatic dynamic incremental nonlinear analysis. theory and modeling guide. Watertown, USA: ADINA R&D, Inc.; 2008.

[69] Esmaeilzadeh Seylabi, E., Jeong, C., Dashti, S., Hushmand, A., and Taciroglu, E. (2018). “Seismic response of buried reservoir structures: a comparison of numerical simulations with centrifuge experiments”, Soil Dynamics and Earthquake Engineering, 109(March):89–101.

[70] Abuhajar, O., El Naggar, H., and Newson, T. (2015). “Experimental and numerical investigations of the effect of buried box culverts on earthquake excitation”, Soil Dynamics and Earthquake Engineering, 79:130–148.

[71] Penzien, J. (2000). “Seismically induced racking of tunnel linings”, Earthquake Engineering and Structural Dynamics, 29:683-691.

[72] Wang, J. N., (1993) Seismic design of tunnels: a simple state of the art design approach. New York, Parsons Brinckerhoff Inc.

[73] Nishioka, T. and Unjoh, S. (2002). “A Simplified Seismic Design Method for Underground Structures Based on Shear Strain Transmitting Characteristics”, SEWC 2002, Yokohama, Japan.

[74] McKenna F., Fenves L. G., Scott M. H. (2000). “Open System for Earthquake Engineering Simulation”, Pacific Earthquake Engineering Research Center.

[75] Lysmer, J. and Kuhlemeyer, A.M. (1969). “Finite Dynamic Model for Infinite Media”, Journal of the Engineering Mechanics Division, 95(4):859-878.

[76] OpenSEES Examples, Dynamic Effective Stress Analysis of a Slope, http://opensees.berkeley.edu/wiki/index.php/Dynamic_2D_Effective_Stress_Analysis_of_Slope, 1 December 2017.

[77] Uzun, S. and Ayvaz, Y. (2018). “Variation of Buried Box Culvert Deformations with Respect to Various Parameters under Earthquake Loading”, Proceedings of the Advances in Civil Engineering, 12-14 September 2018, İzmir.

[78] Wood, J. (2004). “Earthquake Design Procedures for Rectangular Underground Structures”, Proceedings of the New Zealand Society for Earthquake Engineering, 11-13 March 2005, Wellington, New Zealand.

[79] Tsinidis, G., and Pitilakis, K. (2018). “Improved R-F relations for the transversal seismic analysis of rectangular tunnels”, Soil Dynamics and Earthquake Engineering, 107:48–65.

[80] Hadjian, A. H. (2002). “Fundamental period and mode shape of layered soil profiles”, Soil Dynamics and Earthquake Engineering, 22(9–12):885–891.

[81] Vijayendra, K., Prasad, S., and Nayak, S. (2010). “Computation of Fundamental Period of Soil Deposit: A Comparative Study”, Indian Geotechnical Conference, 16-18 December 2010, Mumbai, Maharashtra, India.

CURRICULUM VITAE

PERSONAL INFORMATION

Name Surname : Sefa UZUN

Date of birth and place : 03.01.1992, İstanbul

Foreign Languages : English

E-mail : sefa.uzun@dpu.edu.tr

EDUCATION

Degree	**Department**	**University**	**Date of Graduation**
Undergraduate	Civil Engineering	Yıldız Technical University	2014
High School	-	Haydarpaşa High School	2010

WORK EXPERIENCE

Year	**Corporation/Institute**	**Enrollment**
2018 - Present	Kütahya Dumlupınar University	Research Assistant

PUBLISHMENTS

Conference Papers

1. Uzun, S. and Ayvaz, Y. (2018). “Variation of Buried Box Culvert Deformations with Respect to Various Parameters under Earthquake Loading”, Proceedings of the Advances in Civil Engineering, 12-14 September 2018, İzmir.